Studies on Structure-Function Relationship and Conversion of Coenzyme Requirement in Bacterial α-Keto Acid Reductases Responsible for Metabolism of Acidic Polysaccharides

Ryuichi TAKASE

2015

CONTENTS

INTRODUCTION……..……..1

CHAPTER I **α-Keto acid (DEH) reductase prerequisite for alginate metabolism in *Sphingomonas* sp. strain A1**……...7

CHAPTER II **NADH-dependent DEH reductase and structure-based conversion of its coenzyme requirement**…….32

CHAPTER III **Recognition of coenzymes by bacterial α-keto acid reductases in SDR family**……55

CONCLUSION……...…72

ACKNOWLEDGMENTS……..…..……...……73

LIST OF PUBLICATIONS……75

INTRODUCTION

Coenzymes NADPH and NADH are electron mediators and are involved in oxidation/reduction enzymatic reactions, although their physiological roles are different in biological reactions (1). NADPH is involved in assimilation or antioxidation by its reducing power. On the other hand, NADH, mainly used in catabolism, accepts electrons from nutrients and plays important roles in the production of bioenergy in the form of ATP. In general, an oxidation/reduction-catalytic enzyme shows specificity for either coenzyme based on their biological roles.

Recently, biofuel production from unused and/or excess biomass has been an area of interest (2). To achieve bioproduction, metabolic pathways are modified through introduction and/or disruption of certain genes. This biotechnology, called synthetic biology, is now being developed in academia and industry (3). However, oxidation/reduction reactions are strictly regulated in innate organisms, with coenzyme balance properly maintained. In the case of microbial production of useful substances, intracellular oxidation/reduction imbalance of coenzymes occurs because of the artificial improvement and/or addition of metabolic reactions. The imbalance often causes low yield production. Two attempts have been conducted to solve this problem. One is to regenerate each coenzyme by coupling reactions using dehydrogenases of formate or glucose (4), and the other is to convert the coenzyme requirement of metabolic enzymes such as xylose reductase (5). The latter method is suitable for continuous production because addition of substrates such as formate/glucose and introduction of coenzyme-regenerating enzymes are unnecessary. A lot of studies have been carried out to convert the coenzyme requirement. However, in many cases, resulting mutants show low enzyme activity compared with the wild-type (WT) enzyme (6-27). There are some successful cases (28-36), although general methods for conversion of the coenzyme requirement are being sought.

Short-chain dehydrogenase/reductase (SDR) family enzymes use NADPH or NADH as a coenzyme to metabolize sugars, fatty acids, and steroids (37). From bacteria to humans, a large number of organisms produce SDR family enzymes. More than 120,000 enzymes in the SDR family are registered in UniProtKB (www.uniprot.org/) (38). Structural determinants for the coenzyme requirement in some SDR family enzymes are valuable to establish a basic biotechnology regarding molecular conversion of coenzyme specificity in SDR family enzymes because their crystal structures thus far analyzed are mutually similar (39). Increasingly larger amounts of structural data regarding enzymes and proteins are being deposited in the Protein Data

Bank (PDB) (www.wwpdb.org/) (40), in proportion to the progress in the field of structural biology. Structure-based biotechnology is expected to become an important part of post-structural biology. For example, the structure-based conversions of polysaccharide-degrading enzymes from the exo to the endo mode of action have been achieved (41,42).

Alginate is a heteropolysaccharide consisting of two uronic acids, β-D-mannuronic acid and α-L-guluronic acid (43). The polysaccharide is abundant as a major component of the cell wall matrix in marine algae, such as brown seaweeds. Currently, effective utilization of marine biomass alginate is desirable because brown seaweeds are readily cultivated and cause no serious competing interests for food-stuffs (44). The Gram-negative bacterium, *Sphingomonas* sp. strain A1, directly uptakes alginate into the cytoplasm through a superchannel consisting of a cell-surface pit and ATP-binding cassette (ABC) transporter (45,46). Subsequently, alginate is degraded to monosaccharides by the action of cytoplasmic endotype alginate lyases A1-I, -II, and -III and exotype lyase A1-IV (47,48). All of the resultant monosaccharides are nonenzymatically converted to α-keto acid, 4-deoxy-L-*erythro*-5-hexoseulose uronic acid (DEH). However, metabolic pathway of alginate after DEH formation in strain A1 remains to be clarified. Because α-keto acid is often produced in the bacterial metabolism of some acidic polysaccharides such as pectin and glycosaminoglycan, α-keto acid-acting enzymes are important to reveal the acidic polysaccharide metabolism.

This thesis deals with molecular identification, enzymatic characterization, structure determination, and conversion of coenzyme requirement of bacterial α-keto acid reductases involved in the metabolism of acidic polysaccharides. In addition, this study intends to establish a structure-based methodology to design the coenzyme requirement in SDR family enzymes.

References

1. Moat, A. G., and Foster, J. W. (1987) in *Pyridine Nucleotide Coenzymes Part A* (Avramovic, D. D., and Poulson, R., eds) pp. 1–24, John Wiley & Sons, Inc., New York
2. Vertès, A. A., Qureshi, N., Blaschek, H. P., and Yukawa, H. (2010) *Biomass to Biofuels: Strategies for Global Industries*, pp. 1-22, John Wiley & Sons Ltd., Chichester, UK
3. Colin, V. L., Rodriguez, A., and Cristobal, H. A. (2011) The role of synthetic biology in the design of microbial cell factories for biofuel production. *J. Biomed. Biotechnol.* **2011**, 601834
4. Kaup, B., Bringer-Meyer, S., and Sahm, H. (2004) Metabolic engineering of *Escherichia coli*: construction of

an efficient biocatalyst for D-mannitol formation in a whole-cell biotransformation. *Appl. Microbiol. Biotechnol.* **64**, 333-339

5. Watanabe, S., Saleh, A. A., Pack, S. P., Annaluru, N., Kodaki, T., and Makino, K. (2007) Ethanol production from xylose by recombinant *Saccharomyces cerevisiae* expressing protein engineered $NADP^+$-dependent xylitol dehydrogenase. *J. Biotechnol.* **130**, 316-319
6. Galkin, A., Kulakova, L., Ohshima, T., Esaki, N., and Soda, K. (1997) Construction of a new leucine dehydrogenase with preferred specificity for $NADP^+$ by site-directed mutagenesis of the strictly NAD^+-specific enzyme. *Protein Eng.* **10**, 687-690
7. Petschacher, B., Leitgeb, S., Kavanagh, K. L., Wilson, D. K., and Nidetzky, B. (2005) The coenzyme specificity of *Candida tenuis* xylose reductase (AKR2B5) explored by site-directed mutagenesis and X-ray crystallography. *Biochem. J.* **385**, 75-83
8. Clermont, S., Corbier, C., Mely, Y., Gerard, D., Wonacott, A., and Branlant, G. (1993) Determinants of coenzyme specificity in glyceraldehyde-3-phosphate dehydrogenase: role of the acidic residue in the fingerprint region of the nucleotide binding fold. *Biochemistry* **32**, 10178-10184
9. Banta, S., Swanson, B. A., Wu, S., Jarnagin, A., and Anderson, S. (2002) Alteration of the specificity of the cofactor-binding pocket of *Corynebacterium* 2,5-diketo-D-gluconic acid reductase A. *Protein Eng.* **15**, 131-140
10. Holmberg, N., Ryde, U., and Bulow, L. (1999) Redesign of the coenzyme specificity in L-lactate dehydrogenase from *Bacillus stearothermophilus* using site-directed mutagenesis and media engineering. *Protein Eng.* **12**, 851-856
11. Yaoi, T., Miyazaki, K., Oshima, T., Komukai, Y., and Go, M. (1996) Conversion of the coenzyme specificity of isocitrate dehydrogenase by module replacement. *J. Biochem.* **119**, 1014-1018
12. Rane, M. J., and Calvo, K. C. (1997) Reversal of the nucleotide specificity of ketol acid reductoisomerase by site-directed mutagenesis identifies the NADPH binding site. *Arch. Biochem. Biophys.* **338**, 83-89
13. Shiraishi, N., Croy, C., Kaur, J., and Campbell, W. H. (1998) Engineering of pyridine nucleotide specificity of nitrate reductase: mutagenesis of recombinant cytochrome *b* reductase fragment of *Neurospora crassa* NADPH: nitrate reductase. *Arch. Biochem. Biophys.* **358**, 104-115
14. Eppink, M. H., Overkamp, K. M., Schreuder, H. A., and Van Berkel, W. J. (1999) Switch of coenzyme specificity of *p*-hydroxybenzoate hydroxylase. *J. Mol. Biol.* **292**, 87-96
15. Elmore, C. L., and Porter, T. D. (2002) Modification of the nucleotide cofactor-binding site of cytochrome P-450 reductase to enhance turnover with NADH *in vivo*. *J. Biol. Chem.* **277**, 48960-48964
16. Kristan, K., Stojan, J., Adamski, J., and Lanisnik-Rizner, T. (2007) Rational design of novel mutants of fungal 17 β-hydroxysteroid dehydrogenase. *J. Biotechnol.* **129**, 123-130

17. Dambe, T. R., Kuhn, A. M., Brossette, T., Giffhorn, F., and Scheidig, A. J. (2006) Crystal structure of NADP(H)-dependent 1,5-anhydro-D-fructose reductase from *Sinorhizobium morelense* at 2.2 Å resolution: construction of a NADH-accepting mutant and its application in rare sugar synthesis. *Biochemistry* **45**, 10030-10042

18. Medina, M., Luquita, A., Tejero, J., Hermoso, J., Mayoral, T., Sanz-Aparicio, J., Grever, K., and Gomez-Moreno, C. (2001) Probing the determinants of coenzyme specificity in ferredoxin-$NADP^+$ reductase by site-directed mutagenesis. *J. Biol. Chem.* **276**, 11902-11912

19. Chen, R., Greer, A., and Dean, A. M. (1995) A highly active decarboxylating dehydrogenase with rationally inverted coenzyme specificity. *Proc. Natl. Acad. Sci. U.S.A.* **92**, 11666-11670

20. Hoelsch, K., Suhrer, I., Heusel, M., and Weuster-Botz, D. (2013) Engineering of formate dehydrogenase: synergistic effect of mutations affecting cofactor specificity and chemical stability. *Appl. Microbiol. Biotechnol.* **97**, 2473-2481

21. Bernard, N., Johnsen, K., Holbrook, J. J., and Delcour, J. (1995) D175 discriminates between NADH and NADPH in the coenzyme binding site of *Lactobacillus delbrueckii* subsp. *bulgaricus* D-lactate dehydrogenase. *Biochem. Biophys. Res. Commun.* **208**, 895-900

22. Serov, A. E., Popova, A. S., Fedorchuk, V. V., and Tishkov, V. I. (2002) Engineering of coenzyme specificity of formate dehydrogenase from *Saccharomyces cerevisiae*. *Biochem. J.* **367**, 841-847

23. Capone, M., Scanlon, D., Griffin, J., and Engel, P. C. (2011) Re-engineering the discrimination between the oxidized coenzymes NAD^+ and $NADP^+$ in clostridial glutamate dehydrogenase and a thorough reappraisal of the coenzyme specificity of the wild-type enzyme. *FEBS J.* **278**, 2460-2468

24. Baroni, S., Pandini, V., Vanoni, M. A., and Aliverti, A. (2012) A single tyrosine hydroxyl group almost entirely controls the NADPH specificity of *Plasmodium falciparum* ferredoxin-$NADP^+$ reductase. *Biochemistry* **51**, 3819-3826

25. Lerchner, A., Jarasch, A., Meining, W., Schiefner, A., and Skerra, A. (2013) Crystallographic analysis and structure-guided engineering of NADPH-dependent *Ralstonia* sp. alcohol dehydrogenase toward NADH cosubstrate specificity. *Biotechnol. Bioeng.* **110**, 2803-2814

26. Scrutton, N. S., Berry, A., and Perham, R. N. (1990) Redesign of the coenzyme specificity of a dehydrogenase by protein engineering. *Nature* **343**, 38-43

27. Marohnic, C. C., Bewley, M. C., and Barber, M. J. (2003) Engineering and characterization of a NADPH-utilizing cytochrome b_5 reductase. *Biochemistry* **42**, 11170-11182

28. Zhang, L., Ahvazi, B., Szittner, R., Vrielink, A., and Meighen, E. (1999) Change of nucleotide specificity and enhancement of catalytic efficiency in single point mutants of *Vibrio harveyi* aldehyde dehydrogenase.

Biochemistry **38**, 11440-11447

29. Hsieh, J. Y., Liu, G. Y., Chang, G. G., and Hung, H. C. (2006) Determinants of the dual cofactor specificity and substrate cooperativity of the human mitochondrial $NAD(P)^+$-dependent malic enzyme: functional roles of glutamine 362. *J. Biol. Chem.* **281**, 23237-23245
30. Miller, S. P., Lunzer, M., and Dean, A. M. (2006) Direct demonstration of an adaptive constraint. *Science* **314**, 458-461
31. Tomita, T., Fushinobu, S., Kuzuyama, T., and Nishiyama, M. (2006) Structural basis for the alteration of coenzyme specificity in a malate dehydrogenase mutant. *Biochem. Biophys. Res. Commun.* **347**, 502-508
32. Watanabe, S., Kodaki, T., and Makino, K. (2005) Complete reversal of coenzyme specificity of xylitol dehydrogenase and increase of thermostability by the introduction of structural zinc. *J. Biol. Chem.* **280**, 10340-10349
33. Ehrensberger, A. H., Elling, R. A., and Wilson, D. K. (2006) Structure-guided engineering of xylitol dehydrogenase cosubstrate specificity. *Structure* **14**, 567-575
34. Chen, R., Greer, A., and Dean, A. M. (1996) Redesigning secondary structure to invert coenzyme specificity in isopropylmalate dehydrogenase. *Proc. Natl. Acad. Sci. U.S.A.* **93**, 12171-12176
35. Zheng, H., Bertwistle, D., Sanders, D. A., and Palmer, D. R. (2013) Converting NAD-specific inositol dehydrogenase to an efficient NADP-selective catalyst, with a surprising twist. *Biochemistry* **52**, 5876-5883
36. Brinkmann-Chen, S., Flock, T., Cahn, J. K., Snow, C. D., Brustad, E. M., McIntosh, J. A., Meinhold, P., Zhang, L., and Arnold, F. H. (2013) General approach to reversing ketol-acid reductoisomerase cofactor dependence from NADPH to NADH. *Proc. Natl. Acad. Sci. U.S.A.* **110**, 10946-10951
37. Kavanagh, K. L., Jornvall, H., Persson, B., and Oppermann, U. (2008) Medium- and short-chain dehydrogenase/reductase gene and protein families: the SDR superfamily: functional and structural diversity within a family of metabolic and regulatory enzymes. *Cell. Mol. Life Sci.* **65**, 3895-3906
38. Wu, C. H., Apweiler, R., Bairoch, A., Natale, D. A., Barker, W. C., Boeckmann, B., Ferro, S., Gasteiger, E., Huang, H., Lopez, R., Magrane, M., Martin, M. J., Mazumder, R., O'Donovan, C., Redaschi, N., and Suzek, B. (2006) The Universal Protein Resource (UniProt): an expanding universe of protein information. *Nucleic Acids Res.* **34**, D187-191
39. Persson, B., and Kallberg, Y. (2013) Classification and nomenclature of the superfamily of short-chain dehydrogenases/reductases (SDRs). *Chem. Biol. Interact.* **202**, 111-115
40. Berman, H. M., Westbrook, J., Feng, Z., Gilliland, G., Bhat, T. N., Weissig, H., Shindyalov, I. N., and Bourne, P. E. (2000) The Protein Data Bank. *Nucleic Acids Res.* **28**, 235-242
41. Proctor, M. R., Taylor, E. J., Nurizzo, D., Turkenburg, J. P., Lloyd, R. M., Vardakou, M., Davies, G. J., and

Gilbert, H. J. (2005) Tailored catalysts for plant cell-wall degradation: redesigning the exo/endo preference of *Cellvibrio japonicus* arabinanase 43A. *Proc. Natl. Acad. Sci. U.S.A.* **102**, 2697-2702

42. Ochiai, A., Itoh, T., Mikami, B., Hashimoto, W., and Murata, K. (2009) Structural determinants responsible for substrate recognition and mode of action in family 11 polysaccharide lyases. *J. Biol. Chem.* **284**, 10181-10189
43. Gacesa, P. (1988) Alginates. *Carbohydr. polym.* **8**, 161-182
44. Stokstad, E. (2012) Biofuels. Engineered superbugs boost hopes of turning seaweed into fuel. *Science* **335**, 273
45. Hisano, T., Kimura, N., Hashimoto, W., and Murata, K. (1996) Pit structure on bacterial cell surface. *Biochem. Biophys. Res. Commun.* **220**, 979-982
46. Momma, K., Okamoto, M., Mishima, Y., Mori, S., Hashimoto, W., and Murata, K. (2000) A novel bacterial ATP-binding cassette transporter system that allows uptake of macromolecules. *J. Bacteriol.* **182**, 3998-4004
47. Yoon, H.-J., Hashimoto, W., Miyake, O., Okamoto, M., Mikami, B., and Murata, K. (2000) Overexpression in *Escherichia coli*, purification, and characterization of *Sphingomonas* sp. A1 alginate lyases. *Protein Expr. Purif.* **19**, 84-90
48. Hashimoto, W., Miyake, O., Momma, K., Kawai, S., and Murata, K. (2000) Molecular identification of oligoalginate lyase of *Sphingomonas* sp. strain A1 as one of the enzymes required for complete depolymerization of alginate. *J. Bacteriol.* **182**, 4572-4577

CHAPTER I

α-Keto acid (DEH) reductase prerequisite for alginate metabolism in *Sphingomonas* sp. strain A1

Alginate is composed of two uronic acids, β-D-mannuronic acid and α-L-guluronic acid (1). *Sphingomonas* sp. strain A1 assimilates alginate in a characteristic manner. Strain A1 forms a pit-like structure on the cell surface to concentrate alginate and directly incorporates the macromolecule alginate into the cytoplasm by periplasmic binding proteins-dependent ABC transporter. The mechanism and components involved in the molecular machinery called a super channel are described previously (2). The incorporated alginate is then depolymerized into

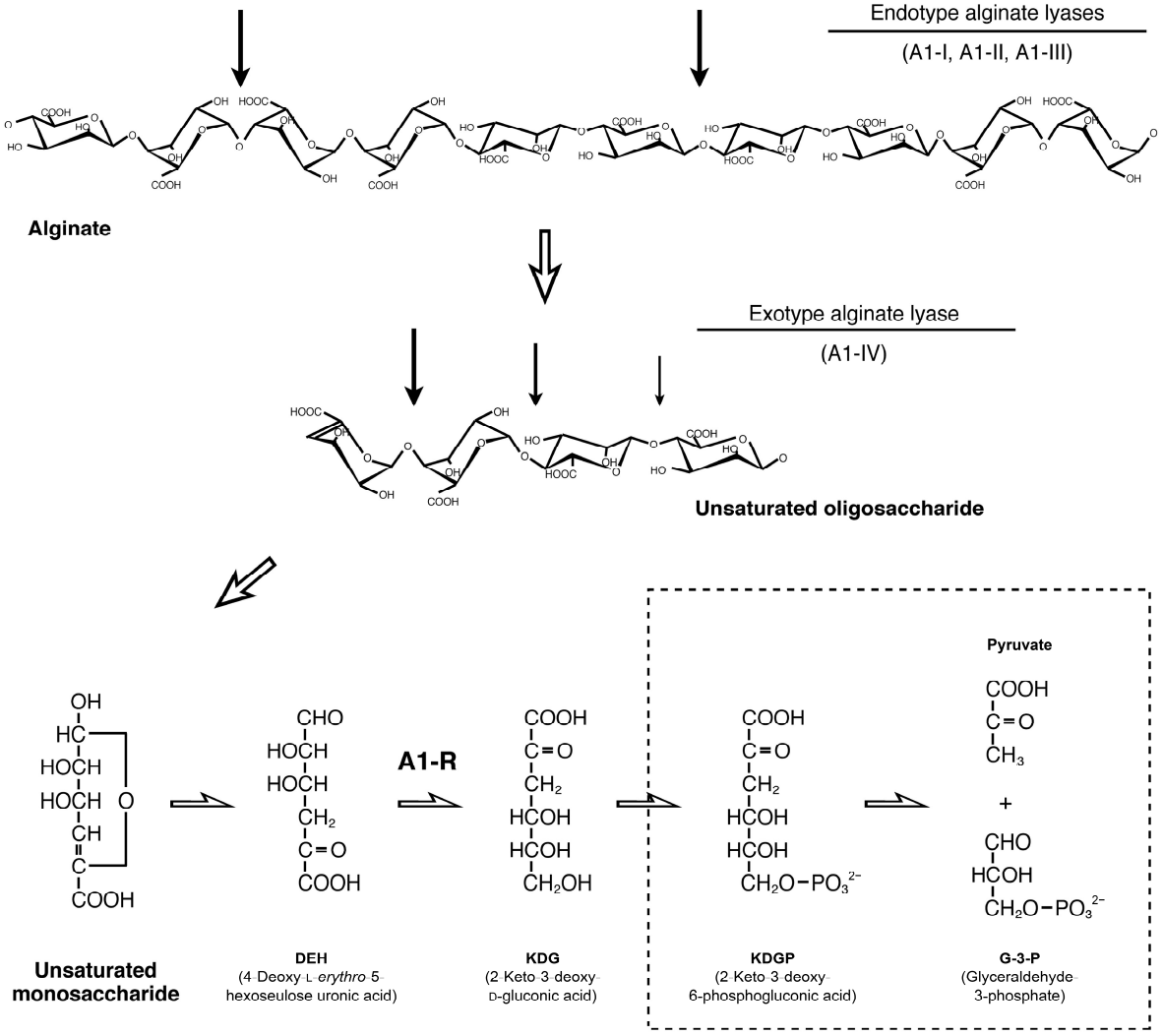

Fig. 1-1. Alginate metabolic pathway in strain A1. The thick arrows indicate the cleavage sites of each alginate lyase against the substrate. Hypothetical pathways are shown in the dotted frame.

disaccharides, trisaccharides, and tetrasaccharides through the action of three cytoplasmic endotype alginate lyases A1-I, -II, and -III (3). The oligosaccharides thus formed are finally degraded by a cytoplasmic exotype alginate lyase, A1-IV, into monosaccharides, which are then nonenzymatically converted to 4-deoxy-L-*erythro*-5-hexoseulose uronic acid (DEH) (4) (Fig. 1-1).

The α-keto acid, DEH, has been shown to be converted to 2-keto-3-deoxy-D-gluconic acid (KDG) by a certain reductase (5). However, the genetic, enzymatic, and structural features of this reductase remain to be clarified. This CHAPTER deals with molecular identification, characterization, and structural determination of a strain A1 DEH-specific reductase, A1-R.

Materials and Methods

Materials. Sodium alginate (viscosity of 1% (w/v) solution; 1000 cP) from *Eisenia bicyclis* and Hydroxylapatite were purchased from Nacalai Tesque. Silica gel 60/Kieselguhr F_{254} thin-layer chromatography (TLC) plates were obtained from Merck. TOYOPEARL DEAE-650 M, TOYOPEARL Butyl-650 M, and TOYOPEARL Butyl-650 S were from Tosoh. HiLoad 26/10 Q-Sepharose HP, HiLoad 16/60 Superdex 75 pg, HiLoad 16/60 Superdex 200 pg, and Mono Q HR 5/5 were from GE Healthcare. Restriction endonucleases and PCR-related enzymes were from Toyobo. Other analytical grade chemicals were obtained from commercial sources.

Microorganisms and Culture Conditions. Strain A1 cells were routinely cultured at 30 °C in minimal medium containing 0.5% (w/v) sodium alginate, 0.1% (w/v) $(NH_4)_2SO_4$, 0.1% (w/v) KH_2PO_4, 0.1% (w/v) Na_2HPO_4, 0.01% (w/v) yeast extract, and 0.01% (w/v) $MgSO_4 \cdot 7H_2O$. The cells were also aerobically cultured at 30 °C in minimal medium containing 0.5% (w/v) pectin, D-glucuronic acid, or glucose as the sole carbon source instead of sodium alginate. As a host for plasmid amplification, *Escherichia coli* strain DH5α (Toyobo) was routinely cultured at 37 °C in LB medium (1% (w/v) tryptone, 0.5% (w/v) yeast extract, and 1% (w/v) NaCl) (pH 7.2) containing sodium ampicillin (100 μg ml^{-1}). *E. coli* strain BL21(DE3) (Novagen) was used as a host for the overexpression of A1-R. For the expression of A1-R, *E. coli* cells were aerobically cultured at 30 °C in LB medium supplemented with sodium ampicillin (100 μg ml^{-1}). When the turbidity at 600 nm reached 0.6, isopropyl-β-D-thiogalactopyranoside was added to the culture at a final concentration of 0.4 mM, and the cells were further cultured at 16 °C for 42 h.

Enzymatic and Protein Assays. The DEH reducing activity of A1-R was assayed at 30 °C for 5 min in a reaction mixture (0.5 ml) consisting of 1 mM DEH, 0.2 mM NADPH, and 50 mM potassium phosphate buffer (KPB) (pH 7.0). The activity was determined by continuously

monitoring the decrease in absorbance at 340 nm, which corresponds to the oxidation of NADPH. One unit of enzymatic activity was defined as the amount of enzyme required to produce 1 μmol of reduced product per min at 30 °C. The protein content was determined according to the procedure of Bradford (6), with bovine serum albumin as the standard. The kinetic parameters (k_{cat} and K_m) for A1-R were calculated by using the Michaelis-Menten equation with the KaleidaGraph program (Synergy Software).

Purification of A1-R from Strain A1 Cells. A1-R was purified from strain A1 cells as follows. Unless otherwise specified, all procedures were performed at 4 °C. Cells were grown in 1.5 liters of alginate minimal medium (1.5 liters per flask), collected by centrifugation (6,000 × *g*, 5 min), and resuspended in 20 mM Tris-HCl (pH 7.5). Strain A1 cells were ultrasonically disrupted (Insonator Model 201 M; Kubota) at 9 kHz for 20 min, and the clear solution obtained on centrifugation (20,000 × *g*, 20 min) was used as the cell extract. The extract was applied to a TOYOPEARL DEAE-650 M column (2.5 × 10 cm) previously equilibrated with 20 mM Tris-HCl (pH 7.5). The absorbed proteins were eluted with a linear gradient of NaCl (0–500 mM, 200 ml) in 20 mM Tris-HCl (pH 7.5), with a 1-ml fraction collected every minute. The A1-R active fractions, eluted with 100–200 mM NaCl, were combined and dialyzed for 3 h against 20 mM Tris-HCl (pH 7.5). The dialysate was applied to a HiLoad 26/10 Q-Sepharose HP column (2.6 × 10 cm) previously equilibrated with 20 mM Tris-HCl (pH 7.5). These absorbed proteins were eluted with a linear gradient of NaCl (0–1 M, 250 ml) in 20 mM Tris-HCl (pH 7.5), with a 3-ml fraction collected every 0.5 min. The active fractions, eluted with 200–250 mM NaCl, were combined and applied to a HiLoad 16/60 Superdex 200 pg column (1.6 × 60 cm) previously equilibrated with 20 mM Tris-HCl (pH 7.5) containing 0.15 M NaCl. A1-R was eluted with the same buffer (120 ml) with a 2-ml fraction collected every 2 min, and the active fractions were combined and dialyzed for 3 h against 5 mM KPB (pH 7.0). The dialysate was applied to a Hydroxylapatite column (1 × 1.5 cm) previously equilibrated with 5 mM KPB (pH 7.0). The absorbed proteins were eluted with a linear gradient of KPB (5–500 mM, 20 ml), with a 1-ml fraction collected every minute. The active fractions obtained on elution with 50–100 mM KPB were combined and saturated with $(NH_4)_2SO_4$ (30%). The enzyme solution was then applied to a TOYOPEARL Butyl-650 S column (1 × 1.5 cm) previously equilibrated with 20 mM Tris-HCl (pH 7.5), containing 30% saturated $(NH_4)_2SO_4$. The absorbed proteins were eluted with a linear gradient of saturated $(NH_4)_2SO_4$ (30–0%, 20 ml), with a 1-ml fraction collected every minute. The active fractions, eluted with 20–10% saturated $(NH_4)_2SO_4$, were combined and applied to a HiLoad 16/60 Superdex 75 pg column (1.6 × 60 cm) previously

equilibrated with 20 mM Tris-HCl (pH 7.5) containing 0.15 M NaCl. A1-R was eluted with the same buffer (120 ml), with a 1-ml fraction collected every minute, and the active fractions were combined and dialyzed for 3 h against 20 mM Tris-HCl (pH 7.5). The dialysate was applied to a Mono Q HR 5/5 column (0.5 × 5 cm) previously equilibrated with 20 mM Tris-HCl (pH 7.5). The absorbed proteins were eluted with a linear gradient of NaCl (0–300 mM, 30 ml) in 20 mM Tris-HCl (pH 7.5), with a 1-ml fraction collected every minute. The active fractions obtained on elution with 200–250 mM NaCl were combined and dialyzed at 4 °C overnight against 20 mM Tris-HCl (pH 7.5). This dialysate was used as the native A1-R (nA1-R).

Liquid Chromatography/tandem Mass Spectrometry (LC-MS/MS). Protein identification by MS was performed as described elsewhere (7). Briefly, A1-R resolved on sodium dodecyl sulfate-polyacrylamide gel electrophoresis (SDS-PAGE) was excised and digested with trypsin at 37 °C overnight. The generated peptides were investigated by determining the molecular masses by LC-MS/MS analysis. Paradigm MS-4 (Michrom Bioresources) with reversed-phase column chromatography (Magic C18, Michrom Bioresources) was used for the LC analysis. The sample was injected into the column at a flow rate of 1 μl min^{-1} for mobile phase buffer A. The chromatography was developed with a 50-min linear gradient from 5% to 65% for buffer B. Buffer A consists of 2% (v/v) acetonitrile, 0.1% (v/v) formic acid, and 0.1% (v/v) trifluoroacetic acid, and buffer B comprises 90% (v/v) acetonitrile, 0.1% (v/v) formic acid, and 0.1% (v/v) trifluoroacetic acid. Subsequent MS/MS was performed using a LCQ Advantage (Thermo Finnigan) in positive mode with a capillary voltage of 2 kV. For protein identification, the experimentally obtained masses were compared with the theoretical peptide masses, derived from proteins loaded in the strain A1 genome database (8). The Mascot system (9) was used for the MS/MS ion search.

Construction of Plasmid for Overexpression of A1-R and DNA Sequencing. The overexpression system for A1-R was constructed in *E. coli* cells as follows. To clone the A1-R gene, PCR was performed in a reaction mixture (100 μl) containing 5 units of KOD polymerase (Toyobo), 0.25 μg of strain A1 genomic DNA, 40 pmol each of forward primer (A1-R_NdeI) and reverse primer (A1-R_BamHI), 20 nmol of dNTPs, 100 nmol of $MgCl_2$, 5 μl of dimethyl sulfoxide, and KOD buffer (Toyobo). The forward and reverse primers with *Nde*I and *Bam*HI sites (double underlined) added to each of their 5′-regions were used for the A1-R gene amplification (Table 1-1).

Table 1-1
Primers for cloning and site-directed mutagenesis

Primer		Oligonucleotides
A1-R_NdeI	forward	5′- GGCATATGTTCCCAGACCTCAAAGGCAAGC -3′
A1-R_BamHI	reverse	5′- CCGGATCCTCAGTGCTTGTACTGCCCGCC -3′
S150A	sense	5′- GTGATCAGCACCGGGGCGATCGCTGGCCAC -3′
	antisense	5′- GTGGCCAGCGATCGCCCCGGTGCTGATCAC -3′
Y164F	sense	5′- CCGGCGCAGGTCTGTTTGGCGCAGCCAAGG -3′
	antisense	5′- CCTTGGCTGCGCCAAACAGACCTGCGCCGG -3′
K168A	sense	5′- GGTCTGTATGGCGCAGCCGCGGCTTTCCTGCACAACG -3′
	antisense	5′- CGTTGTGCAGGAAAGCCGCGGCTGCGCCATACAGACC -3′
G38D	sense	5′- CCAAGGTCGGCCTGCACGATCGCAAGGCACCCGCC -3′
	antisense	5′- GGCGGGTGCCTTGCGATCGTGCAGGCCGACCTTGG -3′
R39I	sense	5′- GGTCGGCCTGCACGGCATCAAGGCACCCGCCAAC -3′
	antisense	5′- GTTGGCGGGTGCCTTGATGCCGTGCAGGCCGACC -3′
R39V	sense	5′- GGTCGGCCTGCACGGCGTCAAGGCACCCGCCAAC -3′
	antisense	5′- GTTGGCGGGTGCCTTGACGCCGTGCAGGCCGACC -3′
R39W	sense	5′- GGTCGGCCTGCACGGCTGGAAGGCACCCGCCAAC -3′
	antisense	5′- GTTGGCGGGTGCCTTCCAGCCGTGCAGGCCGACC -3′
A41E	sense	5′- CGGCCGCAAGGAACCCGCCAACATCG -3′
	antisense	5′- CGATGTTGGCGGGTTCCTTGCGGCCG -3′
S16Y	sense	5′- GCGTTCTGATCACCGGTTCGTATCAGGGCATTGGC -3′
	antisense	5′- GCCAATGCCCTGATACGAACCGGTGATCAGAACGC -3′
G38E	sense	5′- CCAAGGTCGGCCTGCACGAACGCAAGGCACCCGCC -3′
	antisense	5′- GGCGGGTGCCTTGCGTTCGTGCAGGCCGACCTTGG -3′
R39D	sense	5′- GGTCGGCCTGCACGGCGATAAGGCACCCGCCAAC -3′
	antisense	5′- GTTGGCGGGTGCCTTATCGCCGTGCAGGCCGACC -3′
G38D/R39D	sense	5′- GGTCGGCCTGCACGATGATAAGGCACCCGCCAACATCG -3′
	antisense	5′- CGATGTTGGCGGGTGCCTTATCATCGTGCAGGCCGACC -3′
R39D/K40D	sense	5′- GGTCGGCCTGCACGGCGATGATGCACCCGCCAACATCG -3′
	antisense	5′- CGATGTTGGCGGGTGCATCATCGCCGTGCAGGCCGACC -3′
K40D/A41D	sense	5′- CGGCCTGCACGGCCGCGATGATCCCGCCAACATCGATG -3′
	antisense	5′- CATCGATGTTGGCGGGATCATCGCGGCCGTGCAGGCCG -3′
G38D/R39E/K40E	forward	5′- GAAGAAGCACCCGCCAACATCGATGAGACCA -3′
	reverse	5′- ATCGTGCAGGCCGACCTTGGCGCCT -3′

Double and solid underlines show identical sequence used in restriction site and mutation site, respectively.

The PCR conditions were as follows: 94 °C for 30 s, 60 °C for 2 s, and 74 °C for 40 s, for a total of 30 cycles. The PCR products were separated by agarose gel electrophoresis, and the DNA fragment corresponding to the A1-R gene was isolated with a MinElute gel extraction kit (Qiagen). The fragment was ligated with *Hin*cII-digested pUC119 (Takara Bio), and the resulting plasmid was digested with *Nde*I and *Bam*HI for isolating the A1-R gene. The *Nde*I-*Bam*HI fragment containing the A1-R gene was then ligated with *Nde*I- and *Bam*HI-digested pET21b (Novagen), yielding pET21b/A1-R. The cloned fragment included the complete sequence of the A1-R gene with the original start and stop codons. Thus, the encoded polypeptide (recombinant A1-R) was not fused to the His-tag encoded by the vector. The nucleotide sequence of the A1-R gene amplified by PCR

was determined by dideoxy chain termination using an automated DNA sequencer (Model 377; Applied Biosystems) (10).

Purification of Recombinant A1-R from E. coli Cells. Unless otherwise specified, all procedures were performed at 4 °C. *E. coli* strain BL21(DE3) cells harboring pET21b/A1-R were grown at 30 °C in 6 liters of LB medium (1.5 liters per flask), collected by centrifugation (6,000 × *g*, 5 min), and resuspended in 20 mM Tris-HCl (pH 7.5). The cells were ultrasonically disrupted at 9 kHz for 20 min, and the clear solution obtained on centrifugation (20,000 × *g*, 20 min) was used as the cell extract. The extract was applied to a TOYOPEARL DEAE-650 M column (5.5 × 20 cm) previously equilibrated with 20 mM Tris-HCl (pH 7.5). The absorbed proteins were eluted with a linear gradient of NaCl (0–700 mM, 1 liter) in 20 mM Tris-HCl (pH 7.5), with a 1-ml fraction collected every minute. The active fractions, eluted with 100–200 mM NaCl, were combined and saturated with $(NH_4)_2SO_4$ (30%). The enzyme solution was applied to a TOYOPEARL Butyl-650 M column (2.5 × 15 cm) previously equilibrated with 20 mM Tris-HCl (pH 7.5) containing 30% saturated $(NH_4)_2SO_4$. The absorbed proteins were eluted with a linear gradient of saturated $(NH_4)_2SO_4$ (30–0%, 200 ml), with a 1-ml fraction collected every minute. The active fractions, eluted with 20–10% saturated $(NH_4)_2SO_4$, were combined and dialyzed overnight at 4 °C against 20 mM Tris-HCl (pH 7.5). This dialysate was used as the purified recombinant A1-R (rA1-R).

Electrospray Ionization (ESI)-MS and Nuclear Magnetic Resonance (NMR) Spectrometry. Structural determination of the reaction product by rA1-R was carried out as follows. The product was prepared from the reaction mixture of rA1-R and substrate, and purified by gel filtration using Bio-Gel P-2 (Bio-Rad) and normal-phase column chromatography using COSMOSIL HILIC (Nacalai Tesque). The LaChrom Elite system (Hitachi), provided with an L-2100 pump (Hitachi), L-2400 UV detector (Hitachi), ERC-3415α on-line degasser (ERC), and SmartChrom chromatographic manager (KYA Technologies) were used for HPLC analysis. The normal-phase column chromatography was developed at a flow rate of 1 ml min^{-1} with an isocratic mobile phase consisting of 30% (v/v) acetonitrile and 14 mM NH_4HCO_3/acetic acid (pH 7.0). ESI-MS and NMR spectrometry were carried out for subsequent structural analyses of the purified reaction product. The mass spectrometer using LCT Premier XE (Waters) was operated in the negative mode with a cone voltage of −50 V. During the analysis, the mass spectrum was scanned from 100 to 400 $m\,z^{-1}$. For NMR analysis using an Inova500 (Varian), the purified product was lyophilized and dissolved in deuterium oxide. ^{1}H NMR and COSY spectra were monitored at a probe temperature of 25 °C with the solvent deuterium signal as an internal reference.

Site-directed Mutagenesis. To investigate the role of amino acid residues in A1-R, the enzyme mutants, except for a triple mutant G38D/R39E/K40E, were constructed using a QuikChange site-directed mutagenesis kit (Stratagene). The mutant G38D/R39E/K40E was constructed by using a KOD-Plus-Mutagenesis Kit (Toyobo), through an inverse PCR method. The plasmid pET21b/A1-R was used as a PCR template and oligonucleotides listed in Table 1-1 as primers. Mutations were confirmed by DNA sequencing with an automated DNA sequencer, as described earlier. Expression and purification of the mutants were performed using the same procedure as for the wild-type rA1-R from *E. coli*.

Crystallization and Structure Determination. The purified rA1-R was concentrated by ultrafiltration with a Centriprep centrifugal filter (Millipore). Commercial screening kits (Hampton Research, Emerald BioSystems, and Jena Bioscience) were used to search for the crystallization conditions of rA1-R. The enzyme was crystallized by sitting-drop vapor diffusion on a 96-well Intelli-Plate (Veritas). The reservoir solution volume in each well was 100 μl, and the droplet was prepared by mixing 1 μl of the protein solution with 1 μl of the reservoir solution. A crystal of A1-R in complex with $NADP^+$ (A1-R·$NADP^+$) was prepared in the solution containing $NADP^+$ by cocrystallization. Each crystal of A1-R and A1-R·$NADP^+$ on nylon loop was placed directly in a cold nitrogen gas stream at −173 °C. X-ray diffraction images of the crystal were collected at −173 °C under the nitrogen gas stream with a Jupiter 210 CCD detector and synchrotron radiation of wavelength 1.0000 Å at the BL-38B1 station of SPring-8 (Hyogo, Japan). The distance between the crystal and detector was set to 150 mm, and 1° oscillation images were recorded with an exposure time of 4 s. Diffraction data were processed, merged, and scaled using the HKL2000 program package (DENZO and SCALEPACK) (11). The structure of A1-R was determined by molecular replacement with the MOLREP program (12), supplied in the CCP4 program package (13) using coordinates of *Caenorhabditis elegans* glucose dehydrogenase (PDB-ID, 1SPX) as an initial model. In the case of A1-R·$NADP^+$, molecular replacement was conducted using A1-R as an initial model. Structure refinement was conducted with the Refmac5 program (14). Randomly selected 5% reflections were excluded from refinement and used to calculate R_{free}. After each refinement cycle, the model was adjusted manually using the Coot program (15). Water molecules were incorporated where the difference in density exceeded 3.0σ above the mean and the 2 $F_o - F_c$ map showed a density of over 1.0σ. Final model quality was checked with the PROCHECK program (16). Protein models were superimposed and their root mean square deviation (r.m.s.d.) was determined with the LSQKAB program (17), part of CCP4. Figures for the protein structure

were prepared using the PyMOL program (18). Coordinates used in this CHAPTER were obtained from the Protein Data Bank (PDB) (www.wwpdb.org/) (19).

Analytical Methods. SDS-PAGE was performed on a 12.5% polyacrylamide gel, as previously described (20). Proteins in the gel were visualized by Coomassie Brilliant Blue R-250. DEH derived from alginate was prepared by digesting sodium alginate with two purified exotype alginate lyases, namely, A1-IV (4,21) and Atu3025 (22), and then purified using an Amicon Ultra-4 centrifugal filter (Millipore) and Bio-Gel P-2. The purified DEH was confirmed to be almost homogeneous by TLC. The molecular mass of nA1-R was estimated by native-PAGE. Native-PAGE was performed with a Native-PAGE Novex Bis-Tris gel system (Invitrogen), following the manufacturer's instructions. The products derived from DEH incubated with the strain A1 cell extract were separated by TLC using a solvent system consisting of 1-butanol, acetic acid, and water (3:2:2, v/v/v), and visualized by heating the TLC plate at 130 °C for 5 min after spraying it with 10% (v/v) sulfuric acid in ethanol. Standard alginate disaccharides, with a molecular weight of 352, and trisaccharides, with a molecular weight of 528, were prepared by Bio-Gel P-2 column chromatography, as described previously (23).

Results

DEH Reductase Activity in Strain A1 Cells

Extracts prepared from strain A1 cells grown on alginate were incubated with DEH in the presence or absence of various coenzymes. Reaction products were formed only in the presence of NADPH (Fig. 1-2 A), indicating that an NADPH-dependent reductase, designated as A1-R, was responsible for the DEH metabolism. The expression level of A1-R was examined in strain A1 cells grown on various carbon sources. A1-R activity was detected in the cells grown on all carbon sources tested, but the highest activity was found in the presence of alginate (Table 1-2).

Table 1-2
A1-R activity in strain A1 cells grown on different carbon sources

Carbon source	Growth (OD_{600})[a]	Specific activity (units mg^{-1})
Alginate	0.74	2.9
Pectin	0.71	0.023
Glucuronic acid	0.59	0.57
Glucose	0.54	0.26

All cells were cultured until late log phase.

[a] Optical density at 600 nm.

Enzymatic Properties of nA1-R

nA1-R was purified 143-fold from strain A1 cells grown on alginate through seven steps of column chromatography, with a recovery of 1.51% (Table 1-3). The purified enzyme was homogeneous on SDS-PAGE analysis (Fig. 1-2 B, left). The properties were as follows:

(i) Molecular mass

The molecular mass of nA1-R was estimated to be 27 kDa through SDS-PAGE analysis (Fig. 1-2 B, left). Native-PAGE analysis indicated nA1-R was about 130 kDa (Fig. 1-2 C), suggesting that, as is the case with the homologous protein (24), nA1-R may be active in a tetrameric form. This is also supported by crystal structure of the enzyme as described below.

(ii) Optimal pH and temperature

nA1-R was the most active at pH 6.5–7.5 (KPB) and 50 °C, and stable below at 50 °C (Fig. 1-2 D). Replacement of KPB (pH 7.5) with Tris-HCl (pH 7.5) inhibited the activity (10–40%) of the enzyme (data not shown).

(iii) Chemicals

The reaction was conducted at 30 °C in the presence or absence of different compounds, and the residual activity was assayed (Table 1-4). About 65% of the enzymatic activity was lost in the presence of Hg^{2+} at 0.04 mM. Co^{2+} at 1 mM enhanced the enzymatic activity to 153%. Thiol reagents (dithiothreitol, glutathione (reduced form), 2-mercaptoethanol, iodoacetic acid, *p*-chloromercuribenzoic acid (1 mM)), a chelator of EDTA (1 mM), and sugars (L-fucose, D-galactose, D-glucose, D-glucuronic acid, D-mannose, L-rhamnose, D-xylose, D-sucrose, D-galacturonic acid, 2-deoxy glucose, D-glucosamine, (5 mM)) had no effect (94–112%) on the reaction of nA1-R (Table 1-4). Various ketones (4-methyl-2-pentanone, 2,5-hexanedione, 3-chloropropiophenone), aldehydes (benzaldehyde, 4-methoxybenzaldehyde, *trans*-cinnamaldehyde), keto esters (ethyl pyruvate, ethyl benzoylacetate), and α-keto acid (sodium phenylpyruvate) were not utilized as substrates (data not shown). Thus, nA1-R was almost specific for NADPH and DEH.

(iv) Kinetic parameters

k_{cat} and K_m of nA1-R were 274 s^{-1} and 101 μM towards DEH and 241 s^{-1} and 9.0 μM towards NADPH. nA1-R was considered specific for NADPH rather than NADH since the enzyme activity in the presence of NADPH was 50-fold higher than that in the presence of NADH (Table 1-4).

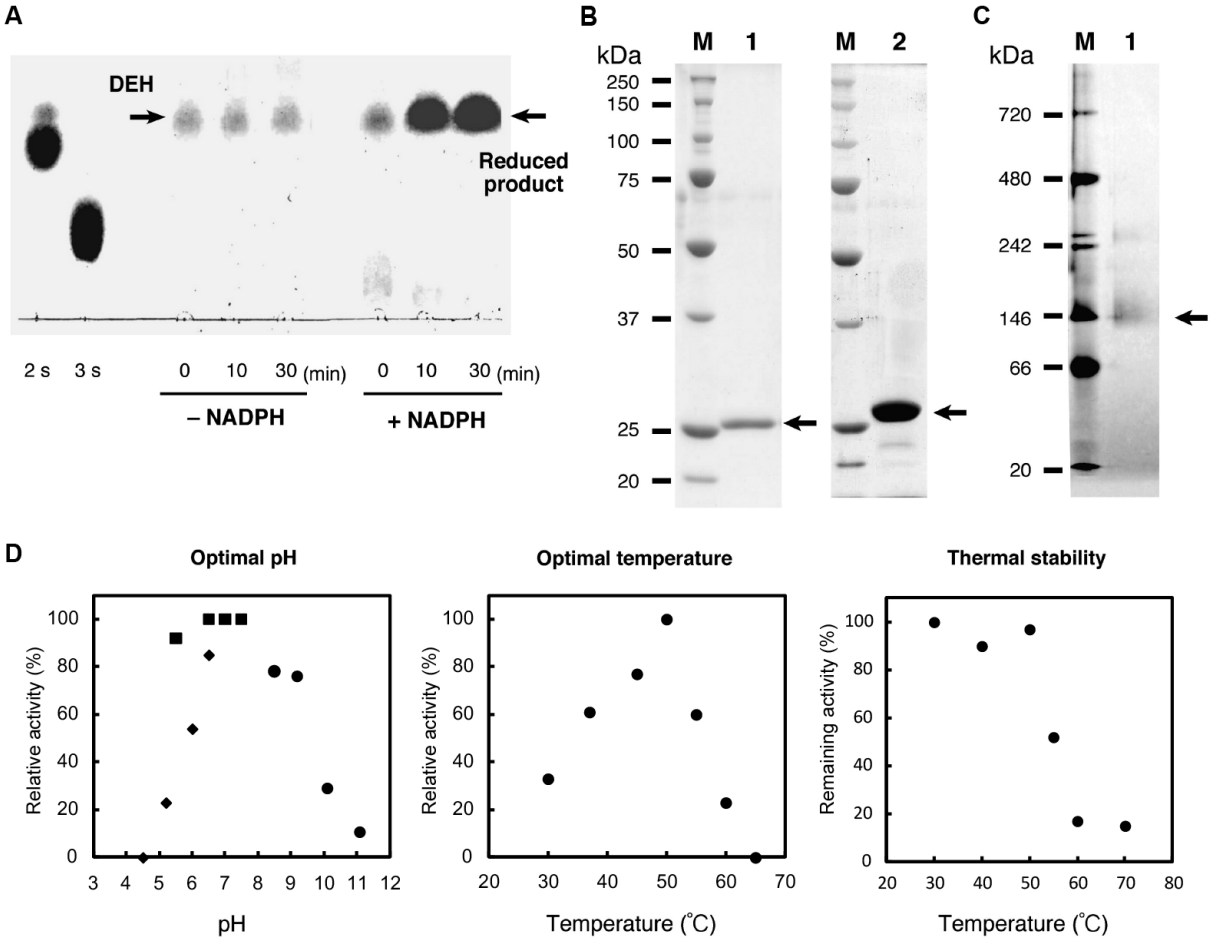

Fig. 1-2. Properties of nA1-R. (A) DEH reducing activity in the strain A1 cell extract. The reaction was performed at 30 °C in a reaction mixture consisting of 5 mg ml^{-1} DEH, 50 mM Tris-HCl (pH 7.5), 1 mM NADPH, and the appropriate amount of strain A1 cell extract. The reaction products were periodically sampled and analyzed on TLC plates, followed by staining with sulfuric acid. Alginate disaccharide (2 s) and trisaccharide (3 s) were used for marker control. (B) SDS-PAGE of purified A1-R followed by protein staining with Coomassie Brilliant Blue R-250. Lane M, molecular weight standards; lane 1, purified nA1-R from strain A1 cells (1 μg of protein); lane 2, purified rA1-R from *E. coli* cells (5 μg of protein). The arrow indicates the position of the enzyme. (C) Native-PAGE of purified nA1-R followed by protein staining with Coomassie Brilliant Blue R-250. Lane M, molecular weight standards; lane 1, nA1-R from strain A1 cells (5 μg of protein). The arrow indicates the position of the enzyme. (D) Effects of pH and temperature on the activity and stability of nA1-R. Left, optimal pH. Activity was assayed with sodium acetate (pH 4.5, 5.2, 6.0, and 6.5), KPB (pH 5.5, 6.5, 7.0, and 7.5), and glycine–NaOH (pH 8.5, 9.0, 10.0, and 11.0). Activity at pH 6.5–7.5 in KPB was taken as 100%. Center, optimal temperature. Activity at 50 °C was taken as 100%. Right, thermal stability. The purified enzyme was preincubated for 5 min at various temperatures (as indicated) and the residual enzyme activity was measured. The activity of the enzyme preincubated at 4 °C for 5 min was taken as 100%.

Table 1-3
Purification of nA1-R and rA1-R

Step	Total protein (mg)	Total activity (units)	Specific activity (units mg^{-1})	Yield (%)	Purification (fold)
nA1-R					
Cell extract	284	468	1.65	100	1.00
TOYOPEARL DEAE-650 M	52.8	243	4.60	51.9	2.79
Q-Sepharose HP	26.7	144	5.39	30.8	3.25
Superdex 200 pg	2.37	36.7	15.5	7.84	9.39
Hydroxylapatite	0.85	32.8	38.6	7.01	23.4
TOYOPEARL Butyl-650 S	0.067	10.9	163	2.33	98.8
Superdex 75 pg	0.050	8.36	167	1.79	101
Mono Q HR	0.030	7.07	236	1.51	143
rA1-R					
Cell extract	2672	60.4	22.6	100	1.00
TOYOPEARL DEAE-650 M	711	35.5	49.9	58.7	2.21
TOYOPEARL Butyl-650 M	492	28.0	56.9	46.3	2.52

Molecular Identification of A1-R

The purified nA1-R was subjected to peptide mass fingerprinting. After excision from the SDS-PAGE gel, the enzyme was digested with trypsin, and the resulting peptide fragments were used for subsequent LC-MS/MS and MS/MS ion search in the strain A1 genome database. The molecular masses of most fragments completely matched those of the partial amino acid sequence of SPH3227, with sequence coverage of 47% (Fig. 1-3). SPH3227 is categorized into the

```
  1  MFPDLKGKRV LITGSSQGIG LATARLFARA GAKVGLHGRK APANIDETIA
 51  SMRADGGDAA FFAADLATSE ACQQLVDEFV AKFGGIDVLI NNAGGLVGRK
101  PLPEIDDTFY DAVMDANIRS VVMTTKFALP HLAAAAKASG QTSAVISTGS
151  IAGHTGGGPG AGLYGAAKAF LHNVHKNWVD FHTKDGVRFN IVSPGTVDTA
201  FHADKTQDVR DRISNGIPMG RFGTAEEMAP AFLFFASHLA SGYITGQVLD
251  INGGQYKH
```

Fig. 1-3. Amino acid sequence of SPH3227 from strain A1. Peptide fragments, identified as the partial sequences of SPH3227 by peptide mass fingerprinting, are colored in red.

"function-unknown protein family" in the strain A1 genome database. The protein consists of 258 amino acid residues with a theoretical molecular mass of 26,931 Da, which is in good agreement with that obtained from SDS-PAGE (27 kDa; Fig. 1-2 B, left) and matrix-assisted laser desorption/ionization time-of-flight (MALDI-TOF)-MS (26,956.6 Da; Fig. 1-4 A). These results

indicated that SPH3227 is A1-R, an NADPH-dependent and DEH-specific reductase. Although the A1-R gene is located far from the genetic cluster for alginate import and degradation in the strain A1 genome, the A1-R gene is in the vicinity of the cluster of iron-related genes such as the outer membrane transporter for siderophore-iron complex and cytochrome. Since alginate is known to bind to iron, the transporter possibly incorporates iron using alginate as a siderophore. The cluster including the A1-R gene was also suggested related to alginate import and metabolism.

Table 1-4
Effects of various compounds on the activity of nA1-R

Compounds	Concentration (mM)	Activity (%)[a]
None	(NADPH)	100
	(NADH)	2.3[b]
Thiol reagents		
Dithiothreitol	1	94
Glutathione (reduced form)	1	96
2-Mercaptoethanol	1	108
Iodoacetic acid	1	97
p-Chloromercuribenzoic acid	1	104
Chelator		
EDTA	1	112
Sugars		
L-Fucose	5	97
D-Galactose	5	105
D-Glucose	5	96
D-Glucuronic acid	5	107
D-Mannose	5	104
L-Rhamnose	5	101
D-Xylose	5	103
D-Sucrose	5	111
D-Galacturonic acid	5	95
2-Deoxy glucose	5	95
D-Glucosamine	5	95
Metals		
$AlCl_3$	1	98
$MgCl_2$	1	108
$MnCl_2$	1	96
$CaCl_2$	1	116
$CoCl_2$	1	153
$ZnCl_2$	1	104
$HgCl_2$	0.04	35
NaCl	1	104
KCl	1	104
LiCl	1	108

[a] Relative activities (%) in a reaction mixture containing various compounds at the indicated concentrations are shown. The activity in the absence of the compound was taken as 100%.

[b] The value was determined when 0.2 mM NADPH was replaced with 0.2 mM NADH.

The sequence similarity analysis was carried out using BLAST (blast.ncbi.nlm.nih.gov). A1-R showed high sequence identity (40–71%) with 239 proteins. All of them belong to the short-chain dehydrogenase/reductase (SDR) family. Based on the primary structure, A1-R is also a member of the SDR family. The subcellular localization prediction program PSORTb (psort.org/psortb/) suggested that A1-R exclusively located in the cytoplasm as strain A1 alginate lyases responsible for depolymerization of alginate does.

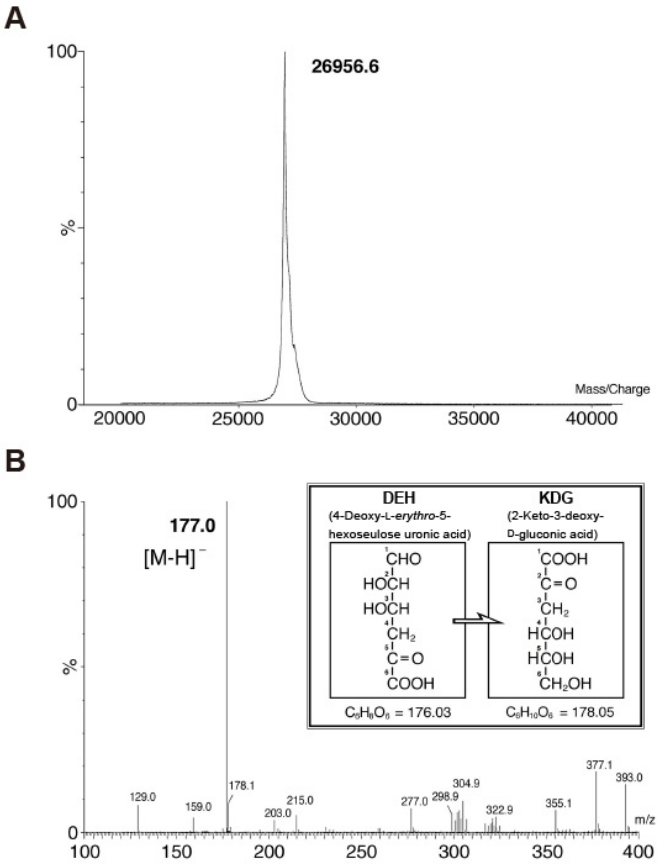

Fig. 1-4. MS. (A) MALDI-TOF-MS spectrum of nA1-R. (B) ESI-MS spectrum of the reduced product from DEH through the rA1-R reaction. The main peak in negative mode coincided with the molecular weight of the deprotonated form of reduced DEH, namely KDG, indicated in the box.

rA1-R from *E. coli* Cells

An overexpression system of A1-R was constructed in *E. coli* cells. rA1-R was purified 2.52-fold through two steps of column chromatography, with a recovery of 46.3% (Table 1-3). The purified enzyme was homogeneous by SDS-PAGE (Fig. 1-2 B, right) and showed DEH reducing activity. The N-terminal amino acid sequence of rA1-R was determined to be ^{1}MFPDLK^{6}, indicating that no excision of the N-terminal amino acid residues occurred in the *E. coli* cells. This

result coincided with the subcellular localization prediction (cytoplasm) of A1-R. The enzymatic properties of rA1-R were similar to those of nA1-R from strain A1 cells, except for the specific activity (nA1-R, 236 units mg^{-1}; rA1-R, 56.9 units mg^{-1}) and affinity to DEH (K_m for nA1-R, 101 μM; K_m for rA1-R, 1930 μM) (Table 1-5). The difference in kinetic parameters between native and recombinant A1-Rs will be attributed to the inappropriate folding of rA1-R in overexpression system.

Table 1-5
Kinetic parameters of rA1-R and A1-R mutant for DEH

Enzyme	k_{cat} (s^{-1})	K_m (mM)	$k_{cat}\ K_m^{-1}$	
			($s^{-1}\ mM^{-1}$)	(%)[a]
rA1-R	197 ± 8.9	1.93 ± 0.098	102	100
S150A	8.53 ± 0.25	16.2 ± 4.82	0.53	0.52
Y164F	0.129 ± 0.017	3.37 ± 0.78	0.038	0.037
K168A	35.2 ± 1.45	2.06 ± 0.17	17.1	16.8

[a] Relative activities (%) are shown. The $k_{cat}\ K_m^{-1}$ value of the wild-type enzyme was taken as 100%.

Identification of the Reaction Product of A1-R

The reaction product of rA1-R was purified and subjected to MS. In the ESI-MS spectrum (Fig. 1-4 B), the major peak of deprotonated ion $[M-H]^-$ in negative mode indicated $m\ z^{-1}$ 177.0, demonstrating that the molecular weight of the product corresponded to that of the reduced form ($C_6H_{10}O_6$, MW = 178.05) derived from DEH ($C_6H_8O_6$, MW = 176.03). Furthermore, ^1H NMR and COSY spectra provided evidence that reduction of the aldehyde group at the 1-position carbon occurred in the A1-R product. These data revealed that A1-R catalyzed the reduction of DEH to KDG (Fig. 1-1).

Crystal Structure of A1-R

To clarify the reaction mechanism of NADPH-dependent DEH reduction, X-ray crystallography of A1-R was conducted. An A1-R crystal was obtained in a reservoir solution consisting of 85 mM Tris-HCl (pH 8.4), 170 mM Li_2SO_4, 25.5% (w/v) PEG4000, 15% (v/v) glycerol, and 32.0 mg ml^{-1} rA1-R. The crystal structure of A1-R was determined at a resolution of 1.65 Å by the molecular replacement method, with an R-factor of 17.6% and R_{free}-factor of 20.4%. Data collection and refinement statistics are summarized in Table 1-6.

The refined model in an asymmetric unit consists of two identical monomers, termed molecules A and B. All the residues could be assigned in the 2 $F_o - F_c$ map of the molecule A, although residues 195-215 and 256-258 were absent in the 2 $F_o - F_c$ map of the molecule B. The r.m.s.d.

Table 1-6
Statistics for X-ray diffraction and structure refinement

	A1-R	A1-R·NADP$^+$
Data collection		
Wavelength (Å)	1.0000	1.0000
Space group	$P3_221$	$P1$
Unit cell parameters (Å, °)	$a = b = 106.2$, $c = 70.4$	$a = 60.4$, $b = 64.2$, $c = 74.4$
		$\alpha = 80.2$, $\beta = 66.1$, $\gamma = 65.0$
Resolution limit (Å)	50.0 – 1.65 (1.71 – 1.65)[a]	50.0 – 1.63 (1.69 – 1.63)[a]
Total reflections	840,225	287,719
Unique reflections	55,401	115,155
Redundancy	15.2 (14.3)	2.6 (2.4)
Completeness (%)	99.9 (99.8)	95.9 (88.8)
I/σ (I)	15.6 (4.99)	19.7 (3.82)
R_{merge} (%)	5.1 (40.1)	3.5 (17.2)
Refinement		
Final model	492 residues,	1028 residues, 4 *tert*-butanol,
	560 water molecules	4 NADP$^+$, 927 water molecules
Resolution limit (Å)	31.2 – 1.65 (1.69 – 1.65)	22.7 – 1.63 (1.67 – 1.63)
Used reflections	52,496 (3,796)	104,849 (6,945)
Completeness (%)	99.9 (99.7)	95.9 (86.2)
R-factor (%)	17.6 (25.3)	17.2 (26.9)
R_{free} (%)	20.4 (31.0)	20.9 (31.7)
Average B-factor (Å^2)		
Protein		
Molecule A	15.6	17.3
Molecule B	16.2	17.3
Molecule C		18.9
Molecule D		19.0
Waters	30.4	32.6
NADP$^+$		
Molecule A		18.5
Molecule B		23.9
Molecule C		23.8
Molecule D		18.9
tert-butanol molecules		19.9
r.m.s.d.		
Bond (Å)	0.007	0.007
Angle (°)	0.96	1.06
Ramachandran plot (%)		
Favored regions	98.8	99.0
Allowed regions	1.2	1.0

[a] Data on highest shells are given in parenthesis.

between molecules A and B was calculated as 0.438 Å for all residues (228 Cα atoms). Because of the inclusion of almost all residues, molecule A is focused on hereafter. On the basis of theoretical curves in the plot, calculated according to the procedure of Luzzati (25), the absolute positional error was estimated to be 0.166 Å at a resolution of 1.65 Å. Ramachandran plot analysis (26), in

which the stereochemical correctness of the backbone structure is indicated by (ϕ, ψ) torsion angles (27), shows that 98.8% of nonglycine residues lie within the favored regions and 100% of nonglycine residues lie in the allowed regions.

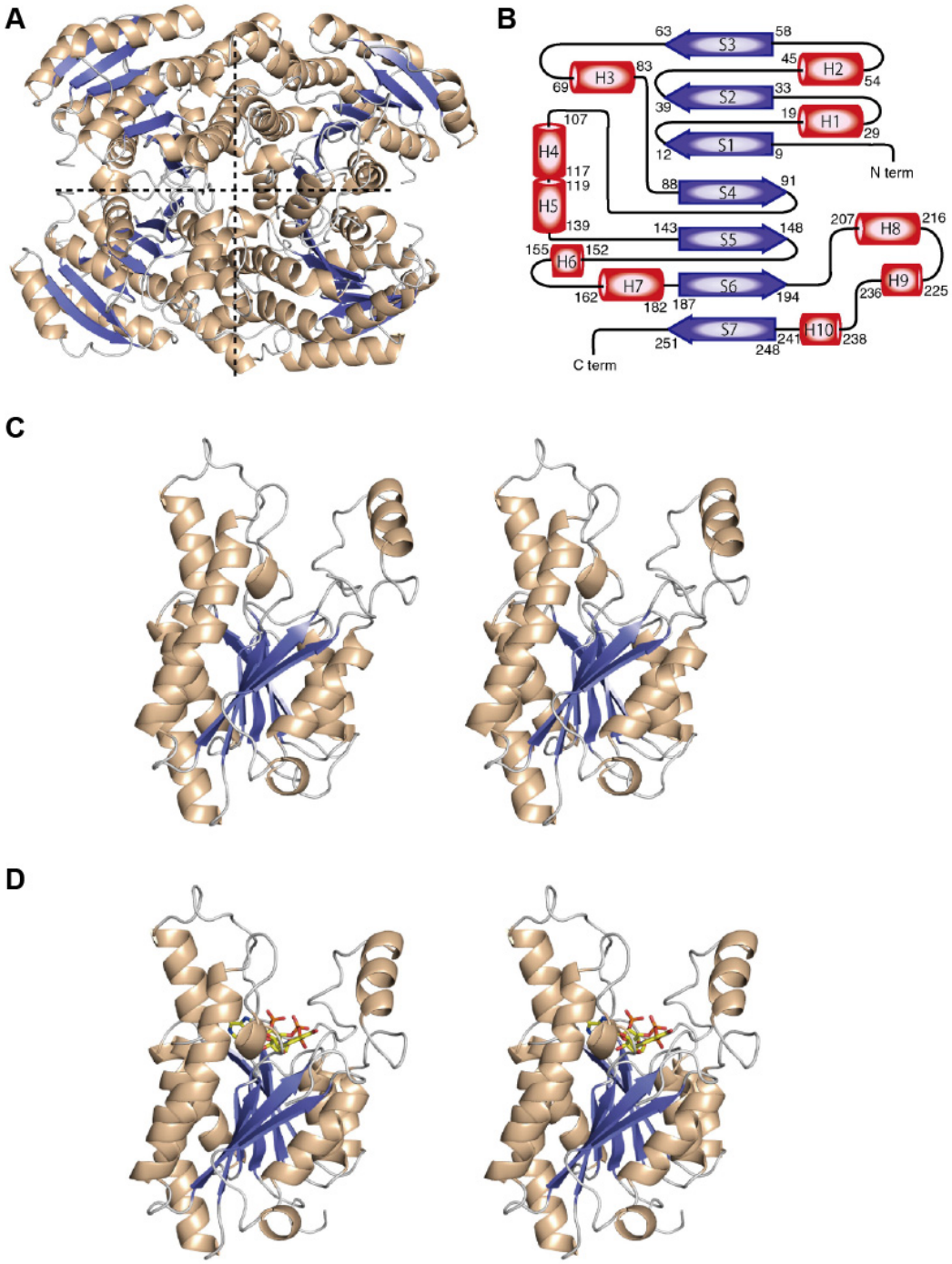

Fig. 1-5. Structure of A1-R. (A) Overall structure of A1-R in a biologically active tetramer form. (B) Topology diagram. Blue, β-strand; red, α-helices. (C) Overall structure of A1-R (stereodiagram). (D) Overall structure of A1-R·$NADP^+$ (stereodiagram). $NADP^+$ is shown as a stick model.

The overall structure and topology of the secondary structure elements indicate that A1-R consists of three-layered structure, α/β/α, with an coenzyme-binding Rossmann fold (28) (Fig. 1-5). The enzyme includes 10 α-helices (H1, residues 19–29; H2, residues 45–54; H3, residues 69–83; H4, residues 107–117; H5, residues 119–139; H6, residues 152–155; H7, residues 162–182; H8, residues 207–216; H9, residues 225–236; H10, residues 238–241) and 7 β-strands (S1, residues 9–12; S2, residues 33–39; S3, residues 58–63; S4, residues 88–91; S5, residues 143–148; S6, residues 187–194; S7, residues 248–251). Structural homologues of A1-R were searched for in the PDB using the Dali program (29). Several proteins included in the SDR family, such as 3-oxoacyl reductase (PDB-ID, 2UVD, Z score = 35.5), were found to exhibit significant structural homology to A1-R (Table 1-7).

Table 1-7
Structural homologs of A1-R

Z score	Protein	r.m.s.d.[a]	Lali[b]	PDB-ID
35.5	3-Oxoacyl reductase	1.4	244	2UVD
35.4	3-Oxoacyl reductase	1.6	246	4JRO
35.3	FABG protein	1.6	244	4NBU
35.3	Glucose-1-dehydrogenase	1.6	250	3AUU
35.0	Gluconate-5-dehydrogenase	1.6	247	1VL8
35.0	β-Keto acyl carrier protein reductase	1.6	244	1EDO
34.8	Glucose dehydrogenase	1.7	250	1GCO
34.5	Putative SDR family enzyme	1.9	246	3RIH
34.5	3-Oxoacyl reductase	1.6	239	4DMM
34.5	3-Oxoacyl reductase	1.5	242	3OSU

[a] A measure of the average deviation in distance between aligned Cα.
[b] Total number of structurally equivalent residues.

Binding Mode to Coenzyme

To identify structural determinants for coenzyme binding, the A1-R·$NADP^+$ crystal was obtained in the solution containing 500 μM $NADP^+$, 47% (v/v) 2-methyl-2,4-pentanediol, 2% (v/v) *tert*-butanol, and 28.8 mg ml^{-1} rA1-R by cocrystallization. The A1-R·$NADP^+$ crystal belongs to space group *P*1 with unit cell parameters of a = 60.4 Å, b = 64.2 Å, and c = 74.4 Å (α = 80.2°, β = 66.1°, γ = 65.0°). Four monomers, termed molecules A, B, C, and D, are present in an asymmetric unit. The initial phase was determined by molecular replacement with the ligand-free A1-R

Table 1-8
Hydrogen bond (≤3.4 Å) between $NADP^+$, water molecules, and A1-R

Direct interaction				Water-mediated interaction					
$NADP^+$ atom	Protein/atom (distance, Å)[a]			$NADP^+$ atom	Water (distance, Å)[b]		Protein/atom (distance, Å)[c]		
Adenosine									
N1A	Leu-66	/N	(2.98)	O5B	Wat-2036	(3.17)	Gly-14	/O	(2.91)
N6A	Asp-65	/OD1	(3.04)				Gln-17	/O	(2.89)
O3B	Gly-14	/O	(3.31)				Ile-19	/N	(3.31)
	Ser-16	/OG	(2.87)				Gly-20	/N	(2.83)
							Asn-92	/OD1	(2.90)
Nicotinamide ribose									
O2D	Tyr-164	/OH	(2.71)	O3D	Wat-2105	(3.20)	Asn-91	/O	(2.97)
O3D	Lys-168	/NZ	(2.99)				Ala-93	/O	(2.95)
	Asn-92	/O	(2.78)				Lys-168	/NZ	(2.90)
O7N	Gly-195	/O	(3.31)	O7N	Wat-2054	(3.26)	Gly-195	/O	(2.73)
	Val-197	/N	(2.66)				His-202	/NE2	(2.93)
	His-202	/NE2	(2.90)						
N7N	Thr-199	/OG1	(3.09)						
	Val-197	/O	(3.33)						
Diphosphate									
O1A	Gln-17	/NE2	(2.81)	O1A	Wat-2056	(2.54)	Ala-200	/N	(2.92)
O1N	Thr-199	/OG1	(2.64)	O2A	Wat-2104	(2.78)	Gly-94	/O	(3.04)
O2N	Ile-19	/N	(2.90)	O2N	Wat-2036	(2.69)	Gly-14	/O	(2.91)
							Gln-17	/O	(2.89)
							Ile-19	/N	(3.31)
							Gly-20	/N	(2.83)
							Asn-92	/OD1	(2.90)
2'-Phosphate									
O2X	Arg-39	/N	(2.77)	O1X	Wat-2095	(3.21)	Ser-16	/OG	(2.74)
	Lys-40	/N	(3.22)				Lys-40	/O	(2.64)
O3X	Arg-39	/NE	(2.70)	O2X	Wat-2095	(2.63)	Ser-16	/OG	(2.74)
	Arg-39	/NH2	(2.74)				Lys-40	/O	(2.64)

[a] Distance between the atom of $NADP^+$ and protein.
[b] Distance between the atom of $NADP^+$ and water.
[c] Distance between the atom of water and protein.

structure as the reference model. Only one N-terminal ^{1}Met could not be assigned in 2 $F_o - F_c$ maps of the four molecules. The r.m.s.d. between ligand-free A1-R and A1-R·$NADP^+$ was calculated as 0.352 Å for all residues (246 Cα atoms); this indicates that no significant conformational change occurs between protein structures with and without $NADP^+$ molecule. $NADP^+$ is accommodated in the Rossmann fold (Figs. 1-5 D and 1-6). There are several hydrogen bond interactions between A1-R and $NADP^+$. Direct and water-mediated hydrogen bonds are listed in Table 1-8. Arg-39 and Lys-40 form direct hydrogen bonds to the 2′-phosphate group of $NADP^+$, and N or O atom of $NADP^+$ is directly bound to Gly-14, Ser-16, Gln-17, Ile-19, Asp-65, Leu-66, Asn-92, Tyr-164, Lys-168, Gly-195, Val-197, Thr-199, and His-202 via hydrogen bonds (Fig. 1-6 B). In addition to hydrogen bond interactions, carbon-carbon contacts were also observed between the enzyme and $NADP^+$. Molecular surface electric charge at pH 7.0 was calculated using the APBS program

(Fig. 1-6 C). Positively charged residues, such as Arg-39 and Lys-40, form a basic pocket around the 2′-phosphate group of $NADP^+$, suggesting that the phosphate group is stabilized by this basic pocket. A multiple sequence alignment between A1-R and some well-known members of the SDR

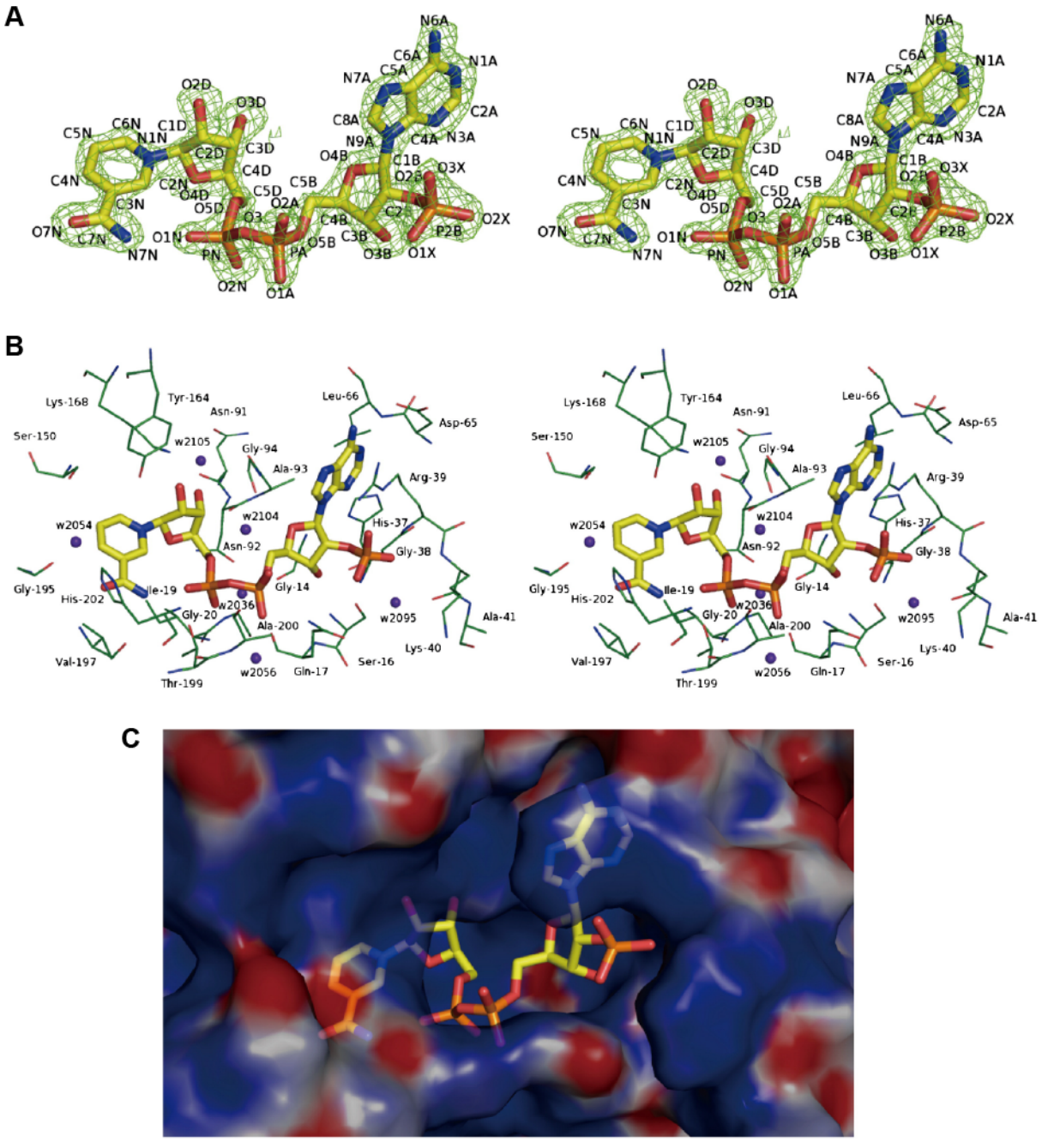

Fig. 1-6. Active site structure. (A) Electron density of $NADP^+$ in the omit map ($F_o - F_c$), calculated at 3.0σ. (B) Residues interacting with $NADP^+$ are shown. Green, carbon atom in residues; yellow, carbon atom in $NADP^+$; red, oxygen atom; blue, nitrogen atom; orange, phosphate atom. Purple balls represent water molecules. (C) Surface electrostatic potentials at pH 7.0 of the A1-R·$NADP^+$ complex. Blue, basic; red, acidic.

family is shown in Fig. 1-7. Arg-39 of A1-R was completely conserved among NADP(H)-dependent enzymes, while Asp was highly conserved among NAD(H)-dependent enzymes in place of Gly-38. In fact, Arg-39 is directly hydrogen bonded to the 2′-phosphate group of $NADP^+$ (Fig. 1-6 B and Table 1-8). To clarify the preference of A1-R for NADPH, 12 A1-R mutants were constructed through site-directed mutagenesis and subjected to the enzyme assay in the presence of NADPH (Table 1-9). The mutants in Gly-38 and Arg-39, such as G38D, R39I, R39V, and R39W, significantly decreased the affinity for NADPH, while there was little difference in the activity for NADH among the mutants.

Table 1-9
Kinetic parameters of rA1-R and A1-R mutants for NADPH and NADH

Enzyme	NADPH				NADH			
	k_{cat} (s^{-1})	K_m (μM)	$k_{cat}\ K_m^{-1}$ ($s^{-1}\ mM^{-1}$)	(%)[a]	k_{cat} (s^{-1})	K_m (μM)	$k_{cat}\ K_m^{-1}$ ($s^{-1}\ mM^{-1}$)	(%)[a]
rA1-R WT	60.8 ± 3.6	7.01 ± 2.2	8700	100	7.59 ± 1.3	188 ± 55	40	100
G38D	5.16 ± 0.29	178 ± 17	29	0.33	8.29 ± 0.72	181 ± 28	46	120
R39I	7.80 ± 1.1	178 ± 43	44	0.51	10.6 ± 2.0	175 ± 59	60	150
R39V	16.2 ± 2.2	139 ± 21	120	1.4	10.2 ± 1.6	153 ± 25	66	170
R39W	2.13 ± 0.25	288 ± 48	7.4	0.085	9.86 ± 1.6	354 ± 84	28	70
A41E	81.7 ± 3.0	15.4 ± 2.3	5300	61	19.2 ± 5.1	402 ± 147	48	120
G38E	0.0767 ± 0.0041	282 ± 24	0.27	0.0031	0.270 ± 0.018	220 ± 22	1.2	3.0
R39D	0.108 ± 0.026	308 ± 105	0.35	0.0040	0.976 ± 0.18	227 ± 64	4.3	11
S16Y	3.59 ± 0.42	88.9 ± 21	40	0.46	0.546 ± 0.067	189 ± 37	2.9	7.3
G38D/R39E/K40E	N.D.	N.D.	N.D.	N.D.	N.D.	N.D.	N.D.	N.D.
G38D/R39D	N.D.	N.D.	N.D.	N.D.	0.0844 ± 0.028	557 ± 233	0.15	0.38
R39D/K40D	0.0618 ± 0.027	448 ± 255	0.14	0.0016	0.558 ± 0.17	446 ± 180	1.3	3.3
K40D/A41D	3.93 ± 0.48	78.0 ± 22	50	0.57	8.98 ± 2.4	160 ± 77	56	140

N.D., not determined due to low activity.
[a] Relative activities (%) are shown. The $k_{cat}\ K_m^{-1}$ value of the wild-type enzyme was considered to be 100%.

Catalytic Triad in A1-R

In the multiple sequence alignment (Fig. 1-7), SDR family enzymes shared sequence identity of 18–32%, with highly conserved sequence motifs, such as the glycine-rich pattern of the cofactor-binding Rossmann fold region (TG*XXX*G*X*G) (24,28,30) and catalytic triad (Ser, Tyr, and Lys) (24). The conserved catalytic triad of A1-R corresponded to Ser-150, Tyr-164, and Lys-168. To confirm that these function as catalytic residues, A1-R mutants were constructed. The mutants were S150A, Y164F, and K168A, in which Ser-150, Tyr-164, and Lys-168 were replaced with Ala, Phe, and Ala, respectively. They were purified and subjected to kinetic analysis (Table 1-5). All the mutants significantly reduced the enzymatic activity ($k_{cat}\ K_m^{-1}$). In particular, Y164F showed

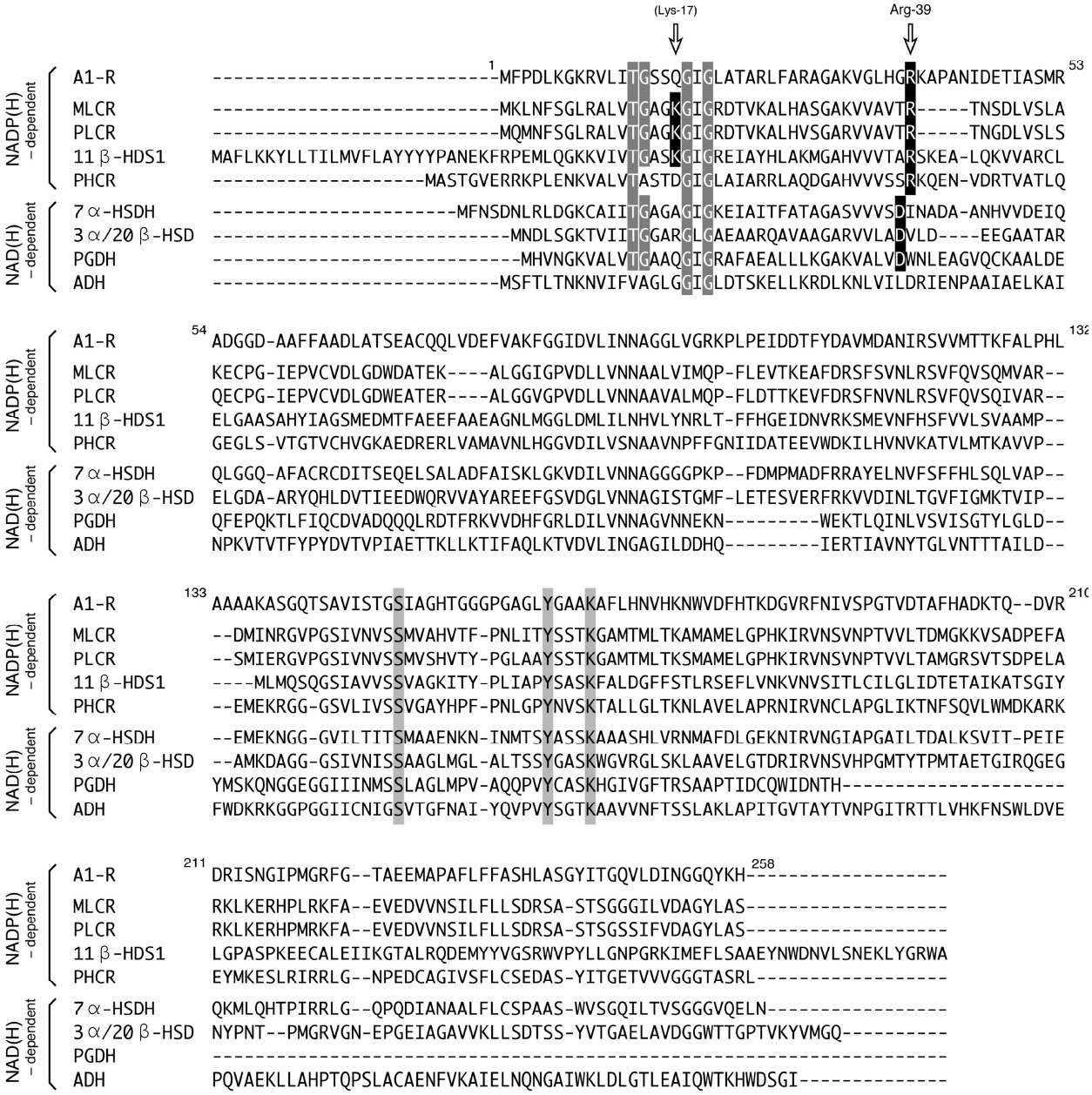

Fig. 1-7. Multiple sequence alignment of A1-R and well-known members of the SDR family. Each enzyme is described as follows: MLCR, lung carbonyl reductase (GenPept-ID, Q542P5) from *Mus musculus*; PLCR, lung carbonyl reductase (GenPept-ID, Q29529) from *Sus scrofa*; 11β-HDS1, 11-β-hydroxysteroid dehydrogenase 1 (GenPept-ID, Q6QLL4) from *Cavia porcellus*; PHCR, heart carbonyl reductase (GenPept-ID, Q8WNV7) from *Sus scrofa*; 7α-HSDH, 7-α-hydroxysteroid dehydrogenase (GenPept-ID, AAC74691) from *E. coli*; 3α/20β-HSD, 3-α (or 20-β)-hydroxysteroid dehydrogenase (GenPept-ID, P19992) from *Streptomyces coelicolor*; PGDH, 15-hydroxyprostaglandin dehydrogenase (GenPept-ID, P15428) from *Homo sapiens*; ADH, alcohol dehydrogenase (GenPept-ID, P00334) from *Drosophila melanogaster*. The amino acid sequences were aligned by using ClustalW (clustalw.ddbj.nig.ac.jp/). The alignment indicates the cofactor-binding TG*XXX*G*X*G motif (outlined characters on a shaded background) and catalytic triad Ser-Tyr-Lys (characters on a light-shaded background) within the enzymes. The residues involved in the specificity of NADP(H) or NAD(H) are shown as outlined characters on a black background.

a significantly low k_{cat} value, suggesting that Tyr-164 may function as a proton donor in the reduction reaction. Ser-150 and Lys-168 may participate in catalysis by stabilizing the intermediates or in proton transfer, as described elsewhere (24,31).

Discussion

In this CHAPTER, a novel bacterial aldose reductase was identified to catalyze the conversion of DEH to KDG. Judging from the data on KDG metabolism in bacteria (5), KDG formed from DEH in strain A1 cells is converted to 2-keto-3-deoxy-6-phosphogluconic acid by 2-keto-3-deoxygluconokinase (A1-K), and then to glyceraldehdye-3-phosphate and pyruvate by 2-keto-3-deoxy-6-phosphogluconic acid aldolase (A1-A) (Fig. 1-1). Candidates for kinase A1-K (35 kDa) and aldolase A1-A (24 kDa) are included in the strain A1 genome database (data not shown). Although the involvement of an NADPH-dependent reductase, like A1-R, in alginate metabolism was reported in a certain pseudomonad in 1962 (5), little information on the molecular identification and physiological function of the enzyme has been accumulated. The A1-R gene was, therefore, first identified to encode the aldose reductase responsible for alginate metabolism. The enzymatic properties of nA1-R were compared with those of the DEH reductase from the pseudomonad (designated PDEHR) (5). nA1-R and PDEHR are similar in terms of the optimal pH, behavior toward various compounds, and substrate specificity, but not susceptibility toward *p*-chloromercuribenzoic acid or affinity for DEH and NADPH.

On the basis of its primary and tertiary structures, A1-R is a member of the SDR family, especially the "classical" SDR family (32). The family members catalyze NAD(P)(H)-dependent redox reactions. They show a limited sequence identity (15–30%) throughout the entire molecules, although sequence motifs, such as the cofactor-binding Rossmann fold (TG*XXX*G*X*G) (24,28,30) and catalytic triad (Ser, Tyr, and Lys) (24), are highly conserved. A1-R also shows sequence identity 18–32% to most of family members, but the catalytic triad formed by Ser-150, Tyr-164, and Lys-168 is well conserved in A1-R. These residues were found to be involved in the catalytic reaction of A1-R by site-directed mutagenesis and to constitute the catalytic triad around the cofactor-binding site by X-ray crystallography.

A glycine-rich pattern is also conserved in A1-R as ^{13}TG*XXX*G*X*G^{20} (Fig. 1-7) and forms the classical β/α/β motif of the Rossmann fold (Fig. 1-5), which facilitates NADPH binding. The specificity for NADP(H), rather than NAD(H), is believed to be conferred by two conserved basic residues in the Rossmann fold. In the mouse lung carbonyl reductase (MLCR), two basic residues,

Lys-17 and Arg-34, have been suggested to promote NADPH binding by interacting with the 2′-phosphate group of NADP(H) (33,34). Based on the sequence alignment, two basic residues in positions corresponding to Lys-17 and Arg-34 in the mouse reductase are conserved in almost all the members of the NADP(H)-dependent SDR family but not in the NAD(H)-dependent members (Fig. 1-7). However, a single basic residue, Arg-39, alone is conserved in A1-R, as observed only rarely in the SDR family members, such as NADP(H)-dependent pig heart carbonyl reductase (Fig. 1-7), suggesting that a specific binding motif for cofactor binding is included in A1-R. Site-directed mutagenesis studies indicate that Gly-38 and Arg-39 play important roles in NADPH binding. The mutant G38D showed no enhanced activity for NADH, suggesting that the preference for NADH in the SDR family may be achieved by complex structural networks. Molecular conversion of A1-R with a preference for NADH requires a further structural study of A1-R in complex with NADH or substrate.

References

1. Gacesa, P. (1988) Alginates. *Carbohydr. polym.* **8**, 161-182
2. Murata, K., Kawai, S., Mikami, B., and Hashimoto, W. (2008) Superchannel of bacteria: biological significance and new horizons. *Biosci. Biotechnol. Biochem.* **72**, 265-277
3. Yoon, H.-J., Hashimoto, W., Miyake, O., Okamoto, M., Mikami, B., and Murata, K. (2000) Overexpression in *Escherichia coli*, purification, and characterization of *Sphingomonas* sp. A1 alginate lyases. *Protein Expr. Purif.* **19**, 84-90
4. Hashimoto, W., Miyake, O., Momma, K., Kawai, S., and Murata, K. (2000) Molecular identification of oligoalginate lyase of *Sphingomonas* sp. strain A1 as one of the enzymes required for complete depolymerization of alginate. *J. Bacteriol.* **182**, 4572-4577
5. Preiss, J., and Ashwell, G. (1962) Alginic acid metabolism in bacteria. II. The enzymatic reduction of 4-deoxy-L-*erythro*-5-hexoseulose uronic acid to 2-keto-3-deoxy-D-gluconic acid. *J. Biol. Chem.* **237**, 317-321
6. Bradford, M. M. (1976) A rapid and sensitive method for the quantitation of microgram quantities of protein utilizing the principle of protein-dye binding. *Anal. Biochem.* **72**, 248-254
7. Thiede, B., Hohenwarter, W., Krah, A., Mattow, J., Schmid, M., Schmidt, F., and Jungblut, P. R. (2005) Peptide mass fingerprinting. *Methods* **35**, 237-247
8. Hashimoto, W., Momma, K., Maruyama, Y., Yamasaki, M., Mikami, B., and Murata, K. (2005) Structure and function of bacterial super-biosystem responsible for import and depolymerization of macromolecules. *Biosci. Biotechnol. Biochem.* **69**, 673-692

9. Perkins, D. N., Pappin, D. J., Creasy, D. M., and Cottrell, J. S. (1999) Probability-based protein identification by searching sequence databases using mass spectrometry data. *Electrophoresis* **20**, 3551-3567

10. Sanger, F., Nicklen, S., and Coulson, A. R. (1977) DNA sequencing with chain-terminating inhibitors. *Proc. Natl. Acad. Sci. U.S.A.* **74**, 5463-5467

11. Otwinowski, Z., and Minor, W. (1997) Processing of X-ray diffraction data. *Methods Enzymol.* **276**, 307-326

12. Vagin, A., and Teplyakov, A. (2010) Molecular replacement with *MOLREP*. *Acta Crystallogr. D Biol. Crystallogr.* **66**, 22-25

13. Collaborative Computational Project, N. (1994) The *CCP4* suite: programs for protein crystallography. *Acta Crystallogr. D Biol. Crystallogr.* **50**, 760-763

14. Murshudov, G. N., Vagin, A. A., and Dodson, E. J. (1997) Refinement of macromolecular structures by the maximum-likelihood method. *Acta Crystallogr. D Biol. Crystallogr.* **53**, 240-255

15. Emsley, P., and Cowtan, K. (2004) *Coot*: model-building tools for molecular graphics. *Acta Crystallogr. D Biol. Crystallogr.* **60**, 2126-2132

16. Laskowski, R. A., MacArthur, M. W., Moss, D. S., and Thornton, J. M. (1993) *PROCHECK*: a program to check the stereochemical quality of protein structures. *J. Appl. Crystallogr.* **26**, 283-291

17. Kabsch, W. (1978) A discussion of the solution for the best rotation to relate two sets of vectors. *Acta Crystallogr. A* **34**, 827-828

18. Delano, W. L. (2002). *The PyMOL Molecular Graphics System*, DeLano Scientific LLC, San Carlos, CA

19. Berman, H. M., Westbrook, J., Feng, Z., Gilliland, G., Bhat, T. N., Weissig, H., Shindyalov, I. N., and Bourne, P. E. (2000) The Protein Data Bank. *Nucleic Acids Res.* **28**, 235-242

20. Laemmli, U. K. (1970) Cleavage of structural proteins during the assembly of the head of bacteriophage T4. *Nature* **227**, 680-685

21. Miyake, O., Hashimoto, W., and Murata, K. (2003) An exotype alginate lyase in *Sphingomonas* sp. A1: overexpression in *Escherichia coli*, purification, and characterization of alginate lyase IV (A1-IV). *Protein Expr. Purif.* **29**, 33-41

22. Ochiai, A., Hashimoto, W., and Murata, K. (2006) A biosystem for alginate metabolism in *Agrobacterium tumefaciens* strain C58: molecular identification of Atu3025 as an exotype family PL-15 alginate lyase. *Res. Microbiol.* **157**, 642-649

23. Hashimoto, W., Okamoto, M., Hisano, T., Momma, K., and Murata, K. (1998) *Sphingomonas* sp. A1 lyase active on both poly-β-D-mannuronate and heteropolymeric regions in alginate. *J. Ferment. Bioeng.* **86**, 236-238

24. Jornvall, H., Persson, B., Krook, M., Atrian, S., Gonzalez-Duarte, R., Jeffery, J., and Ghosh, D. (1995)

Short-chain dehydrogenases/reductases (SDR). *Biochemistry* **34**, 6003-6013

25. Luzzati, V. (1952) Traitement statistique des erreurs dans la determination des structures cristallines. *Acta Crystallogr.* **5**, 802-810

26. Lovell, S. C., Davis, I. W., Arendall, W. B., 3rd, de Bakker, P. I., Word, J. M., Prisant, M. G., Richardson, J. S., and Richardson, D. C. (2003) Structure validation by Cα geometry: φ, ψ and Cβ deviation. *Proteins* **50**, 437-450

27. Ramachandran, G. N., and Sasisekharan, V. (1968) Conformation of polypeptides and proteins. *Adv. Protein Chem.* **23**, 283-438

28. Rossmann, M. G., Moras, D., and Olsen, K. W. (1974) Chemical and biological evolution of nucleotide-binding protein. *Nature* **250**, 194-199

29. Holm, L., Kaariainen, S., Rosenstrom, P., and Schenkel, A. (2008) Searching protein structure databases with DaliLite v.3. *Bioinformatics* **24**, 2780-2781

30. Jornvall, H., Persson, M., and Jeffery, J. (1981) Alcohol and polyol dehydrogenases are both divided into two protein types, and structural properties cross-relate the different enzyme activities within each type. *Proc. Natl. Acad. Sci. U.S.A.* **78**, 4226-4230

31. Cols, N., Atrian, S., Benach, J., Ladenstein, R., and Gonzalez-Duarte, R. (1997) *Drosophila* alcohol dehydrogenase: evaluation of Ser139 site-directed mutants. *FEBS Lett.* **413**, 191-193

32. Persson, B., Kallberg, Y., Oppermann, U., and Jornvall, H. (2003) Coenzyme-based functional assignments of short-chain dehydrogenases/reductases (SDRs). *Chem. Biol. Interact.* **143-144**, 271-278

33. Nakanishi, M., Kakumoto, M., Matsuura, K., Deyashiki, Y., Tanaka, N., Nonaka, T., Mitsui, Y., and Hara, A. (1996) Involvement of two basic residues (Lys-17 and Arg-39) of mouse lung carbonyl reductase in NADP(H)-binding and fatty acid activation: site-directed mutagenesis and kinetic analyses. *J. Biochem.* **120**, 257-263

34. Tanaka, N., Nonaka, T., Nakanishi, M., Deyashiki, Y., Hara, A., and Mitsui, Y. (1996) Crystal structure of the ternary complex of mouse lung carbonyl reductase at 1.8 Å resolution: the structural origin of coenzyme specificity in the short-chain dehydrogenase/reductase family. *Structure* **4**, 33-45

CHAPTER II
NADH-dependent DEH reductase and structure-based conversion of its coenzyme requirement

As described in CHAPTER I, 4-deoxy-L-*erythro*-5-hexoseulose uronic acid (DEH) from alginate was converted to 2-keto-3-deoxy-D-gluconic acid (KDG) by NADPH-dependent DEH reductase, A1-R, in strain A1. KDG is considered to be converted to glyceraldehyde-3-phosphate and pyruvate by strain A1 kinase and aldolase homologues (Fig. 1-1).

Because alginate is an unused and abundant resource, production of useful substances from the polysaccharide is desired (1). Recently, bioethanol production from alginate was achieved using cells of recombinant strain A1, which harbors genes coding for ethanol fermentation (2). Furthermore, ethanologenic bacteria or yeast with an addition of multiple genes involved in alginate import and assimilation have been reported to convert sugars from brown macroalgae to bioethanol (3,4). To optimize the alginate metabolism for biofuel production, an NADH-dependent DEH reductase is also valuable, and two desirable enzymes have been found in *Vibrio* species (3,4). However, the characteristics of these enzymes remain to be clarified.

This CHAPTER deals with molecular identification of a novel NADH-dependent DEH reductase, A1-R′, as a member of the SDR family, structural determination of A1-R′ and its complex with NAD^+, and structure-based conversion of its coenzyme requirement.

Materials and Methods

Materials. Sodium alginate (viscosity of 1% (w/v) solution; 1000 cP) from *Eisenia bicyclis* and Hydroxylapatite were purchased from Nacalai Tesque. TOYOPEARL DEAE-650 M and TOYOPEARL Butyl-650 M were from Tosoh. HiLoad 26/10 Q-Sepharose HP, HiLoad 16/60 Superdex 75 pg, HiLoad 16/60 Superdex 200 pg, and Mono Q HR 5/5 were from GE Healthcare. Restriction endonucleases and PCR-related enzymes were from Toyobo. Bio-Gel P-2 was from Bio-Rad. Other analytical grade chemicals were obtained from commercial sources.

Microorganisms and Culture Conditions. Strain A1 cells were routinely cultured at 30 °C in minimal medium containing 0.5% (w/v) sodium alginate, 0.1% (w/v) $(NH_4)_2SO_4$, 0.1% (w/v) KH_2PO_4, 0.1% (w/v) Na_2HPO_4, 0.01% (w/v) yeast extract, and 0.01% (w/v) $MgSO_4 \cdot 7H_2O$. As a host for plasmid amplification, *Escherichia coli* strain DH5α (Toyobo) was routinely cultured aerobically at 37 °C in LB medium (1% (w/v) tryptone, 0.5% (w/v) yeast extract, and 1% (w/v)

NaCl) (pH 7.2) containing appropriate antibiotics. *E. coli* strain BL21(DE3) (Novagen) was used as a host for the overexpression of A1-R′ or A1-R. For the expression of recombinant proteins, *E. coli* cells were aerobically cultured at 30 °C in LB medium supplemented with sodium ampicillin (100 μg ml^{-1}). When the turbidity at 600 nm reached 0.6, isopropyl-β-D-thiogalactopyranoside was added to the culture at a final concentration of 0.4 mM, and the cells were further cultured at 16 °C for 42 h.

Enzyme and Protein Assays. The DEH reducing activity was assayed at 30 °C in a standard reaction mixture (0.5 ml) consisting of 4 mM DEH, 0.2 mM coenzyme (NADH or NADPH), 50 mM potassium phosphate buffer (KPB) (pH 7.0), and appropriate amount of enzyme. The activity was measured by continuously monitoring the decrease of absorbance at 340 nm, which corresponds to the oxidation of NADH or NADPH. One unit of enzymatic activity was defined as the amount of enzyme required to oxidize 1 μmol of coenzyme per min at 30 °C. The protein content was determined according to the Bradford procedure (5), with bovine serum albumin as the standard. The kinetic parameters (k_{cat} and K_m) for coenzymes or DEH were determined with data from enzyme assays conducted with various concentrations of coenzyme or DEH using the Michaelis-Menten equation with the KaleidaGraph program (Synergy Software).

Construction of A1-R-deficient Strain A1. The strain A1 mutant with a deficiency in A1-R was generated through homologous recombination. Several plasmids were constructed to modify the strain A1 genome (Fig. 2-1). To amplify A1-R gene with upstream and downstream 500-bp regions, PCR was performed using A1-R±500 primers. Each primer used in this CHAPTER is listed in Table 2-1. A reaction mixture (50 μl) contains 1 unit of KOD-FX (Toyobo), 50 ng of strain A1 genomic DNA, 15 pmol each of primers, 20 nmol of dNTPs, and KOD-FX buffer (Toyobo). The PCR conditions were as follows: 94 °C for 2 min and then 20 cycles at 98 °C for 10 s, 66 °C for 30 s, and 68 °C for 2 min. The resultant DNA fragments were ligated with *Hin*cII-digested pUC119 (Takara Bio). The resultant plasmid was designated pUC119/A1-R±500. To mutate Gly-38 to Asp in pUC119/A1-R±500, A1-R_G38D primers were used, and the resultant plasmid was designated pUC119/A1-R±500(G38D). Inverse PCR was performed with A1-R_XhoI primers to insert an *Xho*I recognition site after the stop codon of the A1-R gene. The resultant plasmid after phosphorylation and self-ligation was designated as pUC119/A1-R±500(G38D)_XhoI. The tetracycline resistance gene cassette from pACYC184 (NIPPON GENE) was inserted into the *Xho*I site of pUC119/A1-R±500(G38D)_XhoI, and the resultant plasmid was designated pUC119/A1-R±500(G38D)_Tet. The plasmid was digested with *Pvu*II and *Eco*RI, and the resultant

fragment, including the A1-R gene, was inserted into *Pvu*II- and *Eco*RI-digested pKTY320 (6). The resulting plasmid was designated pKTY320/A1-R±500(G38D)_Tet. DH5α cells transformed with pKTY320/A1-R±500(G38D)_Tet were used as a donor. *E. coli* strain HB101 cells transformed with pRK2013 were used as a helper. To obtain an A1-R-deficient strain A1 mutant, triparental mating (7) was performed using three types of strain A1, donor, and helper. Strain A1 cells were cultured in 0.5% (w/v) alginate minimal medium. Donor cells were cultured in LB medium containing 100 μg ml^{-1} sodium ampicillin and 20 μg ml^{-1} tetracycline hydrochloride. Helper cells were cultured in LB

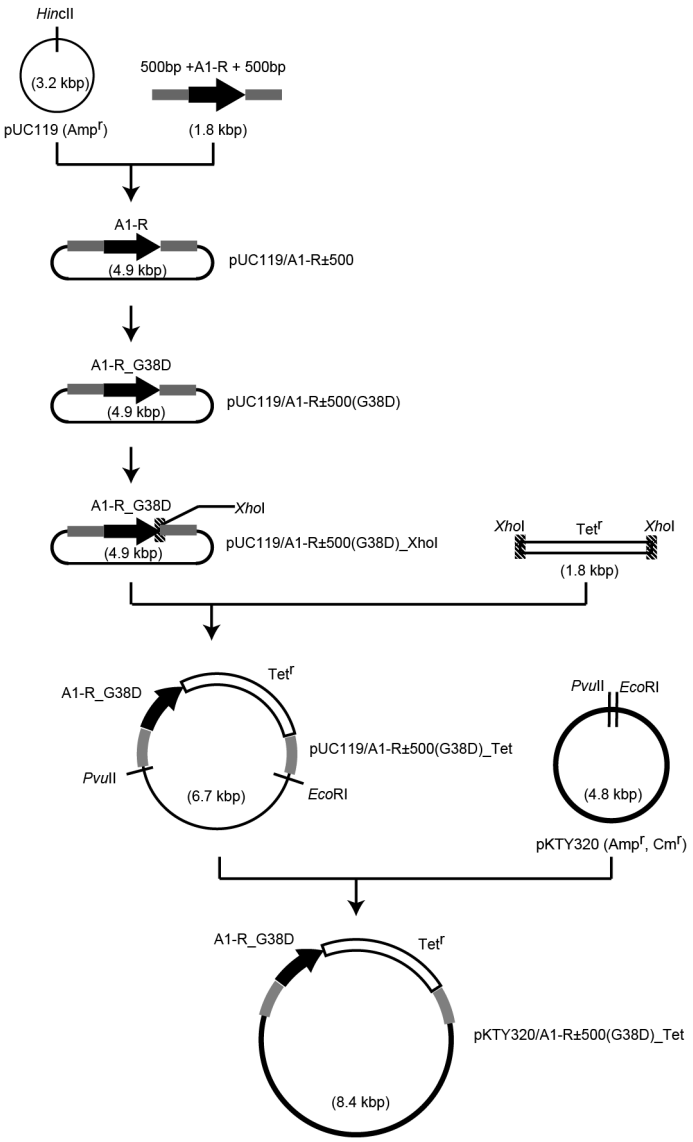

Fig. 2-1. Construction scheme of plasmids for strain A1 mutant with a deficiency in A1-R. Black circle, plasmid; black bold arrow, A1-R gene; gray box, upstream and downstream 500 bp of the A1-R gene; shaded box, *Xho*I recognition site; open box, tetracycline resistance gene cassette.

Table 2-1
Primers for cloning and site-directed mutagenesis

Primer		Oligonucleotides
A1-R±500	forward	5′- CGCCGAGTACGAACAGTTCGCCCGGC -3′
	reverse	5′- CCACCAGCCGCTACGGTCGGTGTCATGC -3′
A1-R_G38D	sense	5′- CCAAGGTCGGCCTGCACGATCGCAAGGCACCCGCC -3′
	antisense	5′- GGCGGGTGCCTTGCGATCGTGCAGGCCGACCTTGG -3′
A1-R_XhoI	forward	5′- CTCGAGTTGCGCGGCGACGTCACTTACAAAC -3′
	reverse	5′- TCAGTGCTTGTACTGCCCGCCGTTGATGTCC -3′
A1-R′_NdeI	forward	5′- AGGAGATATACATATGTTCAGCGATCTGAAGGGCAAGAGAATC -3′
A1-R′_BamHI	reverse	5′- GCTCGAATTCGGATCCTCAGGGGCAGATCTGGCCGCCG -3′
S150A	sense	5′- GTGATCAGTACGGGTGCGATCGCTGCGCGTGAA -3′
	antisense	5′- TTCACGCGCAGCGATCGCACCCGTACTGATCAC -3′
Y164F	sense	5′- GCGCGGGCGTCTTTGCGGCGTCCAA -3′
	antisense	5′- TTGGACGCCGCAAAGACGCCCGCGC -3′
K168A	sense	5′- CTATGCGGCGTCCGCGGCCTGGCTGCAC -3′
	antisense	5′- GTGCAGCCAGGCCGCGGACGCCGCATAG -3′
A1-R′_ex_S	forward	5′- CAGGGTATCGGGATGGCCACGGCCATTGAGC -3′
	reverse	5′- CGACGAGCCGGTGATGAGGATTCTCTTGCCCTTC -3′
A1-R′_ ex_L	forward	5′- CGCAAGGCACCGGCCGATCCGGCGTTGCTACTCGG -3′
	reverse	5′- GCCGTGGAGTCCGACCACGGCTCCATAGCGTGCCAG -3′
A1-R_ ex_S	forward	5′- GAGGGCATTGGCCTTGCCACCGCCCGC -3′
	reverse	5′- GGTCGAACCGGTGATCAGAACGCGCTTGCCTTTG -3′
A1-R_ ex_L	forward	5′- CACGTGGATCCCGCCAACATCGATGAGACCATCGCCAGC -3′
	reverse	5′- TGAATTCAGGCCGACCTTGGCGCCTGCACG -3′

Solid, double, and dotted underlines show identical sequence used in mutation site, restriction site, and In-Fusion reaction, respectively.

medium containing 20 μg ml^{-1} kanamycin sulfate. Each of the bacterial cells was cultured to an exponential growth phase until turbidity at 600 nm reached 0.5–1.0. When turbidity was 1.0, the cell concentration in the culture was regarded as 1.0×10^9 cells ml^{-1}. Bacterial cells were collected and concentrations were adjusted to 2×10^8 strain A1 cells, 1×10^8 donor cells, and 0.4×10^8 helper cells. All cells were collected at 25 °C by centrifugation at 2,500 × *g* for 5 min and washed with 500 μl of 10 mM $MgCl_2$. After centrifugation, bacterial cells were resuspended in 50 μl of 10 mM $MgCl_2$ and spotted onto a 0.2-μm pore size membrane filter placed on a 0.5% (w/v) alginate medium plate containing 0.5% (w/v) yeast extract. After incubating overnight at 30 °C, bacterial cells on the filter were resuspended in 70 μl of 10 mM $MgCl_2$. The cell suspension was spread on a 0.5% (w/v) alginate minimal medium plate containing 20 μg ml^{-1} tetracycline hydrochloride. After incubation at 30 °C for 4 days, single colonies were subjected to streak culture on a fresh alginate minimal medium plate containing tetracycline hydrochloride. As a result, ampicillin-sensitive and tetracycline-resistant cells were obtained. The nucleotide sequence of mutated and inserted regions in the strain A1 mutant genome was confirmed by dideoxy chain termination (8) using an automated DNA sequencer (Model 3730xl; Applied Biosystems). In the strain A1 mutant genome,

the A1-R gene was substituted for the A1-R_G38D gene together with a tetracycline resistance gene.

Purification of Novel DEH Reductase from Strain A1. A novel DEH reductase, A1-R′, was purified from strain A1 cells as follows. Unless otherwise specified, all procedures were performed at 4 °C. Strain A1 cells were aerobically cultured in 6 liters of 0.5% (w/v) alginate minimal medium (1.5 liters per flask) at 30 °C for 48 h, collected by centrifugation at 6,000 × *g* for 5 min, and resuspended in 40 ml of 20 mM Tris-HCl (pH 7.5). Cells were ultrasonically disrupted (Insonator Model 201 M; Kubota) at 9 kHz for 20 min, and the clear solution obtained after centrifugation at 20,000 × *g* for 20 min was dialyzed against 1.5 liters of 20 mM Tris-HCl (pH 7.5) twice and used as the cell extract. The cell extract was applied to a TOYOPEARL DEAE-650 M column (6 × 10 cm) previously equilibrated with 20 mM Tris-HCl (pH 7.5). After washing with 20 mM Tris-HCl (pH 7.5), the absorbed proteins were eluted with a linear gradient of NaCl (0–500 mM, 600 ml) in 20 mM Tris-HCl (pH 7.5), with a 10-ml fraction collected every 10 min. DEH reducing activity was assayed in the presence of NADH or NADPH for all fractions. Fractions including DEH reducing activities in the presence of NADH are called active fractions hereafter. The active fractions, eluted with 200–300 mM NaCl, were dialyzed against 1.5 liters of 20 mM Tris-HCl (pH 7.5) twice. The resultant dialysate was saturated with 30% $(NH_4)_2SO_4$ and applied to a TOYOPEARL Butyl-650 M column (3 × 20 cm) previously equilibrated with 20 mM Tris-HCl (pH 7.5) containing 30% saturated $(NH_4)_2SO_4$. After washing with 20 mM Tris-HCl (pH 7.5) containing 30% saturated $(NH_4)_2SO_4$, the absorbed proteins were eluted with a linear gradient of saturated $(NH_4)_2SO_4$ (30–0%, 200 ml), with a 6-ml fraction collected every 6 min. The active fractions, eluted with 10–0% saturated $(NH_4)_2SO_4$, were combined and dialyzed against 1.5 liters of 20 mM Tris-HCl (pH 7.5) twice. The dialysate was concentrated by ultrafiltration with a Centriprep centrifugal filter (Millipore) to 0.63 ml at a concentration of 20-mg of protein ml^{-1} and applied to a HiLoad 16/60 Superdex 200 pg column (1.6 × 60 cm) previously equilibrated with 20 mM Tris-HCl (pH 7.5) containing 0.15 M NaCl. Proteins were eluted with the same buffer (120 ml) with a 2-ml fraction collected every 2 min. The active fractions were combined and dialyzed against 1.5 liters of 20 mM KPB (pH 7.0) twice. The dialysate was applied to a Hydroxylapatite column (1 × 3 cm) previously equilibrated with 20 mM KPB (pH 7.0). After washing with 20 mM KPB (pH 7.0), the absorbed proteins were eluted with a linear gradient of KPB (20–200 mM, 10 ml), with a 0.5-ml fraction collected every minute. The active fractions obtained on elution with 50–100 mM KPB were dialyzed against 1.5 liters of 20 mM Tris-HCl (pH 7.5) twice. The dialysate was applied to a Mono

Q HR 5/5 column (0.5 × 5 cm) previously equilibrated with 20 mM Tris-HCl (pH 7.5). After washing with 20 mM Tris-HCl (pH 7.5), the absorbed proteins were eluted with a linear gradient of NaCl (0–500 mM, 5 ml) in 20 mM Tris-HCl (pH 7.5), with a 0.5-ml fraction collected every minute. The active fractions, obtained on elution with 10–100 mM NaCl, were combined and applied to a HiLoad 16/60 Superdex 75 pg column (1.6 × 60 cm) previously equilibrated with 20 mM Tris-HCl (pH 7.5) containing 0.15 M NaCl. Proteins were eluted with the same buffer (120 ml), with a 2-ml fraction collected every 2 min, and the active fractions were combined and dialyzed against 1.5 liters of 20 mM Tris-HCl (pH 7.5) twice. The dialysate was applied to a HiLoad 26/10 Q-Sepharose HP column (2.6 × 10 cm) previously equilibrated with 20 mM Tris-HCl (pH 7.5). After washing with 20 mM Tris-HCl (pH 7.5), the absorbed proteins were eluted with a linear gradient of NaCl (0–500 mM, 200 ml) in 20 mM Tris-HCl (pH 7.5), with a 3-ml fraction collected every minute. The active fractions, eluted with 200–250 mM NaCl, were combined and confirmed as homogeneous by sodium dodecyl sulfate-polyacrylamide gel electrophoresis (SDS-PAGE). The purified proteins were dialyzed against 1.5 liters of 20 mM Tris-HCl (pH 7.5) twice and used as the native A1-R′ (nA1-R′).

Overexpression of A1-R′. The overexpression system for A1-R′ was constructed in *E. coli* cells as follows. To clone the A1-R′ gene, PCR was performed in a reaction mixture (50 μl) containing 1 unit of KOD-Plus-Neo (Toyobo), 50 ng of strain A1 genomic DNA, 15 pmol each of forward and reverse primers, 10 nmol of dNTPs, 75 nmol of $MgCl_2$, and KOD-Plus-Neo buffer (Toyobo). The 5′ end of the forward primer (A1-R′_NdeI) contains 15 bases homologous to 15 bases of pET21b (Novagen) from the *Nde*I site toward the opposite direction to the *Bam*HI site. In addition, the reverse primer (A1-R′_BamHI) possesses the same 15 bases of pET21b from the *Bam*HI site toward the opposite direction to the *Nde*I site. PCR conditions were as follows: 94 °C for 2 min, followed by 30 cycles at 98 °C for 10 s, 63 °C for 30 s, and 68 °C for 1 min. The resultant fragment was ligated with *Nde*I- and *Bam*HI-digested pET21b using the In-Fusion HD cloning Kit (Clontech). The resulting plasmid, designated as pET21b/A1-R′, includes the complete sequence of the A1-R′ gene with the original start and stop codons.

Purification of Recombinant A1-R′ from E. coli Cells. Unless otherwise specified, all procedures were performed at 4 °C. For expression, *E. coli* strain BL21(DE3) cells harboring pET21b/A1-R′ were aerobically cultured at 30 °C in 3 liters of LB medium (1.5 liters per flask). Cells were collected by centrifugation at 6,000 × *g* for 5 min and resuspended in 30 ml of 20 mM Tris-HCl (pH 7.5). The cells were ultrasonically disrupted at 9 kHz for 20 min, and the clear solution obtained on

centrifugation at 20,000 × *g* for 20 min was dialyzed against 1.5 liters of 20 mM Tris-HCl (pH 7.5) twice. The dialysate was used as the cell extract. The recombinant A1-R′ (rA1-R′) was purified from the cell extract using four columns: TOYOPEARL DEAE-650 M, TOYOPEARL Butyl-650 M, HiLoad 26/10 Q-Sepharose HP, and HiLoad 16/60 Superdex 200 pg. Each column was operated in the same way as described above.

Site-directed Mutagenesis. To construct multiple amino acid-substituted mutants or to insert the *Xho*I site, the KOD-Plus mutagenesis kit (Toyobo) was used. Single amino acid-substituted mutants were constructed using a QuikChange site-directed mutagenesis kit (Stratagene). The plasmid pET21b/A1-R′ was used as a template for A1-R′ mutants. The plasmid pET21b/A1-R, constructed in CHAPTER I, was used for A1-R mutants. Mutations were confirmed by DNA sequencing as described above. Expression and purification of the mutants were performed in the same way as rA1-R′ from *E. coli*.

Crystallization and Structure Determination. The rA1-R′ solution was concentrated and crystallized by sitting-drop vapor diffusion on a 96-well Intelli-plate (Veritas). Commercial screening kits (Hampton Research, Emerald BioSystems, and Jena Bioscience) were used to search for the crystallization conditions of rA1-R′. The reservoir solution volume was 70 µl in each well, and the droplet was prepared by mixing 1 µl of the protein solution with 1 µl of the reservoir solution. Crystals of A1-R′ in complex with NAD^+ (A1-R′·NAD^+) were prepared in the solution containing NAD^+. Each crystal of A1-R′ and A1-R′·NAD^+ picked off the nylon loop was directly placed in a cold nitrogen gas stream at −173 °C. X-ray diffraction images of the crystals were collected at −173 °C under the nitrogen gas stream and synchrotron radiation of wavelength 1.0000 Å at the BL-38B1 station of SPring-8 (Hyogo, Japan). Diffraction data were processed, merged, and scaled using the HKL2000 program package (DENZO and SCALEPACK) (9). The structure of A1-R′ was determined by molecular replacement using coordinates of A1-R (PDB-ID, 3AFM) as an initial model using the MOLREP program (10), in the CCP4 program package (11). Structure refinement was conducted using the Refmac5 program (12). Randomly selected 5% reflections were excluded from refinement and used to calculate R_{free}. After each refinement cycle, the model was manually adjusted using the Coot program (13). Water molecules were incorporated where the difference in density exceeded 3.0σ in $F_o - F_c$ map. Final model quality was checked using the PROCHECK program (14). Protein models were superimposed, and their root mean square deviation (r.m.s.d.) was determined using the LSQKAB program (15), which is a part of CCP4.

Figures of protein structures were prepared using the PyMOL program (16). Coordinates used in this CHAPTER were obtained from the Protein Data Bank (PDB) (www.wwpdb.org/) (17).

Analytical Methods. Polyacrylamide gel (12.5%) was used for SDS-PAGE (18). Proteins on the gel were stained with Coomassie Brilliant Blue R-250. DEH was prepared from sodium alginate by using exotype alginate lyase, Atu3025 (19), and purified using Centriprep centrifugal filter and Bio-Gel P-2 as described in CHAPTER I. Thiobarbituric acid method (20) was used for determination of DEH concentration. N-terminal amino acid sequence of the enzyme was determined by an Edman degradation method (21). To evaluate structural folding of the enzymes in 50 mM KPB (pH 7.0), circular dichroism (CD) spectra were measured in the far ultraviolet region (260–190 nm) using a J-720C spectropolarimeter (Jasco) at 25 °C. Samples were analyzed in a quartz cell with a path length of 0.1 mm. The content of helix and strand in the enzymes was estimated using the program CDPro. Structural folding in the enzymes was also investigated by measuring their thermal stabilities using differential scanning fluorimetry (DSF) as described previously (22).

Results

DEH Reducing Activity in A1-R-deficient Strain A1

To investigate the physiological significance of A1-R in strain A1, the strain A1 mutant (MT) with a deficiency in A1-R was constructed and characterized. The MT cells seem to produce A1-R_G38D instead of nA1-R. In A1-R_G38D, Gly-38 was replaced with Asp. As described in CHAPTER I, Gly-38 of A1-R was important for accommodating the phosphate group of NADPH due to its lack of side chain. In fact, A1-R_G38D mutant exhibited a significantly reduced enzymatic activity toward NADH (k_{cat}, 8.29 s^{-1}; K_m, 181 μM) as well as NADPH (k_{cat}, 5.16 s^{-1}; K_m, 178 μM). The specific activity of purified A1-R_G38D with 0.2 mM NADPH was drastically decreased to 1/24 (17.2 units mg^{-1}) that of the nA1-R (406 units mg^{-1}). This means that the strain A1 MT, which produces the A1-R_G38D mutant, shows negligible DEH reductase activity even in the presence of NADPH and NADH. MT cells showed little growth in 0.5% (w/v) alginate minimal medium containing 20 μg ml^{-1} tetracycline hydrochloride, although cell growth was observed after several acclimatizations. Specific DEH reducing activities in strain A1 wild-type (WT) and MT cell extracts were measured with 0.2 mM NADPH. The activity in the cell extract of MT corresponded to half as much as that of WT. The MT cell extract showed higher activity with 0.2 mM NADH

than with NADPH. These results suggest the existence of another DEH reductase with a preference for NADH.

Table 2-2
Purification of nA1-R′ and rA1-R′

	Total protein (mg)	Total activity (units)	Specific activity (units mg^{-1})	Yield (%)	Purification (fold)
Step		NADH / NADPH	NADH / NADPH	NADH / NADPH	NADH / NADPH
nA1-R′					
Cell extract	2050	3843 / 2065	1.87 / 1.01	100 / 100	1.00 / 1.00
TOYOPEARL DEAE-650M	330	1887 / 1322	5.72 / 4.01	49.1 / 64.0	3.05 / 3.97
TOYOPEARL Butyl-650M	32.7	1806 / 716.8	55.2 / 21.9	47.0 / 34.7	29.5 / 21.8
Superdex 200 pg	12.5	753.1 / 383.8	60.0 / 30.6	19.6 / 18.6	32.0 / 30.4
Hydroxylapatite	4.28	342.5 / 146.8	80.1 / 34.3	8.91 / 7.11	42.7 / 34.1
Mono Q HR	0.954	100.0 / 54.84	105 / 57.5	2.60 / 2.66	55.9 / 57.1
Superdex 75 pg	0.604	98.37 / 51.74	163 / 85.7	2.56 / 2.51	86.9 / 85.0
Q-Sepharose HP	0.118	51.73 / 25.64	439 / 218	1.35 / 1.24	234 / 216
rA1-R′		[NADH]	[NADH]	[NADH]	[NADH]
Cell extract	1730	458000	265	100	1.00
TOYOPEARL DEAE-650M	945	263000	278	57.5	1.05
TOYOPEARL Butyl-650M	742	240000	323	52.4	1.22
Q-Sepharose HP	313	129000	411	28.1	1.55
Superdex 200 pg	273	117000	428	25.5	1.62

Identification of Another Novel DEH Reductase

A novel DEH reductase, termed A1-R′, with a preference for NADH was purified 234-fold from strain A1 cells through seven steps of column chromatography with recovery of 1.35% (Table 2-2).

The purified nA1-R′ was homogeneous by SDS-PAGE (Fig. 2-2 A, left). The N-terminal amino acid sequence of the purified enzyme was determined to be ^{1}MFSDL^{5}. In a genome database search of strain A1 (23), this protein was assigned ID SPH1210. Based on the primary structure, the molecular weight of A1-R′ was calculated to be 27,337, with 258 amino acid residues. The sequence similarity between A1-R′ and A1-R was compared using ClustalW (clustalw.ddbj.nig.ac.jp/), and the resultant score was high, with 64% identity (Fig. 2-3 A). BLAST search (blast.ncbi.nlm.nih.gov) indicates that A1-R′ shows a high sequence identity (40–71%) with an SDR family enzyme, 3-ketoacyl-CoA reductase. A1-R′ includes a glycine-rich motif of the cofactor-binding Rossmann fold region (^{13}TG*XXX*G*X*G^{20}) and catalytic triad residues (Ser-150, Tyr-164, and Lys-168) conserved in the SDR family (Fig. 2-3 B). These results demonstrate that A1-R′ belongs to the SDR family.

Enzymatic Properties of nA1-R′

(i) Molecular mass

The molecular mass of nA1-R′ was estimated to be 25 kDa via SDS-PAGE (Fig. 2-2 A, left). Elution volume of nA1-R′ after HiLoad 16/60 Superdex 200 pg size exclusion chromatography showed that the molecular mass of nA1-R′ is ~110 kDa (data not shown). These results indicated that nA1-R′ exists as a homotetramer.

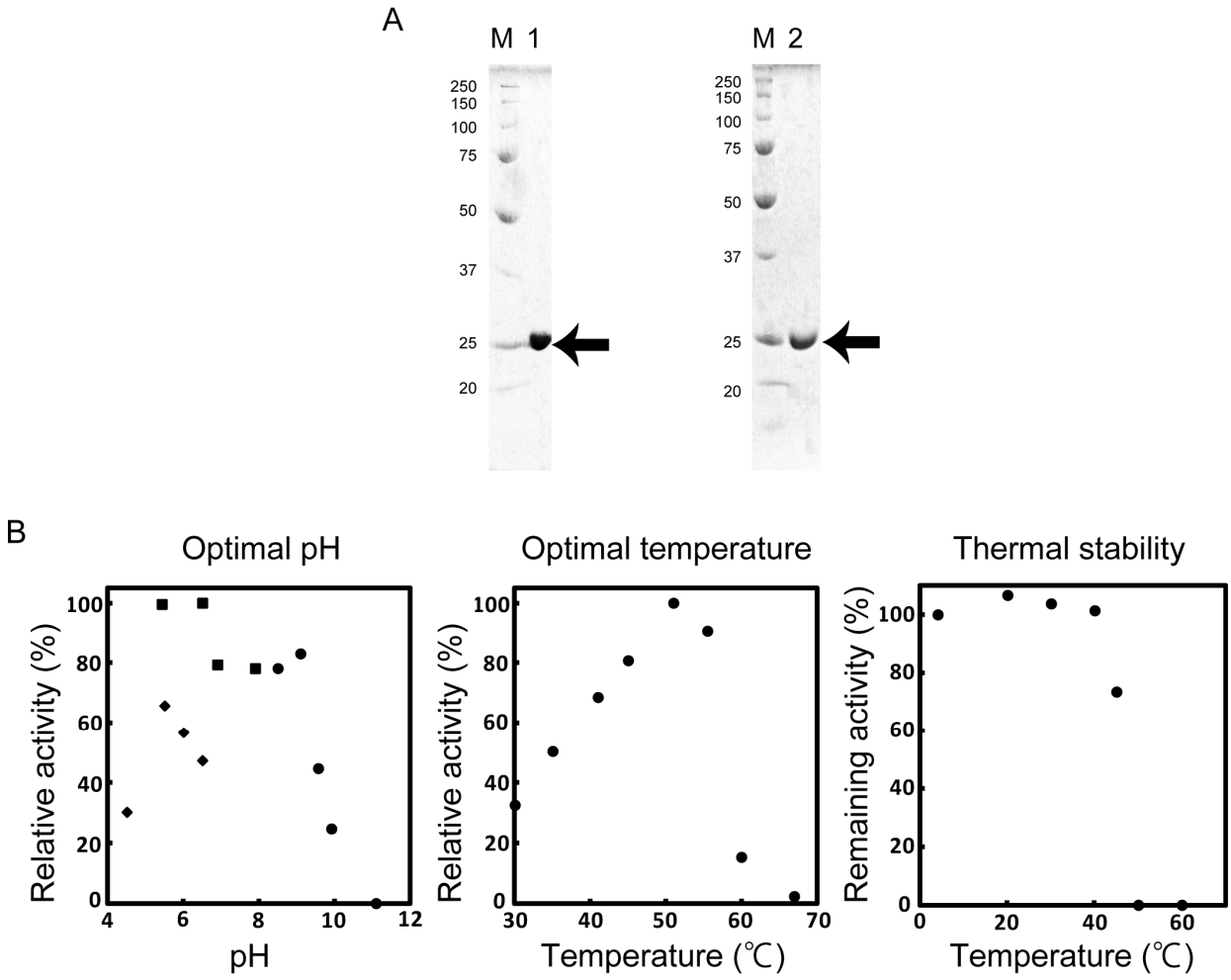

Fig. 2-2. Properties of A1-R′. (A) SDS-PAGE of purified A1-R′. Lane M, molecular weight standards; lane 1, purified nA1-R′ (5 μg); lane 2, purified rA1-R′ (5 μg). The arrow indicates the position of the enzyme. (B) Effects of pH and temperature on the activity and thermal stability of nA1-R′. Left, optimal pH. Activity was assayed with sodium acetate shown as diamond (pH 4.5, 5.5, 6.0, and 6.5), KPB shown as square (pH 5.4, 6.5, 6.9, and 7.9), and glycine-NaOH shown as circle (pH 8.5, 9.1, 9.6, 10, and 11). Sodium acetate appears to inhibit enzymatic activity compared with KPB. Activity at pH 6.5 in KPB was taken as 100%. Center, optimal temperature. Activity at 51 °C was taken as 100%. Right, thermal stability. nA1-R′ was preincubated for 5 min at various temperatures (as indicated), and the residual activity was measured. The activity of the enzyme preincubated at 4 °C for 5 min was taken as 100%.

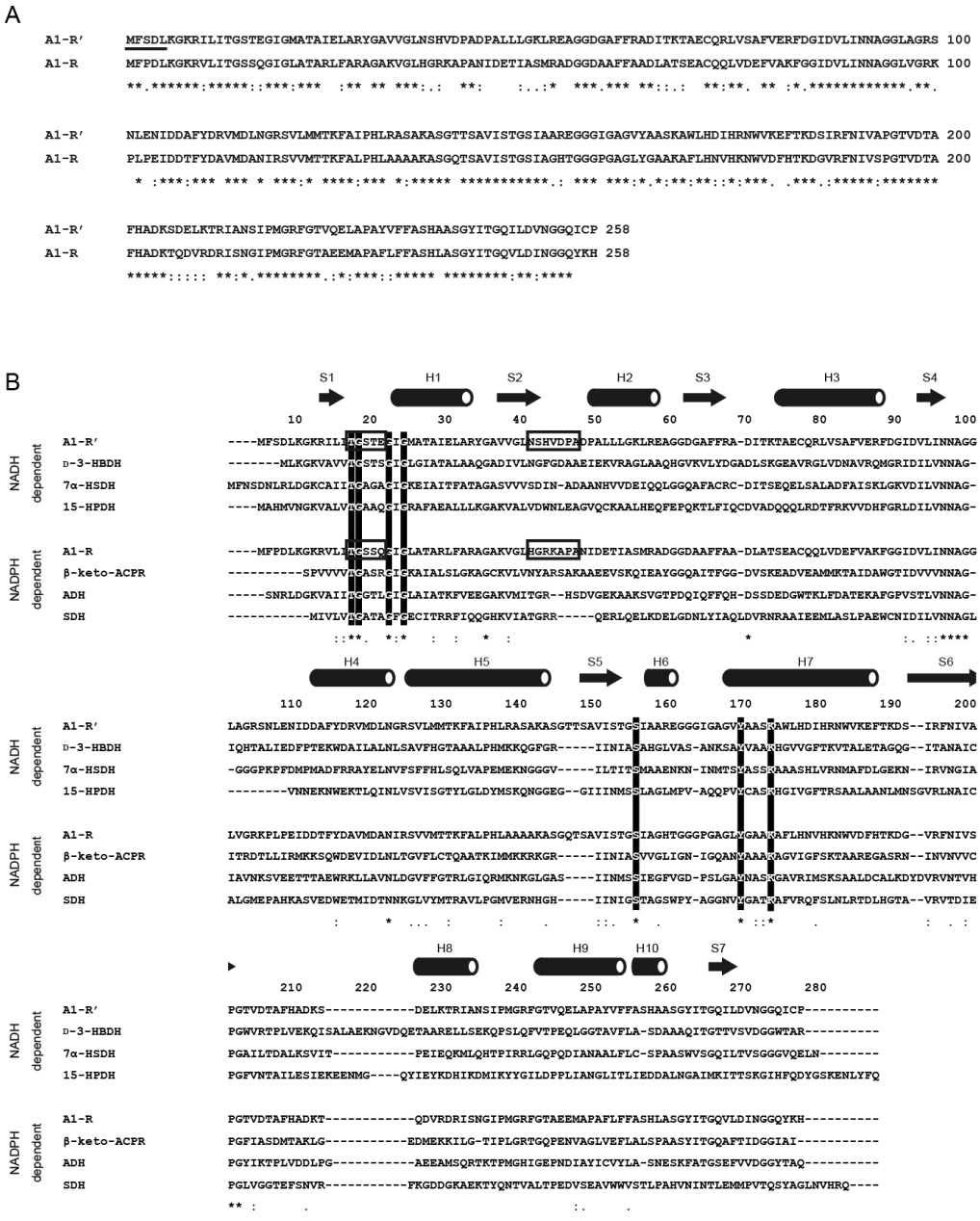

Fig. 2-3. Sequence alignment. (A) Alignment between A1-R′ and A1-R. N-terminal determined residues of A1-R′ are underlined. (B) Alignment between NADH and NADPH-dependent SDR family enzymes. Conserved residues among SDR family enzymes, TG*XXX*G*X*G motif and catalytic triad (Ser, Tyr, and Lys) are indicated by open letters. Asterisk (*), colon (:), and period (.) indicate that residues are identical, highly similar, and moderately similar, respectively. Arrows and tubes over the alignment show β-strand and α-helix, respectively. Structural determinants (two loops) of the coenzyme requirement are boxed. Each enzyme is described as follows: D-3-HBDH, D-3-hydroxybutyrate dehydrogenase (PDB-ID, 2ZTL) from *Pseudomonas fragi*; 7α-HSDH, 7-α-hydroxysteroid dehydrogenase (PDB-ID, 1AHI) from *E. coli*; 15-HPDH, 15-hydroxy prostaglandin dehydrogenase (PDB-ID, 2GDZ) from *Homo sapiens*; β-keto-ACPR, β-keto-acyl carrier protein reductase (PDB-ID, 1EDO) from *Brassica napus*; ADH, alcohol dehydrogenase (PDB-ID, 1NXQ) from *Lactobacillus brevis*; SDH, serine dehydrogenase (PDB-ID, 3ASV) from *E. coli*.

Table 2-3
Effects of various compounds on the activity of nA1-R′

Compounds		Concentration (mM)	Activity (%)[a]
None	(NADPH)		38[b]
	(NADH)		100
Thiol reagents			
Dithiothreitol		1	97
Glutathione (reduced form)		1	107
2-Mercaptoethanol		1	107
Iodoacetic acid		1	98
p-Chloromercuribenzoic acid		1	94
Chelator			
EDTA		1	113
Sugars			
L-Fucose		5	98
D-Galactose		5	98
D-Glucose		5	100
D-Glucuronic acid		5	103
D-Mannose		5	102
L-Rhamnose		5	100
D-Xylose		5	98
D-Sucrose		5	101
D-Galacturonic acid		5	103
Metals			
$AlCl_3$		1	76
$MgCl_2$		1	115
$MnCl_2$		1	106
$CaCl_2$		1	121
$CoCl_2$		1	95
$ZnCl_2$		1	114
$HgCl_2$		0.01	83
NaCl		1	97
KCl		1	95
LiCl		1	102

[a] Relative activities (%) in a reaction mixture containing various compounds at the indicated concentrations are shown. The activity in the absence of the compound was taken as 100%.

[b] The value was determined when 0.2 mM NADH was replaced with 0.2 mM NADPH.

(ii) Optimal pH, optimal temperature, and thermal stability

nA1-R′ was the most active at pH 6.5 (KPB) and 51 °C, and stable below at 40 °C (Fig. 2-2 B).

(iii) Chemicals

The DEH reduction reaction was conducted at 30 °C in the presence or absence of different compounds, such as thiol reagents, the chelator EDTA, sugars, and metals. Almost all the chemicals tested had no significant effect (76–121%) on the reaction of nA1-R′ (Table 2-3).

(iv) Kinetic Parameters

Kinetic parameters of nA1-R′ were determined based on the saturation curve of enzyme activities at various concentrations of substrates (Table 2-4). k_{cat} and K_m values were 227 s^{-1} and 4790 μM toward DEH, 280 s^{-1} and 15.5 μM toward NADH, and 233 s^{-1} and 224 μM toward NADPH. k_{cat} scores toward NADH and NADPH were similar, although the affinity for NADH

was 14.5-fold higher compared with that for NADPH. This indicates that nA1-R′ shows a preference for NADH.

rA1-R′ from *E. coli*

rA1-R′ was purified to 1.62-fold from recombinant *E. coli* cells through four steps of column chromatography (Table 2-2). rA1-R′ was homogeneous via SDS-PAGE (Fig. 2-2 A, right). Kinetic parameters of rA1-R′ were comparable with those of nA1-R′.

Table 2-4
Kinetic parameters of nA1-R′ and rA1-R for DEH, NADH, and NADPH

	nA1-R′			rA1-R		
	k_{cat} (s^{-1})	K_m (μM)	$k_{cat}\,K_m^{-1}$ ($s^{-1}\,mM^{-1}$)	k_{cat} (s^{-1})	K_m (μM)	$k_{cat}\,K_m^{-1}$ ($s^{-1}\,mM^{-1}$)
DEH	227 ± 16.2	4790 ± 630	47.4	197 ± 8.9	1930 ± 98	102[a]
NADH	280 ± 10.2	15.5 ± 2.84	18100	25.3 ± 5.7	192 ± 75	132
NADPH	233 ± 44.6	224 ± 78	1040	220 ± 7.1	9.55 ± 1.4	23000

[a] The kinetic parameters of rA1-R for DEH are cited from CHAPTER I.

Crystal Structure of A1-R′

A1-R′ and A1-R were very similar except for their coenzyme requirements, suggesting that local structural differences cause these variations. X-ray crystallography of A1-R′ was conducted to clarify structural determinants for the coenzyme requirement. An A1-R′ crystal was obtained in a droplet consisting of 20% (v/v) polyethylene glycol 400, 0.05 M sodium potassium phosphate (pH 6.2), 0.1 M NaCl, and 15.6 mg ml^{-1} rA1-R′. The crystal structure of A1-R′ was determined at a resolution of 1.80 Å by the molecular replacement method. After refinement, R- and R_{free}-factors were 18.2 and 20.2%, respectively. Data collection and refinement statistics are summarized in Table 2-5. The refined model had two identical monomers in an asymmetric unit, termed molecules A and B. One phosphate molecule was bound to molecule A, and two phosphate molecules were bound to molecule B. Residues 1 and 199–212 of molecule A, and residues 1 and 197–213 of molecule B were unable to be assigned because the residues in this region of the electron density map are disordered. These residues are considered to form a long flexible loop. Structures of molecules A and B are basically identical because the r.m.s.d. between both was calculated as 0.232 Å. A1-R′ has 10 α-helices and seven β-strands and consists of a three-layered structure, α/β/α, with a coenzyme-binding site, called Rossmann fold (Figs. 2-3 B, and 2-4 A, B) (24). The overall structure of A1-R′ mimics that of A1-R (Fig. 2-4 A, B). The torsion angle of the Thr-141 peptide bond was the outlier in the Ramachandran plot analysis. Thr-141 is on the loop consisting of only

three residues between parallel α-helix H5 and β-strand S5. As a result, Thr-141 forms a hydrogen bond with Ser-139, and the loop is drastically bent.

Catalytic Triad in A1-R′

Based on the sequence alignment (Fig. 2-3 B), Ser-150, Tyr-164, and Lys-168 of A1-R′ are suggested to function as a catalytic triad. To confirm their roles as catalytic residues, three A1-R′ mutants (S150A, Y164F, and K168A, in which Ser-150, Tyr-164, and Lys-168 were replaced with Ala, Phe, and Ala, respectively) were constructed by site-directed mutagenesis. The mutants were purified in the same way as WT rA1-R′, and their kinetic parameters (k_{cat} and K_m) for DEH were determined as follows: WT, 201 s^{-1} and 5.68 mM; S150A, 0.00257 s^{-1} and 13.3 mM; Y164F, 0.000307 s^{-1} and 21.2 mM; and K168A, 0.373 s^{-1} and 5.07 mM. Compared with WT rA1-R′, all the mutants significantly decreased the enzymatic activity (k_{cat} K_m^{-1}) (S150A, 0.00054%; Y164F, 0.000040%; and K168A, 0.21%). In particular, Y164F decreased the k_{cat} value drastically to 0.00015%. The arrangement of each residue of the catalytic triad (Ser-150, Tyr-164, and Lys-168) in the crystal structure of A1-R′ was identical to that of many SDR family enzymes, *e.g.* 3α,20β-hydroxysteroid dehydrogenase (PDB-ID, 2HSD). Because the involvement of the catalytic triad in the reactions catalyzed by SDR family enzymes has been well documented (25-27), the roles of Ser-150, Tyr-164, and Lys-168 in the A1-R′ reaction were postulated based on structural comparison with enzymes of the well characterized SDR family as follows: Ser-150 stabilizes the reaction intermediates; Tyr-164 acts as a catalytic base in the reduction reaction; and Lys-168 is crucial for the proper orientation of the coenzyme and lowering the pK_a of Tyr-164.

Binding Mode to Coenzyme

To clarify the structural difference of the coenzyme-binding mode between A1-R′ and A1-R, the A1-R′·NAD^+ complex crystal was obtained in the solution containing 0.85% (v/v) polyethylene glycol 400, 0.85 M $(NH_4)_2SO_4$, 43 mM sodium Hepes (pH 7.5), 0.5 mM NAD^+, and 15.6 mg ml^{-1} rA1-R′. The initial phase was determined by molecular replacement using coordinates of the ligand-free A1-R′ as a search model. After refinement, final structure was determined at a 2.67 Å resolution. Two monomers, termed molecules A and B, were present in an asymmetric unit. In molecule B, NAD^+ bound to Rossmann fold (Fig. 2-4 C, D). In addition, four sulfate molecules were bound to molecule A, and one sulfate molecule was bound to molecule B. Residues 198–213 of molecule A and residues 197–213 of molecule B were unable to be assigned because the residues in this region of the electron density map are disordered. The r.m.s.d. value between molecules A and B of A1-R′·NAD^+ was calculated as 0.314 Å, demonstrating that there is no significant

Table 2-5
Statistics for X-ray diffraction and structure refinement

	A1-R′	A1-R′·NAD^+
Data collection		
Wavelength (Å)	1.0000	1.0000
Space group	$P3_121$	$P3_121$
Unit cell parameters (Å, °)	$a = b = 87.7$, $c = 139.6$	$a = b = 87.9$, $c = 139.8$
Resolution limit (Å)	50.0 – 1.80 (1.86 – 1.80)[a]	50.0 – 2.67 (2.77 – 2.67)[a]
Total reflections	682,105	219,436
Unique reflections	58,400	18,404
Redundancy	11.7 (11.4)	11.9 (12.2)
Completeness (%)	100 (100)	100 (99.9)
$I/\sigma(I)$	47.3 (5.8)	43.4 (9.0)
R_{merge} (%)	6.0 (38.4)	7.4 (30.6)
Refinement		
Final model	486 residues, 3 PO_4^{3-}, 294 water molecules	483 residues, 5 SO_4^{2-}, 1 NAD^+, 81 water molecules
Resolution limit (Å)	33.4 – 1.80 (1.85 – 1.80)	33.5 – 2.67 (2.73 – 2.67)
Used reflections	55,375 (3,971)	17,397 (1,227)
Completeness (%)	99.8 (98.7)	99.7 (99.4)
R-factor (%)	18.2 (21.7)	19.4 (26.5)
R_{free} (%)	20.2 (24.5)	27.6 (35.5)
Average B-factor (Å^2)		
Protein		
Molecule A	23.5	47.5
Molecule B	24.8	52.2
Waters	33.6	38.5
PO_4^{3-}		
Molecule C1	39.1	
Molecule C2	65.3	
Molecule C3	59.3	
SO_4^{2-}		
Molecule D1		24.2
Molecule D2		62.0
Molecule D3		78.5
Molecule D4		63.8
Molecule D5		83.4
NAD^+		61.3
r.m.s.d.		
Bond (Å)	0.0046	0.0099
Angle (°)	0.97	1.40
Ramachandran plot (%)		
Favored regions	96.6	95.8
Allowed regions	3.0	3.8
Outliers	0.4	0.4

[a] Data on highest shells are given in parenthesis.

conformational change between NAD^+-free and -bound A1-R′. The coenzyme-binding site of A1-R′ was compared with that of A1-R (Fig. 2-5 A, B). In particular, the residues around the nucleoside ribose 2′ region of coenzyme bound were different between A1-R′ and A1-R, postulating that these are involved in coenzyme specificity. The electric charge of the molecular surface at pH 7.0 around the coenzyme-binding site of A1-R′ and A1-R is shown in Fig. 2-5 C, D. In A1-R′·NAD^+, the

A1-R′ site bound to the nucleoside ribose 2′ region of the coenzyme is negatively charged by the influence of Glu-17. However, the corresponding site in A1-R is positively charged by Arg-39 and Lys-40. Negative electric charge of Glu-17 may cause electrostatic repulsion to nucleoside ribose 2′ phosphate group of NADPH. Nevertheless, the positive charge of Arg-39 and Lys-40 is considered to cause electrostatic attraction. The space in A1-R′ is shallower compared with that in A1-R. The difficulty in binding of NADPH to A1-R′ is partly because of this smaller space at the nucleoside ribose 2′-binding site.

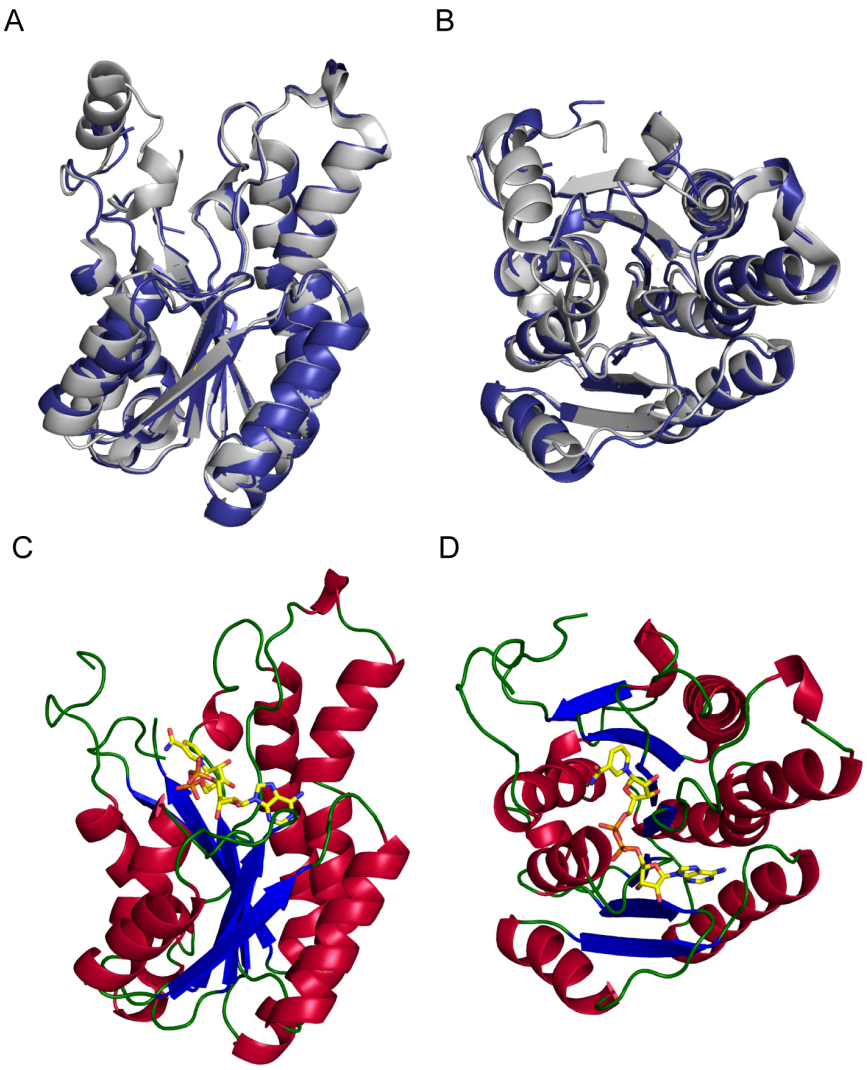

Fig. 2-4. Structures of A1-R′ and A1-R′·NAD$^+$. (A), (B) Overall structure of A1-R′ superimposed on A1-R based on Cα. Blue, A1-R′; gray, A1-R. The structure of (B) is rotated 90° toward the reader relative to that of (A). (C), (D) A1-R′·NAD$^+$ complex structure. A1-R′ molecule is shown as a ribbon model, and each color indicates the following: blue, β-strand; red, α-helix, green, loop. NAD$^+$ molecule is shown by a stick model, and each color indicates following: yellow, carbon atom; blue, nitrogen atom; orange, phosphorus atom; red, oxygen atom. The structure of (D) is rotated 90° toward the reader relative to that of (C).

Conversion of Coenzyme Requirement

The residues involved in electric charge and space formation at the binding site of the nucleoside ribose 2′ region of the coenzyme are on the two loops. In A1-R′, the short and long loops are composed of five residues (^{13}TGSTE^{17}) and seven residues (^{37}NSHVDPA^{43}), respectively (Fig. 2-5 E). These two loops are candidates of structural determinants of the coenzyme requirement because both A1-R′ and A1-R are very similar except for this requirement. To assess this hypothesis, A1-R′ and A1-R mutants were constructed, in which the loops were mutually exchanged. The terms "ex_S", "ex_L", and "ex_W" mean the mutants in which short loop, long loop, and both loops were exchanged, respectively. To validate the structural folding of the A1-R′ and A1-R mutants that have had their loop(s) exchanged, the purified mutants and the WT enzymes were subjected to CD spectroscopy (Fig. 2-6 A, B). The CD spectrum of each mutant was comparable with that of the corresponding WT enzyme. Subsequently, the secondary structural elements were determined by analyzing the CD profiles using the program CDPro. No significant differences in secondary structure were observed between the WT and mutant enzymes. This CD analysis suggested that all the mutants were properly folded, in manners similar to those of their respective WT enzymes, and that the enzymatic activity of the mutants was influenced by mutation, not misfolding. Kinetic parameters of the mutants for NADH, NADPH, and DEH were determined (Table 2-6) after purification in the same way as rA1-R′. There were no significant differences between the K_m values for DEH of the WT enzymes and those of the mutant enzymes as follows: WT rA1-R′, 4.8 mM; A1-R′ mutants, 2.8–4.5 mM; WT rA1-R, 1.9 mM; and A1-R mutants, 1.7–3.5 mM. These results suggest that the affinities of the mutants for the DEH substrate were comparable with those of their respective WT enzymes. Both A1-R′_ex_S and A1-R′_ex_L increased affinity with NADPH. A1-R′_ex_W synergistically increased affinity with NADPH, although these three A1-R′ mutants displayed a decreased k_{cat} for NADPH compared with that for WT rA1-R′. These results suggest that the two loops play a key role in affinity with NADPH. A1-R′_ex_W drastically increased the k_{cat} K_m^{-1} value for NADPH, whereas its k_{cat} K_m^{-1} value for NADH decreased, indicating that A1-R′_ex_W showed an 85-fold preference for NADPH, compared with NADH. Moreover, kinetic parameters of A1-R′_ex_W for NADPH were comparable with those of WT rA1-R for NADPH. In contrast to conversion in dependence from NADH to NADPH, three A1-R mutants exhibited decreased activity for NADH compared with that for WT rA1-R.

TABLE 2-6
Kinetic parameters of the WT and mutants of A1-R′ and A1-R for NADH, NADPH, and DEH

	NADH			NADPH				DEH		
Enzyme	k_{cat} (s^{-1})	K_m (μM)	k_{cat} K_m^{-1} (s^{-1} mM^{-1})	k_{cat} (s^{-1})	K_m (μM)	k_{cat} K_m^{-1} (s^{-1} mM^{-1})	NADH/NADPH [a]	k_{cat} (s^{-1})	K_m (mM)	k_{cat} K_m^{-1} (s^{-1} mM^{-1})
rA1-R′ WT	274 ± 4.8	24.3 ± 1.5	11300	233 ± 15	272 ± 30	857	13	227 ±16.2	4.79 ± 0.63	47.4
A1-R′_ex_S	77.5 ± 4.7	20.4 ± 5.2	3800	109 ± 7.0	28.4 ± 6.9	3840	0.99	172 ± 2.65	3.32 ± 0.11	51.8
A1-R′_ex_L	33.6 ± 10	493 ± 220	68.2	110 ± 11	45.5 ± 15	2420	0.028	161 ± 6.31	2.77 ± 0.24	58.1
A1-R′_ex_W	134 ± 26	217 ± 78	618	149 ± 1.3	2.85 ± 0.31	52300	0.012	225 ± 6.65	4.45 ± 0.25	50.6
rA1-R WT	25.3 ± 5.7	192 ± 75	132	220 ± 7.1	9.55 ± 1.4	23000	0.0057	197 ± 8.9	1.93 ± 0.098	102
A1-R_ex_S	3.77 ± 0.47	623 ± 100	6.05	193 ± 18	512 ± 70	377	0.016	226 ± 6.02	3.54 ± 0.19	48.9
A1-R_ex_L	4.25 ± 2.0	321 ± 240	13.2	N.D.	N.D.	N.D.	N.D.	5.47 ± 0.186	1.66 ± 0.15	1.32
A1-R_ex_W	6.80 ± 3.5	2580 ± 1400	2.64	2.03 ± 3.0	5600 ± 8600	0.363	7.27	8.66 ± 0.257	3.04 ± 0.19	2.85

N.D., not determined due to low activity.

[a] The k_{cat} K_m^{-1} value toward NADH/ the k_{cat} K_m^{-1} value toward NADPH.

Discussion

A novel NADH-dependent DEH reductase, A1-R′, was identified in strain A1. To date, two NADH-dependent DEH reductases from *Vibrios* have been reported (3,4), although their enzyme properties and structures remain to be clarified. In this CHAPTER, structure/function relationship of NADH-dependent DEH reductase was clarified for the first time.

Previously, Tomita *et al.* (28) succeeded in converting the coenzyme requirement in the non-SDR family enzyme, malate dehydrogenase (MDH), by multiple site-directed mutagenesis. Exchange of one of the MDH loops corresponding to the A1-R′ loops also contributes to conversion of the coenzyme requirement, although the loop mutant exhibited a reduced enzymatic activity (k_{cat} K_m^{-1}) compared with the WT enzyme. Recently, Brinkmann-Chen *et al.* (29) established a method for conversion of the coenzyme requirement in the non-SDR family enzymes, ketol-acid reductoisomerase family enzymes, through mutation of some residues in a loop and succeeding random mutations.

Conversion of the coenzyme requirement in A1-R′ was achieved by exchange of two loops close to the coenzyme-binding site. The A1-R′ mutant with A1-R-typed loops showed a high k_{cat} score and low K_m value for NADPH, corresponding to those of WT rA1-R for NADPH. These results demonstrated that the nature of the two loops determines the coenzyme requirement. Because SDR family enzymes commonly have the two loops in the Rossmann fold, the exchange of the two loops is expected to be a potential method to convert the coenzyme requirement of other SDR enzymes. The SDR family includes several metabolic enzymes, and thus the regulation of the coenzyme requirement will enable maintenance of the cellular oxidation/reduction balance. Well

balanced coenzyme concentration can lead to high efficiency and continuous production of useful chemicals.

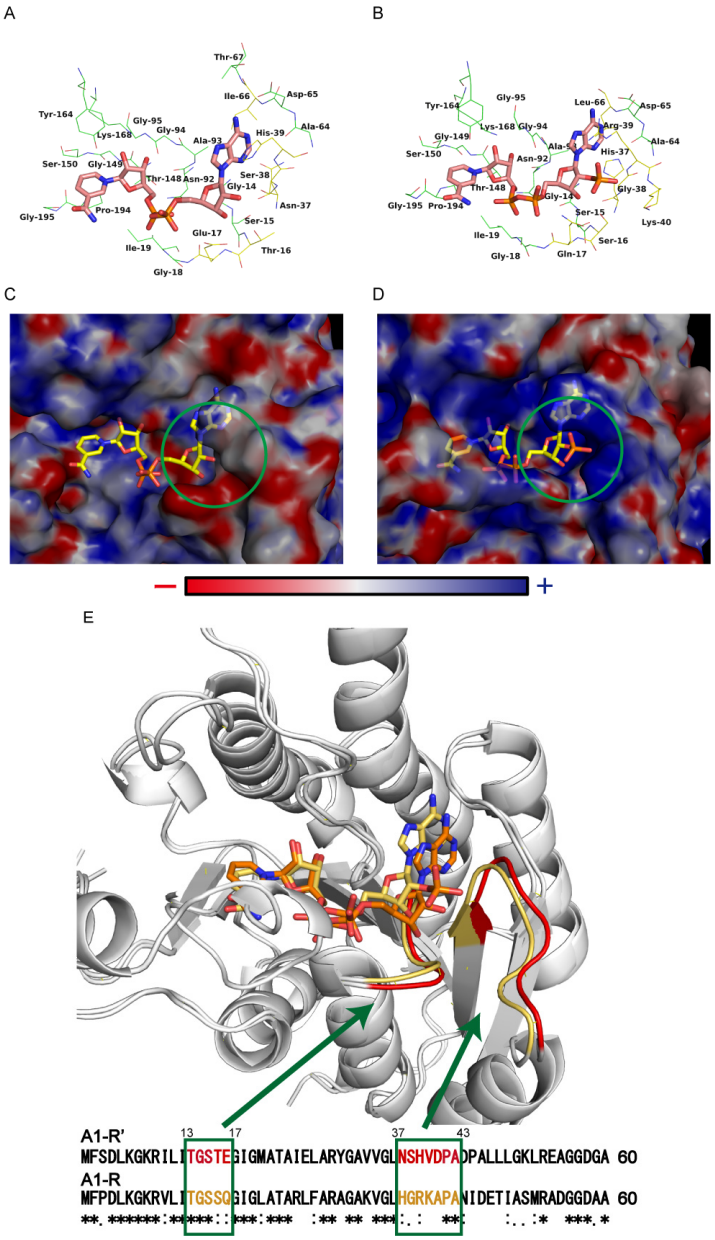

Fig. 2-5. Comparison between A1-R′ and A1-R. (A) Coenzyme-binding site in A1-R′·NAD^+ complex structure. (B) Coenzyme-binding site in A1-R·$NADP^+$ complex structure (PDB-ID, 3AFN). Carbon atoms of NAD^+ or $NADP^+$ are colored pink. Residues within a distance of 4 Å from the coenzyme are shown. Blue, nitrogen atom; orange, phosphorus atom; red, oxygen atom. Carbon atoms of conserved and nonconserved residues between A1-R′ and A1-R are colored green and yellow, respectively. (C) Surface electrostatic potentials around NAD^+ molecule in A1-R′·NAD^+ complex structure. (D) Surface electrostatic potentials around $NADP^+$ molecule in A1-R·$NADP^+$ complex structure (PDB-ID, 3AFN). In (C) and (D), electric charges are calculated at pH 7.0. Blue and red indicate basic and acidic, respectively. Green circle shows the binding site around the nucleoside ribose 2′ region of the coenzyme. (E) Relationship between loops and primary structure. A1-R′ is superimposed on A1-R based on Cα. Loops and primary structures of A1-R′ and A1-R are colored red and yellow, respectively.

Interestingly, NADPH-dependent A1-R′_ex_W showed high activity, whereas NADH-dependent A1-R_ex_W showed low activity (Table 2-6). Therefore, the tertiary and quaternary structures of A1-R′_ex_W and A1-R_ex_W were determined by X-ray crystallography, even though no significant difference in secondary structure was observed between the WT enzymes and their respective mutants by CD spectroscopy. The overall structures of A1-R′_ex_W

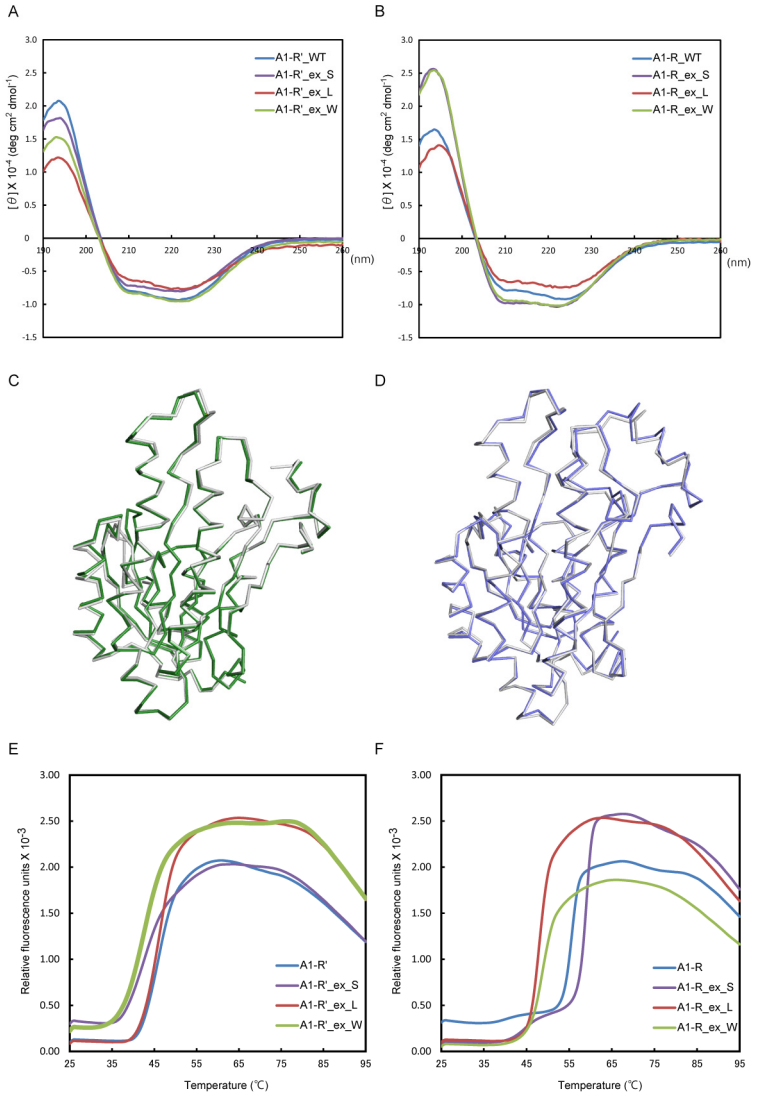

Fig. 2-6. Structural validation of the WT and mutants of A1-R′ and A1-R. (A) CD profiles of WT rA1-R′ and its mutants at 1 mg ml^{-1}. (B) CD profiles of WT rA1-R and its mutants at 1 mg ml^{-1}. WT, ex_S, ex_L, and ex_W are colored blue, purple, red, and green, respectively, in (A) and (B). (C) Superimposition of the main chains of A1-R′_ex_W (green) and WT rA1-R′ (gray). (D) Superimposition of the main chains of A1-R_ex_W (blue) and WT rA1-R (gray). (E) Fluorescence profiles of WT rA1-R′ and its mutants used in the DSF analysis. (F) Fluorescence profiles of WT rA1-R and its mutants used in the DSF analysis. WT, ex_S, ex_L, and ex_W are colored blue, purple, red, and green, respectively, in (E) and (F).

and A1-R_ex_W superimposed well on those of WT A1-R′ and A1-R, respectively (Fig. 2-6 C, D), indicating that the structural folding of both mutants was identical to that of their respective WT enzymes. The significant decrease in enzymatic activity exhibited by A1-R_ex_W is probably due to the exchange of the two loops, not to misfolding. The A1-R′-type loop(s) were considered to be unsuitable for interaction with the basic scaffold of A1-R. In fact, the loop mutants A1-R_ex_W and A1-R_ex_L were found to be less thermally stable than WT rA1-R through DSF analysis. The fluorescence of SYPRO Orange that bound to denatured proteins was measured during heat treatment (from 25 to 95 °C). The melting temperatures (T_m) of the WT and mutant enzymes were determined as the transition midpoint in the fluorescence profile. The fluorescence profiles of A1-R_ex_W (T_m, 49.2 °C) and A1-R_ex_L (T_m, 47.8 °C) were significantly shifted to a lower temperature, compared with that of WT rA1-R (T_m, 55.6 °C) (Fig. 2-6 F), suggesting that WT rA1-R was thermally more stable than the mutants. However, the T_m (42.7 °C) of A1-R′_ex_W was slightly lower than that (T_m, 45.7 °C) of WT rA1-R′ (Fig. 2-6 E).

The question as to why strain A1 has two different DEH reductases will be the focus of future studies. DEH is demonstrated to be toxic to bacterial cells (30), suggesting that strain A1 cells are obliged to reduce DEH immediately to detoxify and metabolize alginate, although the intracellular NAD^+/NADH ratio is influenced by the outer environment (*i.e.* oxygen concentration). To reduce DEH under any circumstance, strain A1 may have two types of reductases with different coenzyme requirements. In the case of a high level of NADH, strain A1 cells reduce DEH by A1-R′ and conserve NADPH for assimilation. As intracellular levels of NADH decrease, A1-R may reduce DEH using NADPH.

References

1. Stokstad, E. (2012) Biofuels. Engineered superbugs boost hopes of turning seaweed into fuel. *Science* **335**, 273
2. Takeda, H., Yoneyama, F., Kawai, S., Hashimoto, W., and Murata, K. (2011) Bioethanol production from marine biomass alginate by metabolically engineered bacteria. *Energy Environ. Sci.* **4**, 2575-2581
3. Wargacki, A. J., Leonard, E., Win, M. N., Regitsky, D. D., Santos, C. N., Kim, P. B., Cooper, S. R., Raisner, R. M., Herman, A., Sivitz, A. B., Lakshmanaswamy, A., Kashiyama, Y., Baker, D., and Yoshikuni, Y. (2012) An engineered microbial platform for direct biofuel production from brown macroalgae. *Science* **335**, 308-313
4. Enquist-Newman, M., Faust, A. M. E., Bravo, D. D., Santos, C. N. S., Raisner, R. M., Hanel, A., Sarvabhowman, P., Le, C., Regitsky, D. D., Cooper, S. R., Peereboom, L., Clark, A., Martinez, Y., Goldsmith, J., Cho, M. Y., Donohoue, P. D., Luo, L., Lamberson, B., Tamrakar, P., Kim, E. J., Villari, J. L., Gill, A.,

Tripathi, S. A., Karamchedu, P., Paredes, C. J., Rajgarhia, V., Kotlar, H. K., Bailey, R. B., Miller, D. J., Ohler, N. L., Swimmer, C., and Yoshikuni, Y. (2013) Efficient ethanol production from brown macroalgae sugars by a synthetic yeast platform. *Nature* **505**, 239-243

5. Bradford, M. M. (1976) A rapid and sensitive method for the quantitation of microgram quantities of protein utilizing the principle of protein-dye binding. *Anal. Biochem.* **72**, 248-254
6. Kimbara, K., Hashimoto, T., Fukuda, M., Koana, T., Takagi, M., Oishi, M., and Yano, K. (1989) Cloning and sequencing of two tandem genes involved in degradation of 2,3-dihydroxybiphenyl to benzoic acid in the polychlorinated biphenyl-degrading soil bacterium *Pseudomonas* sp. strain KKS102. *J. Bacteriol.* **171**, 2740-2747
7. Ruvkun, G. B., and Ausubel, F. M. (1981) A general method for site-directed mutagenesis in prokaryotes. *Nature* **289**, 85-88
8. Sanger, F., Nicklen, S., and Coulson, A. R. (1977) DNA sequencing with chain-terminating inhibitors. *Proc. Natl. Acad. Sci. U.S.A.* **74**, 5463-5467
9. Otwinowski, Z., and Minor, W. (1997) Processing of X-ray diffraction data. *Methods Enzymol.* **276**, 307-326
10. Vagin, A., and Teplyakov, A. (2010) Molecular replacement with *MOLREP*. *Acta Crystallogr. D Biol. Crystallogr.* **66**, 22-25
11. Collaborative Computational Project, N. (1994) The *CCP4* suite: programs for protein crystallography. *Acta Crystallogr. D Biol. Crystallogr.* **50**, 760-763
12. Murshudov, G. N., Vagin, A. A., and Dodson, E. J. (1997) Refinement of macromolecular structures by the maximum-likelihood method. *Acta Crystallogr. D Biol. Crystallogr.* **53**, 240-255
13. Emsley, P., and Cowtan, K. (2004) *Coot*: model-building tools for molecular graphics. *Acta Crystallogr. D Biol. Crystallogr.* **60**, 2126-2132
14. Laskowski, R. A., MacArthur, M. W., Moss, D. S., and Thornton, J. M. (1993) *PROCHECK*: a program to check the stereochemical quality of protein structures. *J. Appl. Crystallogr.* **26**, 283-291
15. Kabsch, W. (1978) A discussion of the solution for the best rotation to relate two sets of vectors. *Acta Crystallogr. A* **34**, 827-828
16. Delano, W. L. (2002). *The PyMOL Molecular Graphics System*, DeLano Scientific LLC, San Carlos, CA
17. Berman, H. M., Westbrook, J., Feng, Z., Gilliland, G., Bhat, T. N., Weissig, H., Shindyalov, I. N., and Bourne, P. E. (2000) The Protein Data Bank. *Nucleic Acids Res* **28**, 235-242
18. Laemmli, U. K. (1970) Cleavage of structural proteins during the assembly of the head of bacteriophage T4. *Nature* **227**, 680-685
19. Ochiai, A., Hashimoto, W., and Murata, K. (2006) A biosystem for alginate metabolism in *Agrobacterium*

tumefaciens strain C58: molecular identification of Atu3025 as an exotype family PL-15 alginate lyase. *Res. Microbiol.* **157**, 642-649

20. Nedjma, M., Hoffmann, N., and Belarbi, A. (2001) Selective and sensitive detection of pectin lyase activity using a colorimetric test: application to the screening of microorganisms possessing pectin lyase activity. *Anal. Biochem.* **291**, 290-296
21. Edman, P. (1950) Method for determination of the amino acid sequence in peptides. *Acta Chem. Scand.* **4**, 7
22. Nishitani, Y., Maruyama, Y., Itoh, T., Mikami, B., Hashimoto, W., and Murata, K. (2012) Recognition of heteropolysaccharide alginate by periplasmic solute-binding proteins of a bacterial ABC transporter. *Biochemistry* **51**, 3622-3633
23. Hashimoto, W., Momma, K., Maruyama, Y., Yamasaki, M., Mikami, B., and Murata, K. (2005) Structure and function of bacterial super-biosystem responsible for import and depolymerization of macromolecules. *Biosci. Biotechnol. Biochem.* **69**, 673-692
24. Rossmann, M. G., Moras, D., and Olsen, K. W. (1974) Chemical and biological evolution of nucleotide-binding protein. *Nature* **250**, 194-199
25. Kavanagh, K. L., Jornvall, H., Persson, B., and Oppermann, U. (2008) Medium- and short-chain dehydrogenase/reductase gene and protein families: the SDR superfamily: functional and structural diversity within a family of metabolic and regulatory enzymes. *Cell. Mol. Life Sci.* **65**, 3895-3906
26. Persson, B., and Kallberg, Y. (2013) Classification and nomenclature of the superfamily of short-chain dehydrogenases/reductases (SDRs). *Chem. Biol. Interact.* **202**, 111-115
27. Hoffmann, F., and Maser, E. (2007) Carbonyl reductases and pluripotent hydroxysteroid dehydrogenases of the short-chain dehydrogenase/reductase superfamily. *Drug Metab. Rev.* **39**, 87-144
28. Tomita, T., Fushinobu, S., Kuzuyama, T., and Nishiyama, M. (2006) Structural basis for the alteration of coenzyme specificity in a malate dehydrogenase mutant. *Biochem. Biophys. Res. Commun.* **347**, 502-508
29. Brinkmann-Chen, S., Flock, T., Cahn, J. K., Snow, C. D., Brustad, E. M., McIntosh, J. A., Meinhold, P., Zhang, L., and Arnold, F. H. (2013) General approach to reversing ketol-acid reductoisomerase cofactor dependence from NADPH to NADH. *Proc. Natl. Acad. Sci. U.S.A.* **110**, 10946-10951
30. Hashimoto, W., Kawai, S., and Murata, K. (2010) Bacterial supersystem for alginate import/metabolism and its environmental and bioenergy applications. *Bioeng. Bugs* **1**, 97-109

CHAPTER III

Recognition of coenzymes by bacterial α-keto acid reductases in SDR family

The coenzyme requirement of the two DEH reductases, A1-R and A1-R′, was converted by exchange of the two loops close to the coenzyme-binding site (CHAPTER II). Because the two loops are commonly included in short-chain dehydrogenase/reductase (SDR) family enzymes, the relationship between the two loops and coenzyme requirement was postulated to be conserved among the SDR family enzymes. To reveal this, another two SDR family reductases, KduD and DhuD, are focused in this CHAPTER. Both of KduD and DhuD reduce the identical α-keto acid, 2,5-diketo-3-deoxy-D-gluconic acid (DK-II), to give 2-keto-3-deoxy-D-gluconic acid (KDG) (1,2), although there is a difference in coenzyme utilization between KduD and DhuD. DK-II was generated from pectin or glycosaminoglycan (GAG) through subsequent reactions of lyase, unsaturated uronate hydrolase, and 4-deoxy-L-*threo*-5-hexosulose-uronate ketol-isomerase (KduI or DhuI) (2-8). KDG is converted to pyruvate and glyceraldehyde-3-phosphate by the following kinase (KdgK) and aldolase (KdgA) (Fig. 3-1) (1,2).

Metabolic pathway of pectin was determined in bacteria such as *Pseudomonas* and *Pectobacterium* (formerly known as *Erwinia*) (1,3,9). KduD from these bacteria has been known to be able to utilize both NADH and NADPH as coenzyme (1,10,11). The three-dimensional structure of KduD remains to be determined except for an enzyme regarded as KduD from *Thermus thermophilus* HB8 (PDB-ID, 4JP2) (12). There is no direct evidence that the *Thermus* enzyme is KduD since no data regarding the enzyme activity has been included in the reference and the reaction catalyzed by the enzyme has been shown to be different from that by KduD (12). In this CHAPTER, KduD from *Pectobacterium carotovorum* subsp. *carotovorum*, a plant pathogenic bacterium, was functionary and structurally characterized.

On the other hand, GAGs are degraded and metabolized by pathogenic bacteria such as streptococci (13,14). The enzyme, DhuD, of streptococci (*Streptococcus agalactiae*, *Streptococcus pneumoniae*, and *Streptococcus pyogenes*) has recently been identified to be DK-II reductase (2). The metabolic pathway of unsaturated glucuronic/iduronic acids derived from GAGs corresponds to that of unsaturated galacturonic acid from pectin. However, distinct from KduD with dual coenzyme specificity, DhuD is specific for NADH (2).

This CHAPTER deals with molecular characterization and structural determination of both KduD from *P. carotovorum* subsp. *carotovorum* (PcaKduD) and DhuD from *S. pyogenes*

(SpyDhuD). Structural determinants for the coenzyme specificity were identified through functional and structural comparison between PcaKduD and SpyDhuD.

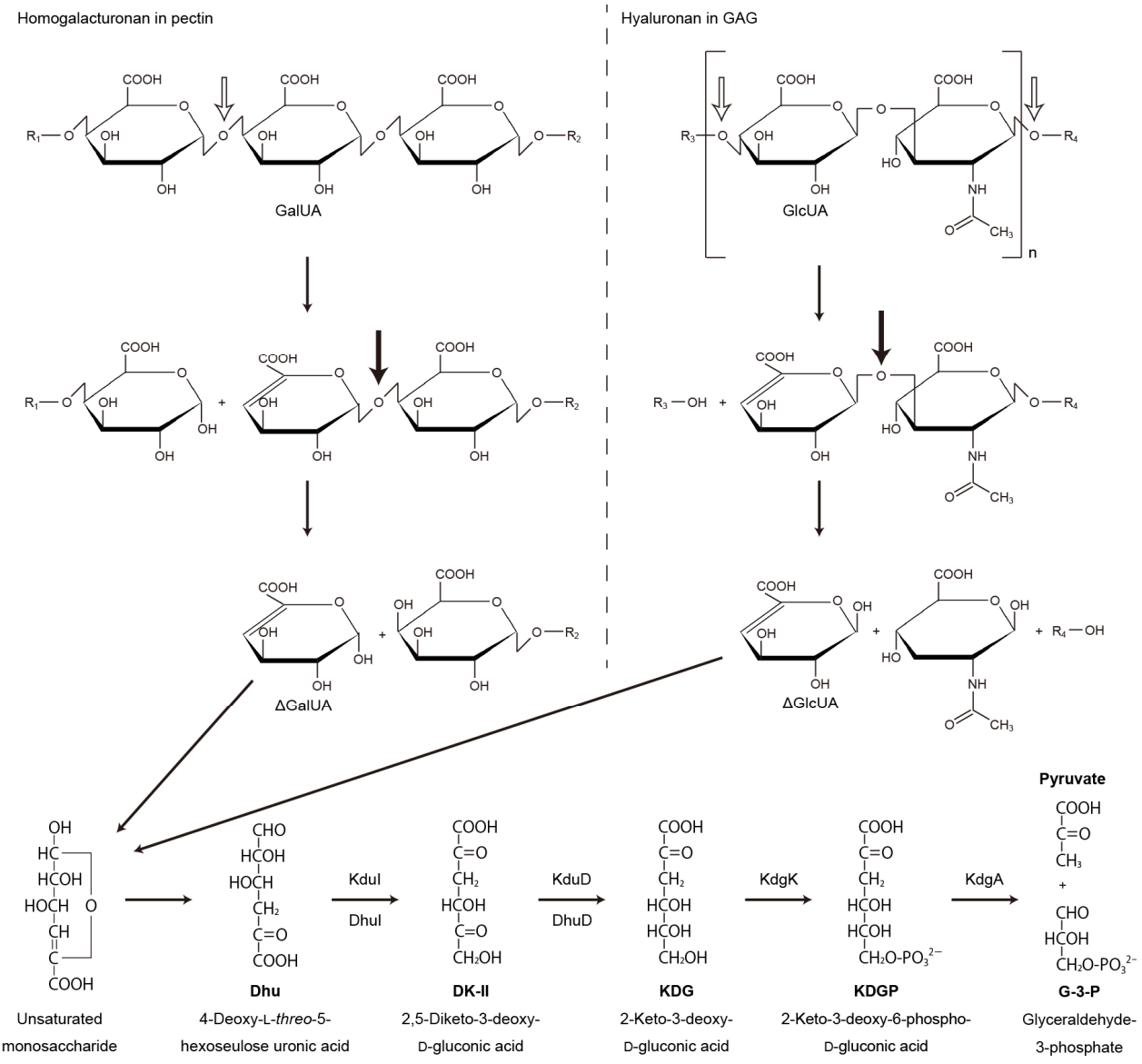

Fig. 3-1. Metabolic pathway of pectin and GAG. The white and thick arrows indicate the cleavage sites of lyase and hydrolase, respectively. GalUA, galacturonic acid; ΔGalUA, unsaturated GalUA; GlcUA, glucuronic acid; ΔGlcUA, unsaturated GlcUA.

Materials and Methods

Materials. TOYOPEARL DEAE-650 M and TOYOPEARL Butyl-650 M were purchased from Tosoh. HiLoad 26/10 Q-Sepharose HP and HiLoad 16/60 Superdex 200 pg were from GE healthcare. Restriction endonucleases and PCR-related enzymes were from Toyobo. Other

analytical grade chemicals were obtained from commercial sources.

Microorganisms and Culture Conditions. Pectobacterium carotovorum subsp. *carotovorum* (NBRC 3380) was purchased from Nite Biological Resource Center (NBRC). *P. carotovorum* was cultured aerobically at 30 °C in medium No. 802 (1% (w/v) polypeptone, 0.2% (w/v) yeast extract, and 0.1% (w/v) $MgSO_4 \cdot 7H_2O$) (pH 7.0). As a host for plasmid amplification, *Escherichia coli* strain DH5α (Toyobo) was routinely cultured at 37 °C in LB medium (1% (w/v) tryptone, 0.5% (w/v) yeast extract, and 1% (w/v) NaCl) (pH 7.2) containing sodium ampicillin (100 μg ml^{-1}). *E. coli* strain BL21(DE3) (Novagen) used as a host for overexpression of recombinant proteins was aerobically cultured at 30 °C in LB medium supplemented with sodium ampicillin (100 μg ml^{-1}). When the turbidity at 600 nm reached 0.6, isopropyl-β-D-thiogalactopyranoside was added to the culture at a final concentration of 0.4 mM, and the cells were further cultured at 16 °C for 42 h.

Enzyme and Protein Assays. The enzyme activity of PcaKduD was assayed at 30 °C in a 0.5 ml of reaction mixture containing 10 mM gellan tetrasaccharide (15), 50 mM Tris-HCl (pH 7.5), 0.2 mM coenzyme (NADH or NADPH), unsaturated glucuronyl hydrolase (UGL) from *Bacillus* sp. GL1 (16), DhuI from *S. agalactiae* (2), and PcaKduD. The enzyme activity of SpyDhuD was assayed using 20 mM 5-keto-D-gluconic acid as a substrate. The activity was measured by monitoring the decrease of absorbance at 340 nm, which corresponds to the oxidation of NADH or NADPH. The activities at various coenzyme concentrations were measured to determine kinetic parameters (k_{cat} and K_m) toward coenzyme using the Michaelis-Menten equation with the KaleidaGraph program (Synergy Software). The concentration of protein was determined by Bradford procedure (17), with bovine serum albumin as the standard.

Overexpression of PcaKduD. PcaKduD was overexpressed in *E. coli* cells as follows. To clone the KduD gene from *P. carotovorum*, PCR was conducted in a 50 μl of reaction mixture containing 1 unit of KOD-Plus-Neo (Toyobo), *P. carotovorum* cells, 15 pmol of forward and reverse primers, 75 nmol of $MgSO_4$, 10 nmol of dNTPs, and KOD-Plus-Neo buffer (Toyobo). The forward and reverse primers with *Nde*I and *Bam*HI sites (underlined) added to each of their 5'-regions were used (forward primer, 5'-GGCCGGCATATGATTTTAAATTCTTTTG-3'; reverse primer, 5'-CCGGATCCTTAGCGAGCCAGCCAGC-3'). PCR conditions were as follows: 94 °C for 2 min, followed by 30 cycles at 98 °C for 10 s, 56 °C for 30 s, and 68 °C for 1 min. The amplified DNA fragment containing the PcaKduD gene was supplied to gel electrophoresis and purified. After digestion with *Nde*I and *Bam*HI, the DNA fragment was ligated with *Nde*I- and *Bam*HI-digested pET21b (Novagen). The resultant plasmid, designated as pET21b/PcaKduD, includes the complete

sequence of the PcaKduD gene with the original start and stop codons. *E. coli* strain BL21(DE3) was transformed with pET21b/PcaKduD and used for overexpression of PcaKduD. The nucleotide sequence of the PcaKduD gene amplified from *P. carotovorum* was confirmed to be completely identical with that of *Pectobacterium atrosepticum* published on the database (GenBank-ID, AJ507294.1) by DNA sequencing (Model 3730xl and Model 3130xl; Applied Biosystems) (18).

Purification of Recombinant PcaKduD from E. coli Cells. *E. coli* strain BL21(DE3) cells harboring pET21b/PcaKduD were aerobically cultured in 3 liters of LB medium (1.5 liters per flask). Following procedures were performed at 4 °C. Cells were collected by centrifugation at 6,000 × *g* for 5 min and resuspended in 20 ml of 20 mM Tris-HCl (pH 7.5). The cells were ultrasonically disrupted (Insonator Model 201 M; Kubota) at 9 kHz for 20 min, and the supernatant was obtained after centrifugation at 20,000 × *g* for 20 min and dialyzed against 1.5 liters of 20 mM Tris-HCl (pH 7.5) twice. The dialysate was used as the cell extract. The cell extract was applied to a TOYOPEARL DEAE-650 M column (6 × 10 cm) previously equilibrated with 20 mM Tris-HCl (pH 7.5). The column was washed with the same buffer and the absorbed proteins were eluted with a linear gradient of NaCl (0–500 mM, 600 ml) in 20 mM Tris-HCl (pH 7.5), with a 10 ml fraction collected every 10 min. After sodium dodecyl sulfate-polyacrylamide gel electrophoresis (SDS-PAGE) analysis, fractions including PcaKduD, eluted with 50–150 mM NaCl, were collected and dialyzed against 1.5 liters of 20 mM Tris-HCl (pH 7.5) twice. The dialysate was saturated with 30% $(NH_4)_2SO_4$ and applied to a TOYOPEARL Butyl-650 M column (3 × 20 cm) previously equilibrated with 20 mM Tris-HCl (pH 7.5) saturated with 30% $(NH_4)_2SO_4$. After washing with 20 mM Tris-HCl (pH 7.5) containing 30% saturated $(NH_4)_2SO_4$, the absorbed proteins were eluted with a linear gradient of saturated $(NH_4)_2SO_4$ (30–0%, 200 ml), with a 6 ml fraction collected every 6 min. The fractions containing PcaKduD, eluted with 15–5% saturated $(NH_4)_2SO_4$, were combined and dialyzed against 1.5 liters of 20 mM Tris-HCl (pH 7.5) twice. The dialysate was applied to a HiLoad 26/10 Q-Sepharose HP column (2.6 × 10 cm) previously equilibrated with 20 mM Tris-HCl (pH 7.5). After washing with 20 mM Tris-HCl (pH 7.5), the absorbed proteins were eluted with a linear gradient of NaCl (0–500 mM, 150 ml) in 20 mM Tris-HCl (pH 7.5), with a 4 ml fraction collected every minute. The fractions containing PcaKduD, eluted with 250–300 mM NaCl, were combined and dialyzed against 1.5 liters of 20 mM Tris-HCl (pH 7.5) twice. The dialysate was concentrated by ultrafiltration with a Centriprep centrifugal filter (Millipore) to 1.3 ml at a concentration of 24-mg protein ml^{-1} and applied to a HiLoad 16/60 Superdex 200 pg column (1.6 × 60 cm) previously equilibrated with 20 mM Tris-HCl (pH 7.5) containing 0.15 M NaCl. Proteins

were eluted with the same buffer (120 ml) with a 2 ml fraction collected every 2 min. The fractions containing PcaKduD were combined and confirmed as homogeneous by SDS-PAGE. The purified proteins were dialyzed against 1.5 liters of 20 mM Tris-HCl (pH 7.5) twice and used as recombinant PcaKduD (rPcaKduD). Recombinant SpyDhuD (rSpyDhuD) was also obtained from recombinant *E. coli* cells and purified to become homogeneous as described previously (2).

Crystallization and Structure Determination. Crystals of PcaKduD and SpyDhuD were obtained by sitting-drop vapor diffusion on a 96-well Intelli-plate (Veritas). To search for the crystallization conditions, commercial screening kits (Hampton Research, Emerald BioSystems, and Jena Bioscience) were used. The volume of reservoir solution was 70 μl in each well, and the droplet was prepared by mixing 1 μl of the protein solution with equal amount of the reservoir solution. Crystals of PcaKduD in complex with NAD^+ (PcaKduD·NAD^+) were prepared in the solution containing NAD^+. Each crystal of PcaKduD, PcaKduD·NAD^+, and SpyDhuD was picked off the nylon loop and was directly placed in a cold nitrogen gas stream at −173 °C. X-ray diffraction images of the crystals were collected at –173 °C under the nitrogen gas stream and synchrotron radiation of wavelength 1.0000 Å at BL-38B1 station in SPring-8 (Hyogo, Japan). Diffraction data were processed, merged, and scaled using the HKL2000 program package (DENZO and SCALEPACK) (19). The structures of PcaKduD, PcaKduD·NAD^+, and SpyDhuD were determined by molecular replacement using coordinates of 3-oxoacyl-(acyl-carrier-protein) reductase (PDB-ID, 2UVD), ligand-free PcaKduD (this CHAPTER), and gluconate 5-dehydrogase from *Streptococcus suis* (PDB-ID, 3CXR), respectively, as an initial model using the MOLREP program (20), in the CCP4 program package (21). The Refmac5 program (22) was used for structure refinement. Randomly selected 5% reflections were excluded from refinement and used to calculate R_{free}. The model was manually adjusted using the Coot program (23). Water molecules were incorporated where the difference in density exceeded 3.0σ in $F_o - F_c$ map. The qualities of final models were checked using the PROCHECK program (24). Superimposition of protein models and determination of their root mean square deviation (r.m.s.d.) were calculated using LSQKAB program (25), part of CCP4. Figures of protein structures were drawn by the PyMOL program (26). Coordinates used in this CHAPTER were obtained from the Protein Data Bank (PDB) (www.wwpdb.org/) (27).

Analytical Methods. SDS-PAGE (28) was conducted using polyacrylamide gel (12.5%). Proteins on the gel were stained using Coomassie Brilliant Blue R-250.

Results and Discussion

Identification and Characterization of PcaKduD

In order to obtain KduD with dual coenzyme specificity, the KduD gene was searched for by BLAST (blast.ncbi.nlm.nih.gov) using primary structure of the enzymatically identified KduD of *Dickeya dadantii* (GenBank-ID, CAA43989.1) (10). As a result, a protein (GenBank-ID, KFX18736.1) was found to show a high sequence identity (89%) with the *D. dadantii* KduD. The protein is putatively annotated to be 2-deoxy-D-gluconate-3-dehydrogenase and encoded in a plant pathogen bacterium, *P. carotovorum* subsp. *carotovorum*. Because KduD was enzymatically identified in *P. carotovorum* subsp. *atrosepticum*, a congeneric bacterium of *P. carotovorum* subsp. *carotovorum* (29), identity of primary structures between the protein (GenBank-ID, KFX18736.1) and *P. carotovorum* subsp. *atrosepticum* KduD was determined using ClustalW (clustalw.ddbj.nig.ac.jp/). The resultant identity was considerably high, 98%. Thus, the protein (GenBank-ID, KFX18736.1) was considered to be KduD. The gene of *P. carotovorum* subsp. *carotovorum* KduD (PcaKduD) was amplified from *P. carotovorum* subsp. *carotovorum* genome, and rPcaKduD was purified from recombinant *E. coli* strain BL21(DE3) harboring pET21b/PcaKduD through four steps of column chromatography to become homogeneous on SDS-PAGE as described above. The purified rPcaKduD reduced DK-II in the presence of coenzyme (NADH or NADPH). Enzymatic properties of rPcaKduD were determined as follows:

(i) Molecular mass

Molecular mass of rPcaKduD was determined to be 25 kDa through analysis of SDS-PAGE (Fig. 3-2 A). Elution profile of gel filtration column, HiLoad 16/60 Superdex 200 pg, indicated that the molecular mass of rPcaKduD was about 90 kDa (data not shown). These results suggested that rPcaKduD was a homotetramer.

(ii) Optimal pH, optimal temperature, and thermal stability

rPcaKduD was most active at 45 °C and pH 7.2, and stable below at 40 °C (Fig. 3-2 B).

(iii) Kinetic parameters toward coenzyme

Kinetic parameters (k_{cat} and K_m) toward NADH and NADPH were calculated using saturation curve of enzyme activities at various coenzyme concentrations. k_{cat} and K_m values of rPcaKduD were 0.024 s^{-1} and 2.1 μM toward NADH, and 0.021 s^{-1} and 5.0 μM toward NADPH. Although k_{cat} scores toward NADH and NADPH were similar, the affinity for NADH was 2.4-fold higher compared with that for NADPH. These indicate that rPcaKduD prefers NADH, although the enzyme utilizes both NADH and NADPH. On the other hand, rSpyDhuD was specific for

NADH (k_{cat}, 0.068 s^{-1}; K_m, 12 μM toward NADH) and exhibited no enzyme activity toward NADPH.

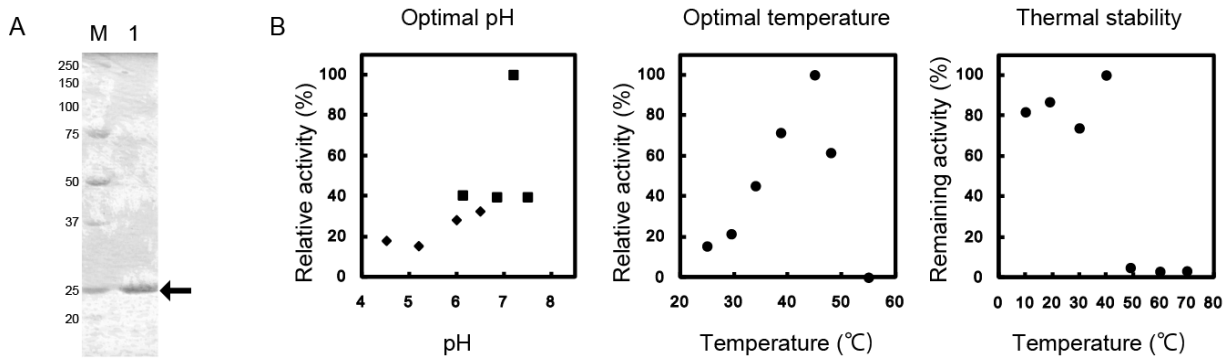

Fig. 3-2. Properties of rPcaKduD. (A) SDS-PAGE analysis of rPcaKduD. Lane M, molecular weight marker; lane 1, Purified rPcaKduD (2 μg). (B) Effects of pH and temperature on the activities of rPcaKduD. Left: optimal pH. Activity was assayed with sodium acetate shown as diamond (♦) (pH 4.5, 5.2, 6.0, 6.5) and potassium phosphate buffer (KPB) shown as square (■) (pH 6.1, 6.9, 7.2, 7.5). Activity at pH 7.2 in KPB was taken as 100%. Center: optimal temperature. Activity at 45 °C was taken as 100%. Right: thermal stability. rPcaKduD was preincubated for 5 min at various temperatures (as indicated) and the residual activity was measured. The activity of the enzyme preincubated at 4 °C for 5 min was taken as 100%.

Sequence Alignment

PcaKduD and SpyDhuD consist of 253 and 264 amino acid residues, respectively. The identity of primary structure between the two reductases was calculated to be 39% using ClustalW. The sequence alignment among PcaKduD, SpyDhuD, and other SDR family enzymes (A1-R and A1-R′) was also conducted using ClustalW. PcaKduD and SpyDhuD have glycine-rich motif of the coenzyme-binding Rossmann fold region (TG*XXX*G*X*G) and catalytic triad (Ser, Tyr, and Lys), conserved in SDR family (Fig. 3-3 A). These results indicate that PcaKduD and SpyDhuD belong to SDR family.

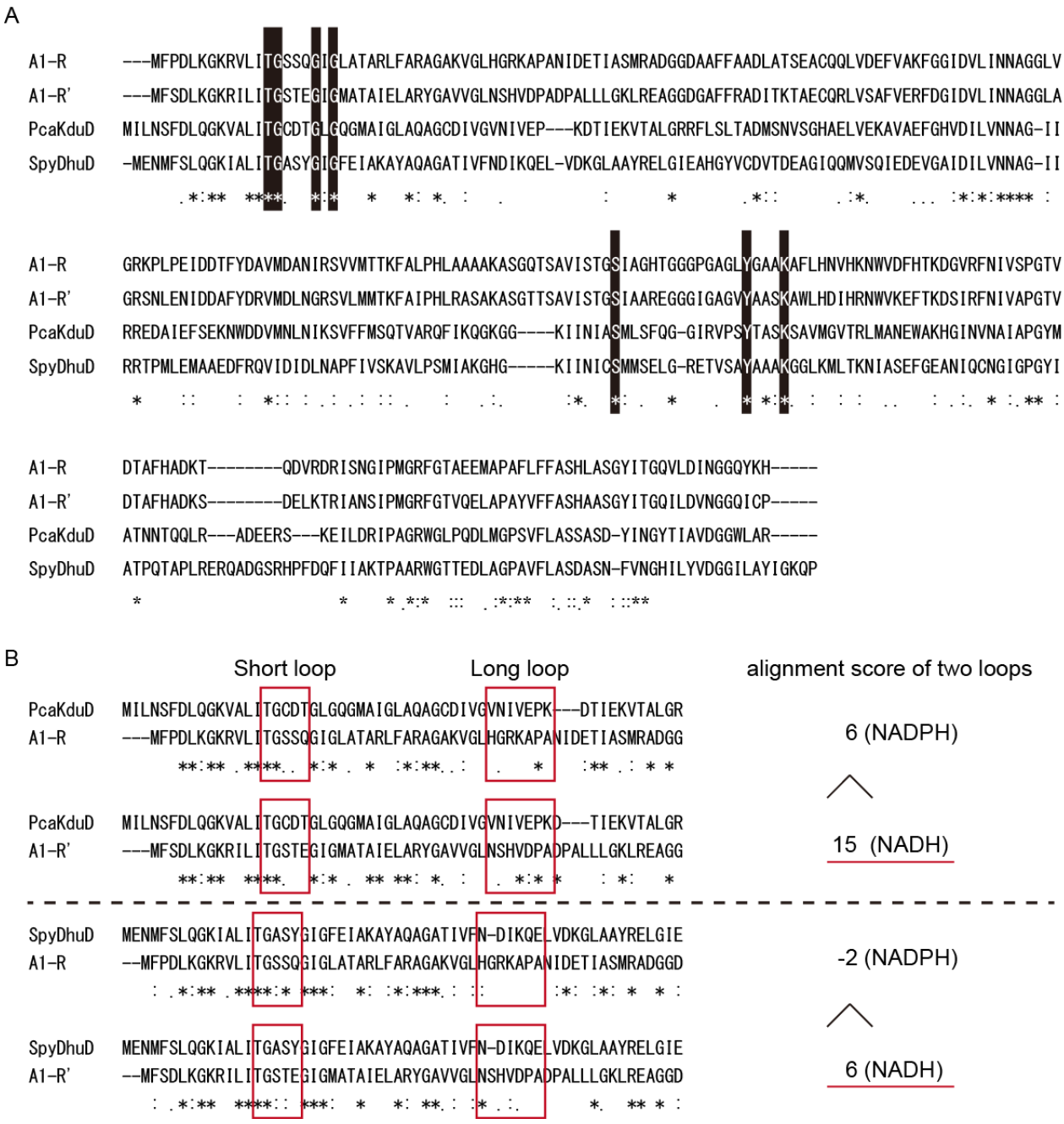

Fig. 3-3. Sequence alignment. (A) Alignment between A1-R, A1-R′, PcaKduD, and SpyDhuD. Conserved residues among SDR family enzymes, TG*XXXGX*G motif and catalytic triad (Ser, Tyr, and Lys) are indicated by open letters. Asterisk (*), colon (:), and period (.) indicate that residues are identical, highly similar, and moderately similar, respectively. (B) Alignment between PcaKduD or SpyDhuD and A1-R or A1-R′, respectively. Alignment scores between two loops (red box) using BLOSUM62 are shown in the right side of the alignment.

Crystal Structures of PcaKduD and SpyDhuD

In order to identify structural determinants in PcaKduD and SpyDhuD for different coenzyme specificity, X-ray crystallography of both enzymes was conducted. A PcaKduD crystal was obtained

in a solution consisting of 6% (w/v) polyethylene glycol 8000, 5% (v/v) glycerol, 0.25 M potassium chloride, and 30.0 mg ml^{-1} rPcaKduD. A PcaKduD·NAD^+ complex crystal was obtained in a droplet containing 5% (w/v) polyethylene glycol 4000, 10% (v/v) isopropanol, 0.5 mM NAD^+, and 30.0 mg ml^{-1} rPcaKduD. A SpyDhuD crystal was obtained in a droplet comprising 25% (w/v) polyethylene glycol 4000, 0.1 M sodium citrate (pH 5.6), 0.2 M $(NH_4)_2SO_4$, 1 mM NADH, 10 mM 5-keto-D-gluconic acid potassium salt, and 11.6 mg ml^{-1} rSpyDhuD. The PcaKduD and SpyDhuD crystals were soaked in mother liquor containing 20% (v/v) glycerol as a cryoprotectant before freezing. The PcaKduD·NAD^+ crystal was soaked in mother liquor containing 40% (v/v) glycerol and freezed immediately. The crystal structures of PcaKduD, PcaKduD·NAD^+, and SpyDhuD were determined at resolutions of 1.63 Å, 1.55 Å, and 1.70 Å, respectively. *R*- and R_{free}-factors of PcaKduD, PcaKduD·NAD^+, and SpyDhuD were 16.7% and 19.6%, 19.9% and 23.4%, and 18.7% and 20.8%, respectively. Data collection and refinement statistics are summarized in Table 3-1. The refined PcaKduD model had four monomers in an asymmetric unit, termed molecules A, B, C, and D. PcaKduD has three-layered structure, α/β/α, and a coenzyme-binding site, Rossmann fold (Fig. 3-4 A, B). Structural homologs of PcaKduD were sought using Dali program (30). A large number of PcaKduD structural homologs were listed and the 147 proteins scored above 30 in Z score. Top 10 proteins in Z score are shown in Table 3-2 and these structural homologs belong to SDR family. The Z score and r.m.s.d. between PcaKduD and possible KduD from *T. thermophilus* HB8 (PDB-ID, 4JP2) were 34.1 and 1.5 Å, respectively. These indicate that both proteins are mutually similar in structure. However, these results are weak to sustain that the protein from *T. thermophilus* is KduD because many other structural homologs with PcaKduD exhibit different enzyme activities. The refined PcaKduD·NAD^+ model also has four monomers in an asymmetric unit. A NAD^+ molecule is included in Rossmann fold region in each molecule C or D. The r.m.s.d. value between NAD^+-free and -bound PcaKduD was calculated as 0.194 Å, indicating that no significant conformational change occurred between NAD^+-free and -bound PcaKduD.

Although SpyDhuD is a homotetramer enzyme, the refined SpyDhuD model contains one monomer in an asymmetric unit. In SpyDhuD, residues 1 and 204-208 were unable to be assigned because the residues in this region of the electron density map are disordered. SpyDhuD has three-layered structure, α/β/α, as observed in other SDR family enzymes including PcaKduD (Fig. 3-4 C, D). PcaKduD was well superimposed on SpyDhuD based on Cα. The overall structures of PcaKduD and SpyDhuD were found to be similar (Fig. 3-4 E, F). The arrangements of catalytic triads in the structure of PcaKduD (Ser-145, Tyr-158, and Lys-162) and SpyDhuD (Ser-145,

Tyr-158, and Lys-162) were identical to those of A1-R (PDB-ID, 3AFM) and A1-R′ (PDB-ID, 4TKL).

Table 3-1
Statistics for X-ray diffraction and structure refinement

	PcaKduD	PcaKduD·NAD^+	SpyDhuD
Data collection			
Wavelength (Å)	1.0000	1.0000	1.0000
Space group	$P1_211$	$P1_211$	$P4_22_12$
Unit cell parameters (Å, °)	a = 68.7, b = 72.7, c = 99.0	a = 68.7, b = 72.7, c = 99.0	$a = b$ = 67.6, c = 108.9
	α = 90.0, β = 90.8, γ = 90.0	α = 90.0, β = 90.8, γ = 90.0	
Resolution limit (Å)	50.0 – 1.63 (1.69 – 1.63)[a]	50.0 – 1.55 (1.58 – 1.55)[a]	50.0 – 1.70 (1.76 – 1.70)[a]
Total reflections	1,123,367	1,539,230	346,213
Unique reflections	122,189	141,041	28,548
Redundancy	4.1 (4.0)	4.1 (4.1)	12.0 (9.2)
Completeness (%)	99.6 (98.0)	99.7 (99.9)	99.9 (100)
I/σ (I)	39.1 (8.3)	40.5 (4.4)	62.1 (6.2)
R_{merge} (%)	5.6 (24.1)	3.4 (39.8)	4.6 (36.2)
Refinement			
Final model	1,012 residues, 4 SO_4^{2-},	1,012 residues, 2 NAD^+,	258 residues,
	998 water molecules	624 water molecules	106 water molecules
Resolution limit (Å)	41.0 – 1.63 (1.67 – 1.63)	34.1 – 1.55 (1.59 – 1.55)	32.0 – 1.70 (1.74 – 1.70)
Used reflections	115,520 (8,457)	133,413 (9,801)	18,419 (1,344)
Completeness (%)	99.6 (98.4)	99.6 (98.9)	98.7 (98.5)
R-factor (%)	16.7 (22.4)	19.9 (28.0)	18.7 (21.3)
R_{free} (%)	19.6 (27.5)	23.4 (31.7)	20.8 (24.1)
Average B-factor (Å^2)			
Protein			
Molecule A	13.2	17.7	23.7
Molecule B	16.2	22.1	
Molecule C	22.7	28.0	
Molecule D	25.7	32.1	
Waters	30.5	30.3	26.8
NAD^+			
Molecule A		46.0	
Molecule B		47.4	
SO_4^{2-}			
Molecule E1	21.4		
Molecule E2	19.4		
Molecule E3	33.0		
Molecule E4	43.0		
r.m.s.d.			
Bond (Å)	0.0093	0.018	0.0052
Angle (°)	1.35	1.64	1.051
Ramachandran plot (%)			
Favored regions	97.2	96.0	97.6
Allowed regions	2.5	3.3	2.4
Outliers	0.3	0.7	0

[a] Data on highest shells are given in parenthesis.

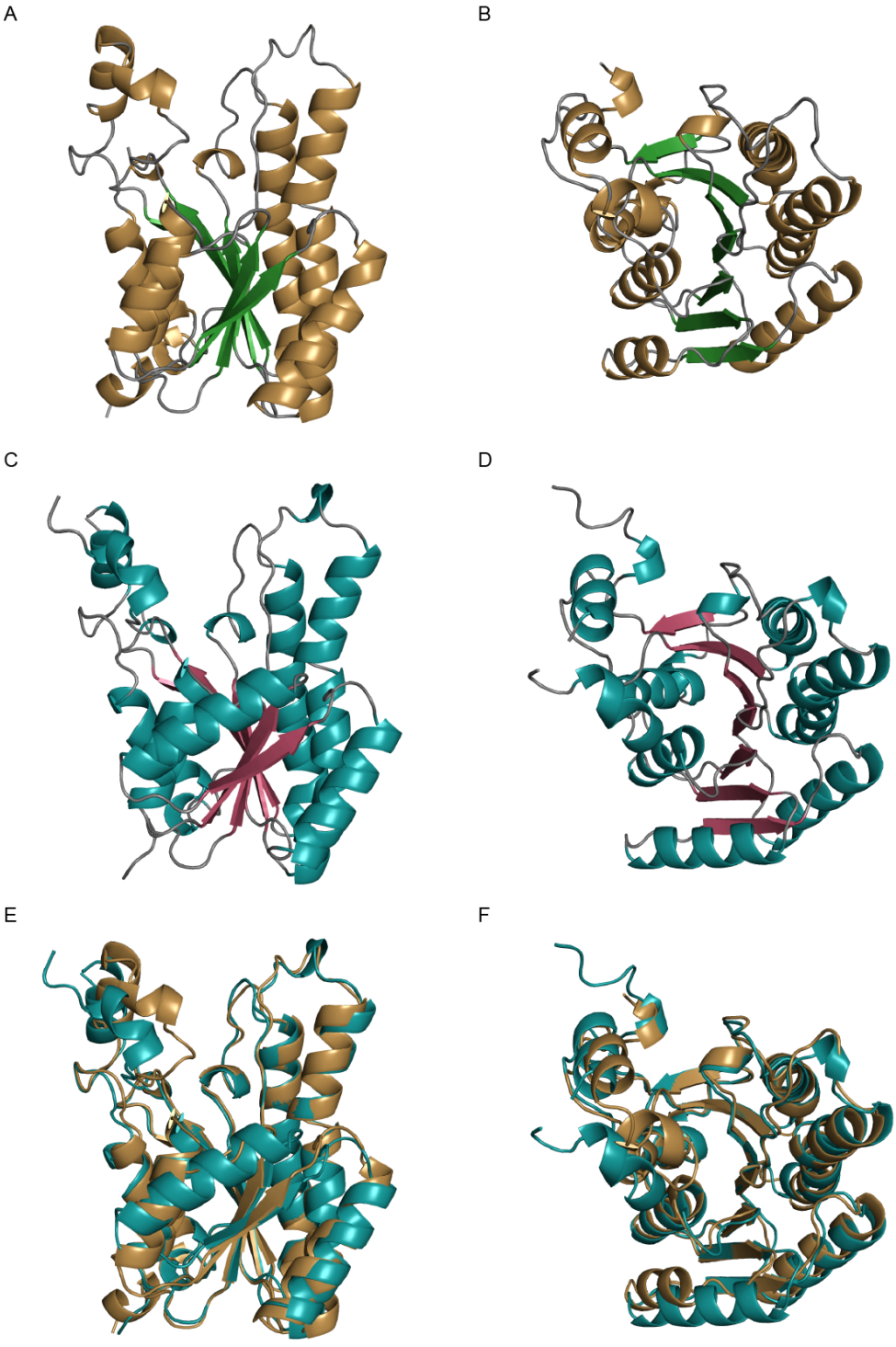

Fig. 3-4. Structures of PcaKduD and SpyDhuD. (A), (B) Overall structure of PcaKduD. Green, β-strand; yellow, α-helix; gray, loop. The structure of (B) is rotated 90° toward the reader relative to that of (A). (C), (D) Overall structure of SpyDhuD. Red, β-strand; blue, α-helix; gray, loop. The structure of (D) is rotated 90° toward the reader relative to that of (C). (E), (F) Superimposed structures of PcaKduD and SpyDhuD based on Cα. Yellow, PcaKduD; blue, SpyDhuD. The structure of (F) is rotated 90° toward the reader relative to that of (E).

Table 3-2
Structural homologs of PcaKduD

Z score	Protein	r.m.s.d.[a]	Lali[b]	PDB-ID
38.5	Putative short-chain alcohol dehydrogenase	1.1	249	4J2H
38.4	2-Deoxy-D-gluconate-3-dehydrogenase	1.3	246	4HP8
38.3	Gluconate-5-dehydrogenase	1.2	248	1VL8
37.7	Nitric oxide synthase	1.5	248	3UFO
37.6	Gluconate dehydrogenase	1.5	252	4IBO
37.6	Monoacylglycerol lipase	1.4	250	3RLI
37.6	Putative hexonate dehydrogenase	1.4	250	4G81
37.3	3-Oxoacyl-(acyl-carrier-protein) reductase	1.2	243	2UVD
37.2	3-Oxoacyl-(acyl-carrier-protein) reductase	1.2	243	4JRO
36.7	Glucose-1-dehydrogenase	1.6	250	1RWB

[a] A measure of the average deviation in distance between aligned Cα.
[b] Total number of structurally equivalent residues.

Primary Structure of the Two Loops

In order to clarify the involvement of the two loops of PcaKduD and SpyDhuD in their coenzyme specificity as described in CHAPTER II, primary structures of PcaKduD and SpyDhuD were compared to those of A1-R and A1-R′ using ClustalW, respectively (Fig. 3-3 B). As a result, the two loops in PcaKduD (short loop, ^{16}TGCDT^{20}; long loop, ^{40}VNIVEPK^{46}) and in SpyDhuD (short loop, ^{15}TGASY^{19}; long loop, ^{39}NDIKQE^{44}) corresponded to those of A1-R (short loop, ^{13}TGSSQ^{17}; long loop, ^{37}HGRKAPA^{43}) and A1-R′ (short loop, ^{13}TGSTE^{17}; long loop, ^{37}NSHVDPA^{43}), respectively. The alignment scores in the two loops were calculated using BLOSUM62 (31), usually used to short sequence alignment in ClustalW. A gap existence cost was set as −10, used routinely in BLOSUM62. The two loops of PcaKduD showed a similarity toward those of A1-R′ rather than those of A1-R (alignment scores: 6 toward loops of A1-R and 15 toward loops of A1-R′). The two loops of SpyDhuD were also similar to those of A1-R′ (alignment scores: −2 toward loops of A1-R and 6 toward loops of A1-R′). Since A1-R′ is an NADH-dependent enzyme (CHAPTER II) similar to PcaKduD and SpyDhuD, these results indicate that there are correlations between primary structures of the two loops and coenzyme requirement in SDR family enzymes, while little identities in entire sequence were observed between PcaKduD or SpyDhuD

and A1-R or A1-R′ (identities between PcaKduD and A1-R, PcaKduD and A1-R′, SpyDhuD and A1-R, and SpyDhuD and A1-R′ were 23%, 26%, 23%, and 24%, respectively). Thus, primary structure analysis of the two loops is considered to be useful to predict coenzyme requirements in SDR family enzymes.

Binding Mode to Coenzyme

As described above, coenzyme requirement of two DK-II reductases was explained by primary structure analysis of the two loops. However, the explanation for difference of NADPH-utilization in PcaKduD and SpyDhuD was difficult based on the primary structure analysis of the two loops. Thus, coenzyme-binding sites of PcaKduD and SpyDhuD were compared (Fig. 3-5). Residues within a distance of 4.0 Å from NAD^+ molecule in PcaKduD are shown in Fig. 3-5 A. Although every effort was done to determine the complex structure of SpyDhuD and NAD^+ molecule, no

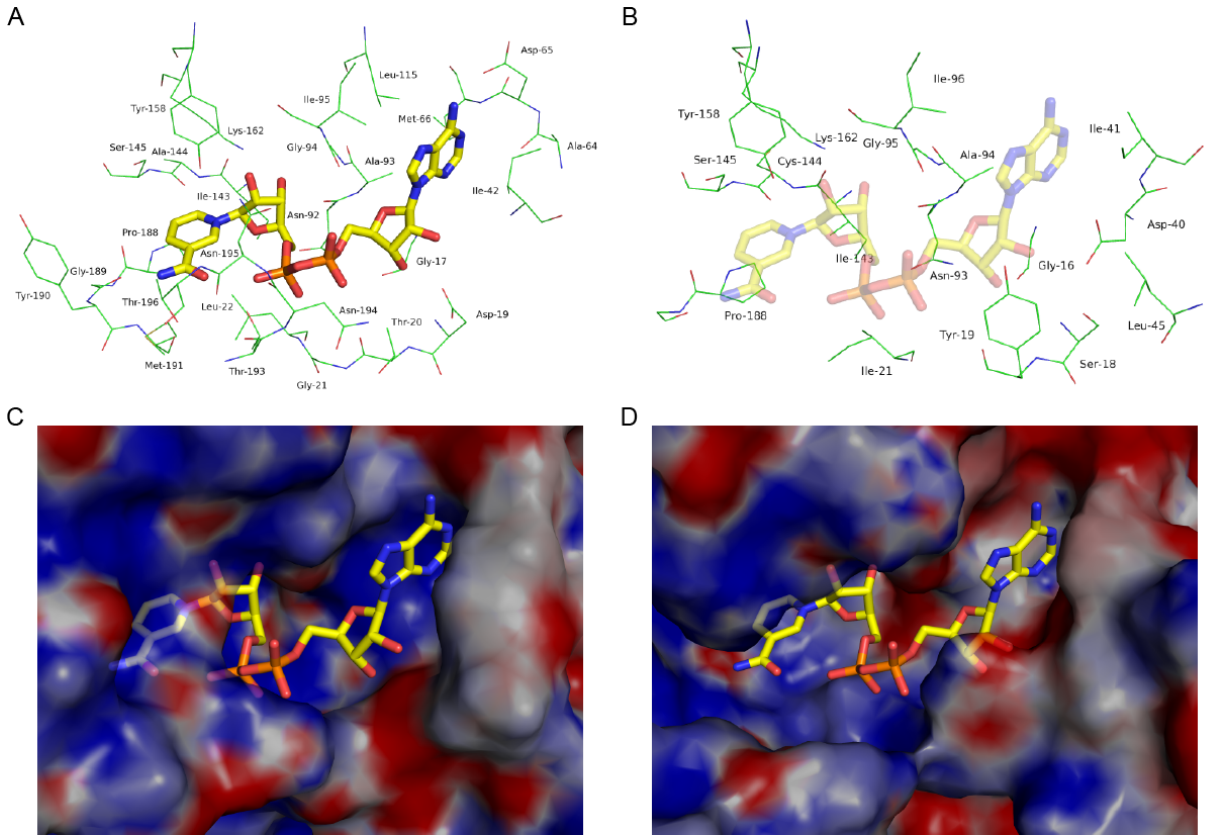

Fig. 3-5. Coenzyme-binding site. (A) Coenzyme-binding site in PcaKduD·NAD^+. (B) Predicted coenzyme-binding site in SpyDhuD. In (A) and (B), residues within a distance of 4.0 Å from NAD^+ are shown. Green, carbon atom of amino acid residues, yellow, carbon atom of NAD^+, blue, nitrogen atom; orange, phosphorus atom; red, oxygen atom. (C) Surface electrostatic potentials around NAD^+ molecule in PcaKduD·NAD^+. (D) Surface electrostatic potentials at predicted coenzyme-binding site in SpyDhuD. Electric charges are calculated at pH 7.0. Blue and red indicate basic and acidic, respectively.

crystal of SpyDhuD·NAD^+ complex formed. Thus, the NAD^+ molecule was docked into the Rossmann fold region of SpyDhuD and shown as half-transparent stick model after superposition of PcaKduD·NAD^+ on SpyDhuD based on Cα atoms and succeeding deletion of PcaKduD molecule (Fig. 3-5 B). The electric charges of the molecular surface at pH 7.0 around the coenzyme-binding site of PcaKduD and SpyDhuD are shown in Fig. 3-5 C, D. The apparent differences were observed around nucleoside ribose 2' region between PcaKduD and SpyDhuD. The nucleoside ribose 2' region in SpyDhuD is negatively charged due to the presence of Asp-40. This electric charge may cause electrostatic repulsion to nucleoside ribose 2' phosphate group of NADPH. On the other hand, the corresponding region in PcaKduD exhibited no apparent electric charge. The region was intermediate between positively and negatively charged areas. Thus, there may be no electric influence between PcaKduD and nucleoside ribose 2' phosphate group of NADPH.

The distances less than 4.5 Å between oxygen atom of nucleoside ribose 2' hydroxyl group in NAD^+ (O2B) and the residues of PcaKduD or SpyDhuD are shown in Table 3-3. Positional relation between SpyDhuD and NAD^+ was the same with that shown in Fig. 3-5 B. The closest interaction between NAD^+ and PcaKduD is formed by hydrogen bond between oxygen atom (O2B) of NAD^+ and oxygen atom (OD1) of side chain in Asp-19. The distance is 3.05 Å. In SpyDhuD, the interaction (1.99 Å) is also formed by hydrogen bond between oxygen atom (O2B) of NAD^+ and oxygen atom (OH) of side chain in Tyr-19. These results indicate that there is less space volume to

Table 3-3
Hydrogen bond (≤ 3.4 Å) and van der waals interaction (≤ 4.5 Å) between the oxygen atom of nucleoside ribose 2' hydroxyl group of NAD^+ (NAD O2B) and PcaKduD or SpyDhuD

PcaKduD			SpyDhuD		
NAD O2B	Protein/atom (distance, Å)[a]		NAD O2B	Protein/atom (distance, Å)[a]	
Hydrogen bond			*Hydrogen bond*		
	Asp-19 /OD1	(3.05)		Tyr-19 /OH	(1.99)
				Asp-40 /OD2	(3.29)
van der waals			*van der waals*		
	Asp-19 /CG	(4.03)		Gly-16 /O	(4.34)
	Asp-19 /OD2	(4.34)		Ser-18 /OG	(4.21)
				Tyr-19 /CG	(4.35)
				Tyr-19 /CD1	(3.53)
				Tyr-19 /CE1	(2.38)
				Tyr-19 /CZ	(2.26)
				Tyr-19 /CE2	(3.37)
				Tyr-19 /CD2	(4.26)
				Asp-40 /OD1	(3.80)
				Asp-40 /CG	(3.97)

[a] Distance between the oxygen atom of nucleoside ribose 2' hydroxyl group in NAD^+ and protein.

make phosphate group of nucleoside ribose 2’ of NADPH fit into the nucleoside ribose 2’-binding site in SpyDhuD. On the other hand, in PcaKduD, the phosphate group can be accommodated in the space at the nucleoside ribose 2’-binding site. Thus, electric charge and space formation at the binding site of nucleoside ribose 2’ region were found to cause the difference in NADPH-utilization between PcaKduD and SpyDhuD. Owing to adequate space formation and non-electric charge at the nucleoside ribose 2’ region, PcaKduD was considered to utilize both NADH and NADPH as coenzyme.

In conclusion, two DK-II reductases, PcaKduD and SpyDhuD, prefer NADH as coenzyme. However, only PcaKduD can utilize NADPH. In order to clarify the reasons why both DK-II reductases prefer NADH and only PcaKduD can utilize NADPH, the two loops around coenzyme-binding site were focused on. As described in CHAPTER II, the two short and long loops around coenzyme-binding site determine the coenzyme requirement in two SDR family enzymes, A1-R and A1-R′. The two loop structures of PcaKduD and SpyDhuD were identified by X-ray crystallography. Sequence alignment between PcaKduD or SpyDhuD and A1-R or A1-R′ revealed that the two loops of two DK-II reductases corresponded to those of A1-R and A1-R′ in the alignment. Especially, the alignment score demonstrated that the two loops of DK-II reductases were similar to those of A1-R′. This result coincided with experimentally determined coenzyme requirement. In addition, structural determinants in KduD for the dual coenzyme specificity were found through structural comparison between KduD and DhuD. The electric charge and space formation at the nucleoside ribose 2’-binding site are crucial for the coenzyme requirement.

References

1. Preiss, J., and Ashwell, G. (1963) Polygalacturonic acid metabolism in bacteria. II. Formation and metabolism of 3-deoxy-D-glycero-2,5-hexodiulosonic acid. *J. Biol. Chem.* **238**, 1577-1583
2. Maruyama, Y., Oiki, S., Takase, R., Mikami, B., Murata, K., and Hashimoto, W. (2015) Metabolic fate of unsaturated glucuronic/iduronic acids from glycosaminoglycans: molecular identification and structure determination of streptococcal isomerase and dehydrogenase. *J. Biol. Chem.* **290**, 6281-6292
3. Preiss, J., and Ashwell, G. (1963) Polygalacturonic acid metabolism in bacteria. I. Enzymatic formation of 4-deoxy-L-*threo*-5-hexoseulose uronic acid. *J. Biol. Chem.* **238**, 1571-1583
4. Pedrolli, D. B., Monteiro, A. C., Gomes, E., and Carmona, E. C. (2009) Pectin and pectinases: production, characterization and industrial application of microbial pectinolytic enzymes. *Open Biotechnol. J.* **3**, 9-18
5. Li, S., Kelly, S. J., Lamani, E., Ferraroni, M., and Jedrzejas, M. J. (2000) Structural basis of hyaluronan

degradation by *Streptococcus pneumoniae* hyaluronate lyase. *EMBO J.* **19**, 1228-1240

6. Hashimoto, W., Kobayashi, E., Nankai, H., Sato, N., Miya, T., Kawai, S., and Murata, K. (1999) Unsaturated glucuronyl hydrolase of *Bacillus* sp. GL1: novel enzyme prerequisite for metabolism of unsaturated oligosaccharides produced by polysaccharide lyases. *Arch. Biochem. Biophys.* **368**, 367-374
7. Maruyama, Y., Nakamichi, Y., Itoh, T., Mikami, B., Hashimoto, W., and Murata, K. (2009) Substrate specificity of streptococcal unsaturated glucuronyl hydrolases for sulfated glycosaminoglycan. *J. Biol. Chem.* **284**, 18059-18069
8. Nakamichi, Y., Maruyama, Y., Mikami, B., Hashimoto, W., and Murata, K. (2011) Structural determinants in streptococcal unsaturated glucuronyl hydrolase for recognition of glycosaminoglycan sulfate groups. *J. Biol. Chem.* **286**, 6262-6271
9. Richard, P., and Hilditch, S. (2009) D-Galacturonic acid catabolism in microorganisms and its biotechnological relevance. *Appl. Microbiol. Biotechnol.* **82**, 597-604
10. Condemine, G., Hugouvieux-Cotte-Pattat, N., and Robert-Baudouy, J. (1984) An enzyme in the pectinolytic pathway of *Erwinia chrysanthemi*: 2-keto-3-deoxygluconate oxidoreductase. *J. Gen. Microbiol.* **130**, 2839-2844
11. Condemine, G., and Robert-Baudouy, J. (1991) Analysis of an *Erwinia chrysanthemi* gene cluster involved in pectin degradation. *Mol. Microbiol.* **5**, 2191-2202
12. Pampa, K. J., Lokanath, N. K., Kunishima, N., and Rai, R. V. (2014) The first crystal structure of NAD-dependent 3-dehydro-2-deoxy-D-gluconate dehydrogenase from *Thermus thermophilus* HB8. *Acta Crystallogr. D Biol. Crystallogr.* **70**, 994-1004
13. Starr, C. R., and Engleberg, N. C. (2006) Role of hyaluronidase in subcutaneous spread and growth of group A *streptococcus*. *Infect. Immun.* **74**, 40-48
14. Marion, C., Stewart, J. M., Tazi, M. F., Burnaugh, A. M., Linke, C. M., Woodiga, S. A., and King, S. J. (2012) *Streptococcus pneumoniae* can utilize multiple sources of hyaluronic acid for growth. *Infect. Immun.* **80**, 1390-1398
15. Hashimoto, W., Maesaka, K., Sato, N., Kimura, S., Yamamoto, K., Kumagai, H., and Murata, K. (1997) Microbial system for polysaccharide depolymerization: enzymatic route for gellan depolymerization by *Bacillus* sp. GL1. *Arch. Biochem. Biophys.* **339**, 17-23
16. Itoh, T., Akao, S., Hashimoto, W., Mikami, B., and Murata, K. (2004) Crystal structure of unsaturated glucuronyl hydrolase, responsible for the degradation of glycosaminoglycan, from *Bacillus* sp. GL1 at 1.8 Å resolution. *J. Biol. Chem.* **279**, 31804-31812
17. Bradford, M. M. (1976) A rapid and sensitive method for the quantitation of microgram quantities of protein

utilizing the principle of protein-dye binding. *Anal. Biochem.* **72**, 248-254

18. Sanger, F., Nicklen, S., and Coulson, A. R. (1977) DNA sequencing with chain-terminating inhibitors. *Proc. Natl. Acad. Sci. U.S.A.* **74**, 5463-5467
19. Otwinowski, Z., and Minor, W. (1997) Processing of X-ray diffraction data. *Methods Enzymol.* **276**, 307-326
20. Vagin, A., and Teplyakov, A. (2010) Molecular replacement with *MOLREP*. *Acta Crystallogr. D Biol. Crystallogr.* **66**, 22-25
21. Collaborative Computational Project, N. (1994) The *CCP4* suite: programs for protein crystallography. *Acta Crystallogr. D Biol. Crystallogr.* **50**, 760-763
22. Murshudov, G. N., Vagin, A. A., and Dodson, E. J. (1997) Refinement of macromolecular structures by the maximum-likelihood method. *Acta Crystallogr. D Biol. Crystallogr.* **53**, 240-255
23. Emsley, P., and Cowtan, K. (2004) *Coot*: model-building tools for molecular graphics. *Acta Crystallogr. D Biol. Crystallogr.* **60**, 2126-2132
24. Laskowski, R. A., MacArthur, M. W., Moss, D. S., and Thornton, J. M. (1993) *PROCHECK*: a program to check the stereochemical quality of protein structures. *J. Appl. Crystallogr.* **26**, 283-291
25. Kabsch, W. (1978) A discussion of the solution for the best rotation to relate two sets of vectors. *Acta Crystallogr. A* **34**, 827-828
26. Delano, W. L. (2002). *The PyMOL Molecular Graphics System*, DeLano Scientific LLC, San Carlos, CA
27. Berman, H. M., Westbrook, J., Feng, Z., Gilliland, G., Bhat, T. N., Weissig, H., Shindyalov, I. N., and Bourne, P. E. (2000) The Protein Data Bank. *Nucleic Acids Res* **28**, 235-242
28. Laemmli, U. K. (1970) Cleavage of structural proteins during the assembly of the head of bacteriophage T4. *Nature* **227**, 680-685
29. Miamin, V. E., Pesniakevich, A. G., Nikolaichik, E. A., and Prokulevich, V. A. (2004) Genetic regulation of pathogenicity and virulence factors in bacteria *Erwinia carotovora* subsp. *atroseptica*: identification of gene *kduD*. *Genetika* **40**, 1187-1193
30. Holm, L., Kaariainen, S., Rosenstrom, P., and Schenkel, A. (2008) Searching protein structure databases with DaliLite v.3. *Bioinformatics* **24**, 2780-2781
31. Henikoff, S., and Henikoff, J. G. (1992) Amino acid substitution matrices from protein blocks. *Proc. Natl. Acad. Sci. U.S.A.* **89**, 10915-10919

CONCLUSION

1. 4-Deoxy-L-*erythro*-5-hexoseulose uronic acid (DEH) derived from alginate is converted to 2-keto-3-deoxy-D-gluconic acid (KDG) in *Sphingomonas* sp. strain A1 by NADPH-dependent reductase, A1-R. Based on the primary structure, A1-R was classified to short-chain dehydrogenase/reductase (SDR) family. The structures of A1-R and A1-R·$NADP^+$ complex were determined by X-ray crystallography. $NADP^+$ molecule was bound to the Rossmann fold. Some residues were identified to be involved in catalytic reaction (Ser-150, Tyr-164, and Lys-168) and NADPH recognition (Ser-16, Gly-38, and Arg-39) by structure-guided site-directed mutagenesis.

2. Distinct from A1-R, another NADH-dependent DEH reductase, A1-R′, was found in A1-R-deficient strain A1 cells. Due to high sequence identity (64%) between A1-R′ and A1-R, A1-R′ also belongs to SDR family. Enzymatic properties of A1-R′ were similar to those of A1-R except for coenzyme requirement. A1-R′ and A1-R′·NAD^+ complex structures were determined by X-ray crystallography. Significant differences in electric charge and space formation at the binding site of nucleoside ribose 2' region of the coenzyme were found between A1-R′ and A1-R. Two short and long loops cause these differences. Coenzyme requirement of A1-R′ was completely converted by exchange of the two loops with those of A1-R. The loop exchange is promising for conversion of coenzyme requirement in the SDR family.

3. Two SDR family enzymes, KduD from *P. carotovorum* (PcaKduD) and DhuD from *S. pyogenes* (SpyDhuD), prefer NADH as coenzyme, although only PcaKduD can utilize NADPH as well as NADH. Both enzymes reduce 2,5-diketo-3-deoxy-D-gluconic acid to produce KDG. PcaKduD and SpyDhuD were crystallized and subjected to X-ray crystallography. Similar to A1-R and A1-R′, both enzymes have the two short and long loops close to the coenzyme-binding site. Primary structures of the two loops in PcaKduD and SpyDhuD were similar to those in A1-R′ rather than those in A1-R. The moderate space formation and non-electric charge at the binding site of nucleoside ribose 2' region of the coenzyme were structurally determined to be crucial for dual coenzyme specificity in KduD.

Throughout this study, structural determinants of coenzyme requirement in SDR family enzymes were identified and the methodology to design the coenzyme requirement was established.

ACKNOWLEDGMENTS

The author is deeply grateful to Dr. Kousaku Murata, Emeritus Professor of Kyoto University (currently Professor at the Faculty of Science and Engineering, Setsunan University). The author would not have been able to complete this study without the comfortable research environment arranged by Dr. Murata. In addition, his comments and suggestions about not only research activities but also private life were of inestimable value to the author.

The author would like to express deep gratitude to Dr. Wataru Hashimoto, Associate Professor at the Graduate School of Agriculture, Kyoto University. His meaningful suggestions and heartfelt instructions were of invaluable help in the author's study.

The author is indebted to Dr. Bunzo Mikami, Professor at the Graduate School of Agriculture, Kyoto University, for his kind instruction regarding X-ray crystallography and for technical advice.

The author would like to express special thanks to Dr. Shigeyuki Kawai, Assistant Professor at the Graduate School of Agriculture, Kyoto University, for his encouragement and enormous help.

The author is deeply indebted to Dr. Yukie Maruyama, Post-Doctoral Fellow at the Graduate School of Agriculture, Kyoto University (currently Assistant Professor at the Faculty of Science and Engineering, Setsunan University), for her heartwarming support.

The author would like to express his gratitude to Dr. Akihito Ochiai, Post-Doctoral Fellow at the Graduate School of Agriculture, Kyoto University (currently Assistant Professor at the Faculty of Engineering, Niigata University), for providing fundamental and careful instructions to the author.

The author would like to express thanks to Dr. Takafumi Itoh, Post-Doctoral Fellow at the Graduate School of Agriculture, Kyoto University (currently Associate Professor at the Faculty of Biotechnology, Fukui Prefectural University), for his sincere encouragement.

The author is indebted to Dr. Jun Ogawa, Professor at the Graduate School of Agriculture, Kyoto University, Dr. Shigenobu Kishino, Assistant Professor at the Graduate School of Agriculture, Kyoto University, and Dr. Nobuyuki Takahashi, Assistant Professor at the Graduate School of Agriculture, Kyoto University, for their help in protein sequence determination and circular dichroism spectroscopy.

The author would like to thank Dr. Kohei Ogura, Ph.D. student at the Graduate School of Agriculture, Kyoto University (currently Assistant Professor at the Graduate School of Medicine, Chiba University), for his instructions regarding laboratory techniques.

The author would like to thank Dr. Kazuto Ohashi, Ph.D. student at the Graduate School of

Agriculture, Kyoto University (currently Post-Doctoral Fellow at the Department of Integrative Structural and Computational Biology, The Scripps Research Institute), for his suggestions and encouragement.

The author also expresses thanks to Dr. Yusuke Nakamichi, Ph.D. student at the Graduate School of Agriculture, Kyoto University (currently Post-Doctoral Fellow at the Institute for Protein Research, Osaka University), for his stimulating discussions.

The author would like to offer special thanks to the members of the Laboratory of Basic and Applied Molecular Biotechnology, Graduate School of Agriculture, Kyoto University, for their help.

The author would also like to express thanks to his family for their support.

This work was supported by a Research Fellowship for Young Scientists from the Japan Society for the Promotion of Science.

Ryuichi TAKASE

LIST OF PUBLICATIONS

Original papers

1. **Ryuichi Takase, Yukie Maruyama, Sayoko Oiki, Bunzo Mikami, Kousaku Murata, and Wataru Hashimoto.** Structural determinants in bacterial 2-keto-3-deoxy-D-gluconic acid dehydrogenase KduD for dual (NADH and NADPH) coenzyme specificity.
   J. Biol. Chem. In preparation (2015).
2. **Ryuichi Takase, Bunzo Mikami, Shigeyuki Kawai, Kousaku Murata, and Wataru Hashimoto.** Structure-based conversion of the coenzyme requirement of a short-chain dehydrogenase/reductase involved in bacterial alginate metabolism.
   J. Biol. Chem. **289,** 33198-33214 (2014).
3. **Ryuichi Takase, Akihito Ochiai, Bunzo Mikami, Wataru Hashimoto, and Kousaku Murata.** Molecular identification of unsaturated uronate reductase prerequisite for alginate metabolism in *Sphingomonas* sp. A1.
   Biochim. Biophys. *Acta* **1804,** 1925-1936 (2010).

Review article

1. **Akihito Ochiai, Ryuichi Takase, Bunzo Mikami, Wataru Hashimoto, and Kousaku Murata.** Structure and function of alginate-metabolizing enzymes.
   Vitamins **84,** 525-531 (2010).

Related article

1. **Chie Hayashi, Ryuichi Takase, Keiko Momma, Yukie Maruyama, Kousaku Murata, and Wataru Hashimoto.** Alginate-dependent gene expression mechanism in *Sphingomonas* sp. strain A1.
   J. Bacteriol. **196,** 2691-2700 (2014).